MAGNESIUM SIALONS

A Dissertation submitted for the Degree of

Doctor of Philosophy

of the University of Newcastle upon Tyne

by

DAYANTHA SHRESHTA PERERA

Department of Metallurgy and Engineering Materials

The University of Newcastle upon Tyne

September 1976

Preface

This dissertation describes original work, and it has not been submitted for a degree at any other university.

The investigations were carried out in the Crystallography Laboratory, Department of Metallurgy and Engineering Materials of the University of Newcastle upon Tyne within the period October 1973 to September 1976, under the supervision of Professor K.H. Jack.

The thesis describes the investigation of the magnesium-silicon-aluminium-oxygen-nitrogen system. Phase relationships have been studied in this system and the physical and chemical properties of some of the more important phases have been measured.

Acknowledgements

I sincerely thank Professor K.H. Jack for the keen interest, enthusiasm and encouragement during the supervision of this work.

My gratitude to Dr. D.P. Thompson for helpful suggestions and invaluable discussions.

I also wish to thank:

Professor R.N. Parkins for providing facilities in the Department of Metallurgy and Engineering Materials of the University of Newcastle upon Tyne;

Dr. A. Hendry and Dr. N.J. Pipkin for assistance in electron microscopy;

Professor E.S. Page and his staff at the Newcastle University Computing Laboratory for the use of computing facilities;

Dr. S. Wild of the Department of Science, Polytechnic of Wales, Mid-Glamorgan, for infra-red measurements;

Joseph Lucas Limited for awarding me a grant from October 1973 to September 1976;

Mrs. A. Rule for typing the script.

Finally I like to thank my wife, Shanthi for her patience and understanding during this project.

To Shevantha.

8th September 1976

Abstract

The Mg-Si-Al-O-N system was investigated for phase relationships from compositions made from Si_3N_4, Al_2O_3, SiO_2, MgO, Mg_3N_2 and pre-prepared spinels and forsterite. These were hot-pressed at 1700-1800°C and the products were analysed by X-ray techniques and from the results behaviour diagrams were constructed.

A single-phase region of β'-magnesium sialon isostructural with β-silicon nitride and similar to the β'-phase in the Si-Al-O-N system was observed in the plane of constant 3:4 metal:non-metal atom ratio. Some property measurements were carried out on a selected β'-magnesium sialon. It has a low isotropic coefficient of expansion of $2.7 \times 10^{-6} {}^{o}C^{-1}$ and slightly better oxidation resistance than β'-sialon.

A homogeneous nitrogen containing spinel region was observed in the Mg_3N_2-MgO-Al_2O_3-AlN plane extending into the Mg-Si-Al-O-N system. Evidence for the formation of spinel with vacant non-metal atom sites is given.

Number of new phases and structural modifications of existing AlN-polytypes were observed. The AlN-polytypes 6H, 12R, 15R, 12H, 21R, 20H and $2H^{\delta}$ corresponding to the metal:non-metal atom ratio of

4:3, 5:4, 5:6, 6:7, 7:8, 10:11 and $>$ 10:11, $<$ 1:1 were found.

A new quaternary nitride, $MgAlSiN_3$ was formed by reacting Mg_3N_2, Si_3N_4 and AlN at 1800°C. This compound has an orthorhombic structure, space group $Cmc2_1$ based on the lithium silicon nitride structure with ordered magnesium atoms occupying lithium positions and disordered Si,Al atoms in silicon sites.

Some glass-forming compositions in the Mg-Si-O-N system and the Mg-Si-Al-O-N system were observed. This glass plays an important role in the hot-pressing of silicon nitride and β'-sialon with magnesium oxide additions.

Contents

List of Figures

List of Tables

I. Introduction

I.1 The meaning of ceramics

It is becoming increasingly difficult to give an all-inclusive definition of ceramics. A meaningful definition is "The art and science of making and using solid articles which have as their essential component, and are composed in large part of, inorganic, nonmetallic materials" (Kingery, 1967).

Over the last 10 to 15 years, there has been a rapidly increasing need for structural and special purpose materials able to withstand severe environmental conditions. Industry has been turning away from the metallic engineering materials towards non-conventional ceramics. This has broadened the field of ceramics to include in addition to the traditional materials made largely from natural raw materials such as clay, quartz and feldspars, the purer materials based on metal oxides, nitrides, silicides and carbides. These form the branch of "Special ceramics". The division between metals and ceramics is somewhat arbitrary and some ceramic materials, the interstitial alloys, also have metallic properties, e.g. TiC, ZrN, WC.

I.2 Technological applications of ceramics

Historically, ceramic materials predate metals. However, metals have been better understood because they are somewhat simpler in structure and are in general made up of identical atoms in a simple close-packed or nearly close-packed arrangement; ceramics are composed of at least two different types of atoms linked together by either ionic or covalent bonds the latter being responsible for high hardness, refractoriness and chemical inertness. From a technological point of view the main disadvantage of ceramics is their brittleness. Some of the more desirable properties that are required of ceramic engineering materials are:

(1) High specific modulus i.e. elastic modulus/specific gravity;

(2) Good high-temperature strength;

(3) Good thermal shock resistance;

(4) Ease of fabrication;

(5) High chemical stability.

Table I.1 shows potential ceramic materials with their high specific moduli and melting or decomposition temperatures, compared with conventional engineering materials like steel and wood. For a high modulus, the bond strength between atoms must be high and for a low density the atoms must have low atomic weights and small co-ordination numbers. This implies covalent bonding. The high-modulus materials also have high melting or

Table I.1 Some high specific modulus materials

(after Jack, 1973)

	elastic modulus / specific gravity		melting or decomposition temperature
	10^6 lb in^{-2}	10^3 Mn m^{-2}	°C
AlN	15	103	2450
Al_2O_3	13	90	2050
BeO	18	124	2530
C whiskers	61	421	3500
SiC	25	172	2600
Si_3N_4	17	117	1900
BN	7	48	2700
steel, glass, aluminium, wood	4	28	

high decomposition temperatures because this also depends on a high interatomic bond strength. Of the materials listed in Table I.1, aluminium nitride is easily hydrolysed, alumina has poor thermal shock resistance, beryllia is toxic, and carbon is easily oxidised. This leaves silicon carbide and silicon nitride as leading contenders for high-temperature engineering applications.

I.3 Development of nitrogen ceramics

Some of the useful properties of silicon nitride, namely its high strength, good wear resistance, high decomposition temperature, oxidation resistance, excellent thermal shock properties, low coefficient of friction and resistance to corrosive environments should make it an ideal material in the gas turbine engine. Figure I.1 illustrates the parts of a gas turbine which would need to be made out of ceramic components. There are other potential applications for nitrogen ceramics, in aerospace as radomes and nozzle materials, in engineering as die materials, ball bearings for abrasive or corrosive environments, crucibles, thermocouple sheaths, gas burner elements. Silicon nitride also being an electrically insulating material, it may be used in microwave dielectric transparency applications such as antenae windows, electron tube windows and envelopes.

Silicon nitride being a covalently bonded solid, it cannot be sintered to maximum density by firing and it

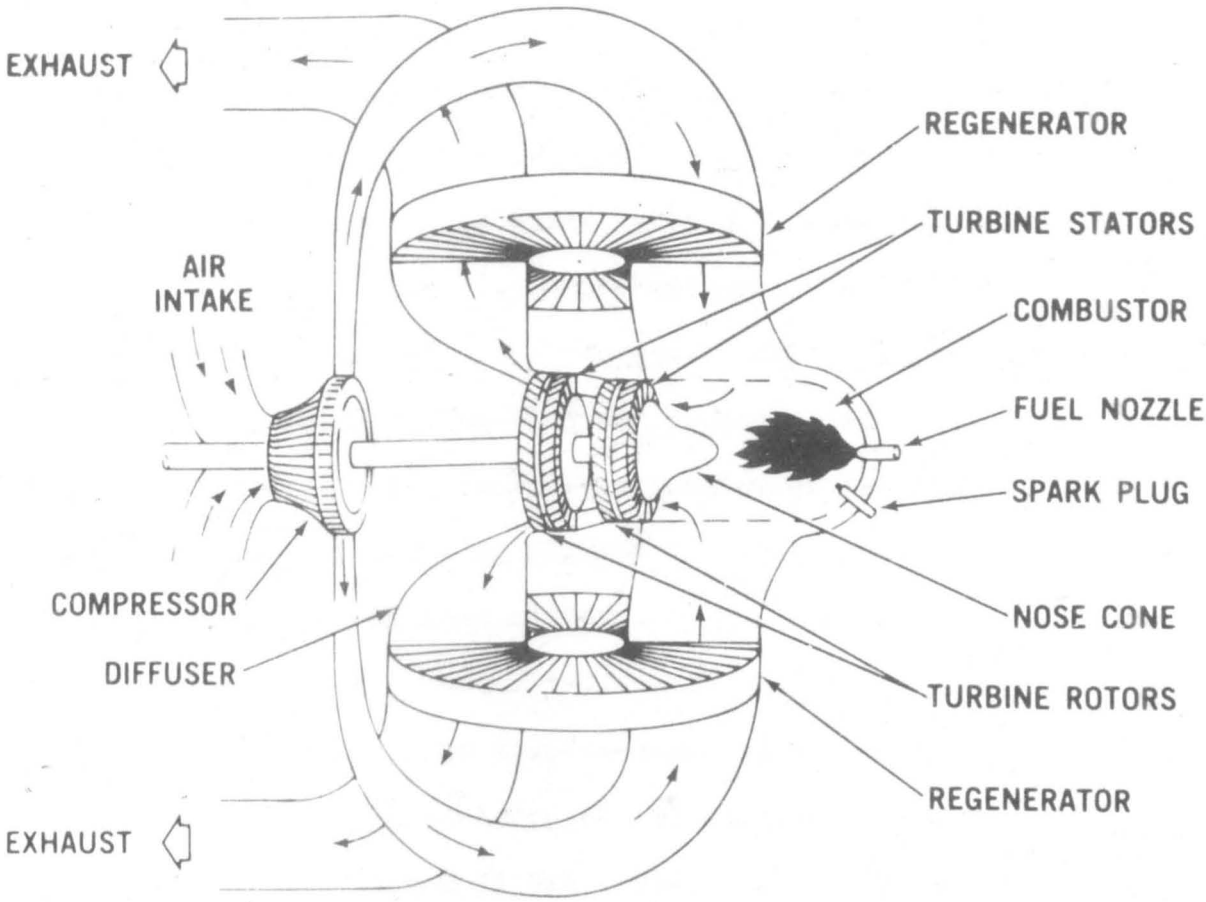

Regenerative gas turbine schematic.

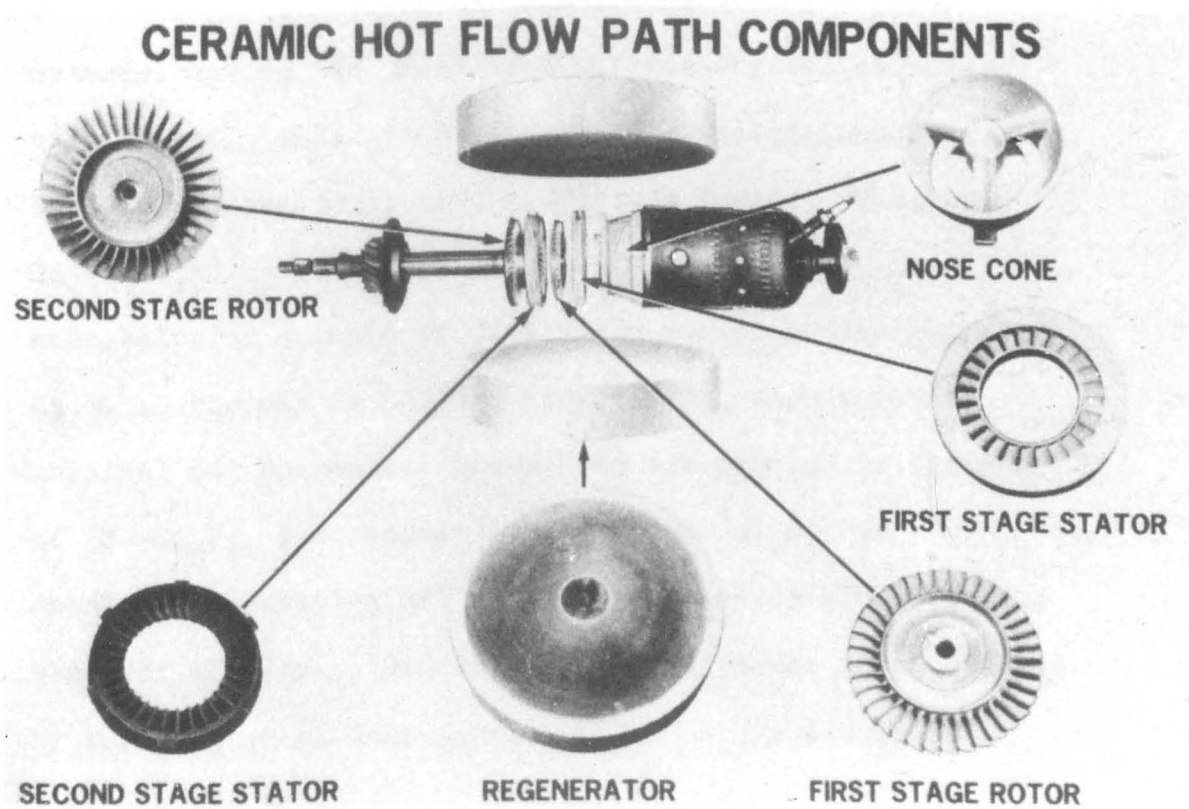

Ceramic hot flow path components.

is possible to reach theoretical density only by hot-pressing α-silicon nitride with small added quantities of metal oxides such as magnesia, alumina, yttria. Hot-pressing is an expensive and time consuming method and complex shapes cannot be fabricated. However complex shapes may be fabricated by "reaction-bonding" as discussed in Chapter II, but it has limitations because of its high porosity. This has led to further investigation of materials based on silicon nitride.

It was found possible to replace silicon by aluminium and at the same time nitrogen by oxygen in silicon nitride without change of structure (Oyama & Kamigaito, 1972; Jack & Wilson, 1972). This opened up a wide field of chemistry based on the Si-Al-O-N system. By hot-pressing mixtures of aluminium nitride and alumina with α-silicon nitride at 1700-1800°C a single-phase material having the β-silicon nitride crystal structure with slightly enlarged unit cell is obtained (Gauckler, Lukas & Petzow, 1975; Lumby, North & Taylor, 1975; Jack, 1976). This is widely known as "sialon", the name being an acronym of Si-Al-O-N, and it is designated as β'; because it has the same crystal structure its physical and mechanical properties are similar to those of β-Si_3N_4, but because it is nearer Al_2O_3 in chemical composition its chemical properties are more like those of alumina. Similar β'-sialon phases were obtained by reacting α-silicon nitride with lithium aluminium

spinel, $LiAl_5O_8$ (Jama, Thompson & Jack, 1974) and also with magnesium-aluminium spinel (Jack, 1973). In other words, properties can be to some extent "tailor-made" by "alloying" silicon nitride with Al_2O_3, MgO, Li_2O and other metal oxides and nitrides. Depending on the extent and the type of combination, the properties of the product varies e.g. high oxygen content gives good oxidation resistance and easier sinterability. Sialons have not only a potential use in the ceramic gas-turbine but also in many other engineering and technological applications.

In earlier work at Newcastle associated with the hot-pressing of silicon nitride, several metal-silicon nitrides including those of magnesium ($MgSiN_2$), manganese ($MnSiN_2$) and lithium ($LiSi_2N_3$) were prepared and characterised (see Chapter II). These all have structures based on that of aluminium nitride (AlN) and are built up of metal-nitrogen tetrahedra MN_4 (M = Mg,Mn,Li,Si). In all these nitrides limited replacement of nitrogen by oxygen is possible, valency requirements being met by some of the metal-atom sites becoming vacant. These considerations suggested that there is every possibility of incorporating magnesium, manganese and lithium as $M(O,N)_4$ (M = Mg,Mn,Li) structural units in β'-sialons which, being isostructural with β-Si_3N_4, are built up of $(Si,Al)(O,N)_4$ tetrahedra. The existence of β'-lithium sialons and β'-magnesium sialons has been confirmed as mentioned above. The range of homogeneity of β'-magnesium sialon was not determined and

needed investigation.

β'-sialon has better oxidation resistance, creep resistance, resistance to chemical attack and has a lower coefficient of expansion than silicon nitride (see Chapter II). Therefore it would be expected that another good refractory oxide like magnesium oxide (m. pt. 2800°C) would "alloy" with α-Si_3N_4, Al_2O_3 and AlN to form materials with chemical resistance superior to that of β'-sialon.

Bell & Wilson (1973) reacted magnesium oxide with mixtures of α-silicon nitride and alumina, and observed AlN-polytypes similar to those found in the Si-Al-O-N system (see Chapter II). It seemed probable that these polytypes could accommodate Mg and an investigation of the Mg-Si-Al-O-N system was considered necessary.

One of the first additives to be used to densify silicon nitride was magnesium oxide. The proposed mechanism for densification is via liquid phase sintering and is discussed in detail in Chapter II. Wild, Grieveson, Jack & Latimer (1972) showed that the liquid phase present at the sintering temperature remains as a glass at room temperature and divitrifies to enstatite and silicon oxynitride. It can therefore be concluded that this glass contains Mg, Si, O and N. Si-N bonds are more covalent than Si-O bonds and make the glass more refractory than a silica glass. These glass systems (Mg-Si-O-N or Mg-Si-Al-O-N) need further investigation.

II. Previous Investigations

II.1 The crystal chemistry of nitrogen ceramics

Silicon nitride exists in two crystallographic forms α and β. β has the atomic arrangement of a silicate structure, phenacite (Be_2SiO_4), and is a typically covalent solid built up of SiN_4 tetrahedra joined in a three-dimensional net-work by sharing corners; each nitrogen corner is common to three tetrahedra (Figure II.1). α-silicon nitride represents another way of joining together SiN_4 tetrahedra except that about 1 in 30 nitrogen atoms are replaced by oxygen (Figure II.2). The unit-cell contents of β-silicon nitride are Si_6N_8 and that of α-silicon nitride are $Si_{12}N_{16}$. A selection of unit-cell dimensions from the literature is presented in Table II.1.

In the Si-O-N system "silicon oxynitride" Si_2N_2O another nitrogen ceramic, is built up of SiN_3O tetrahedra and consists of parallel sheets of Si-N atoms joined by Si-O-Si bonds. It has four formula units in its orthorhombic unit cell and dimensions:

a	b	c	
5.498	8.877	4.853	(Forgeng & Decker, 1958)
5.473	8.843	4.835	(Indrestedt & Brosset, 1964)

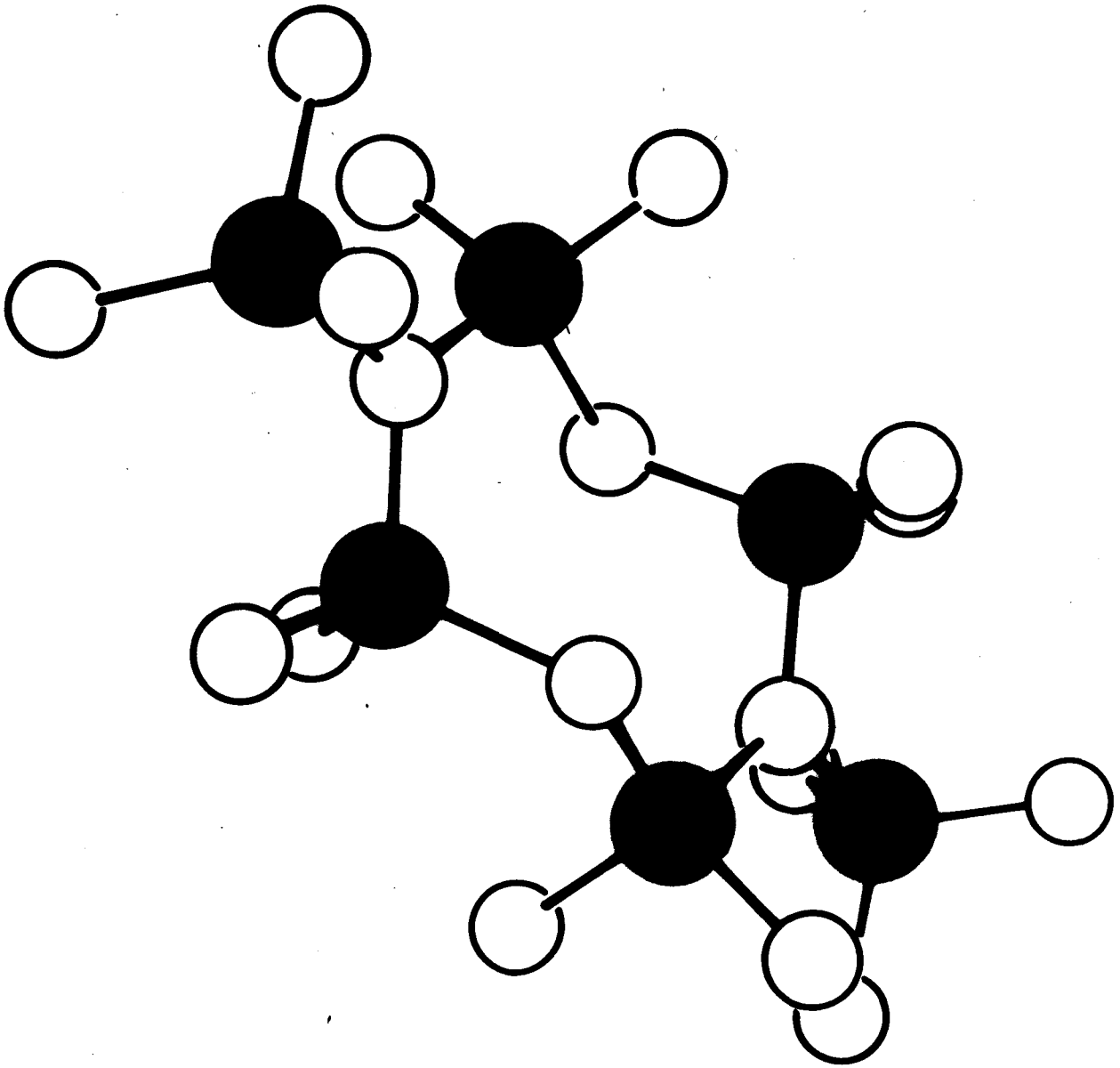

Figure II.1 Structure of β-silicon nitride

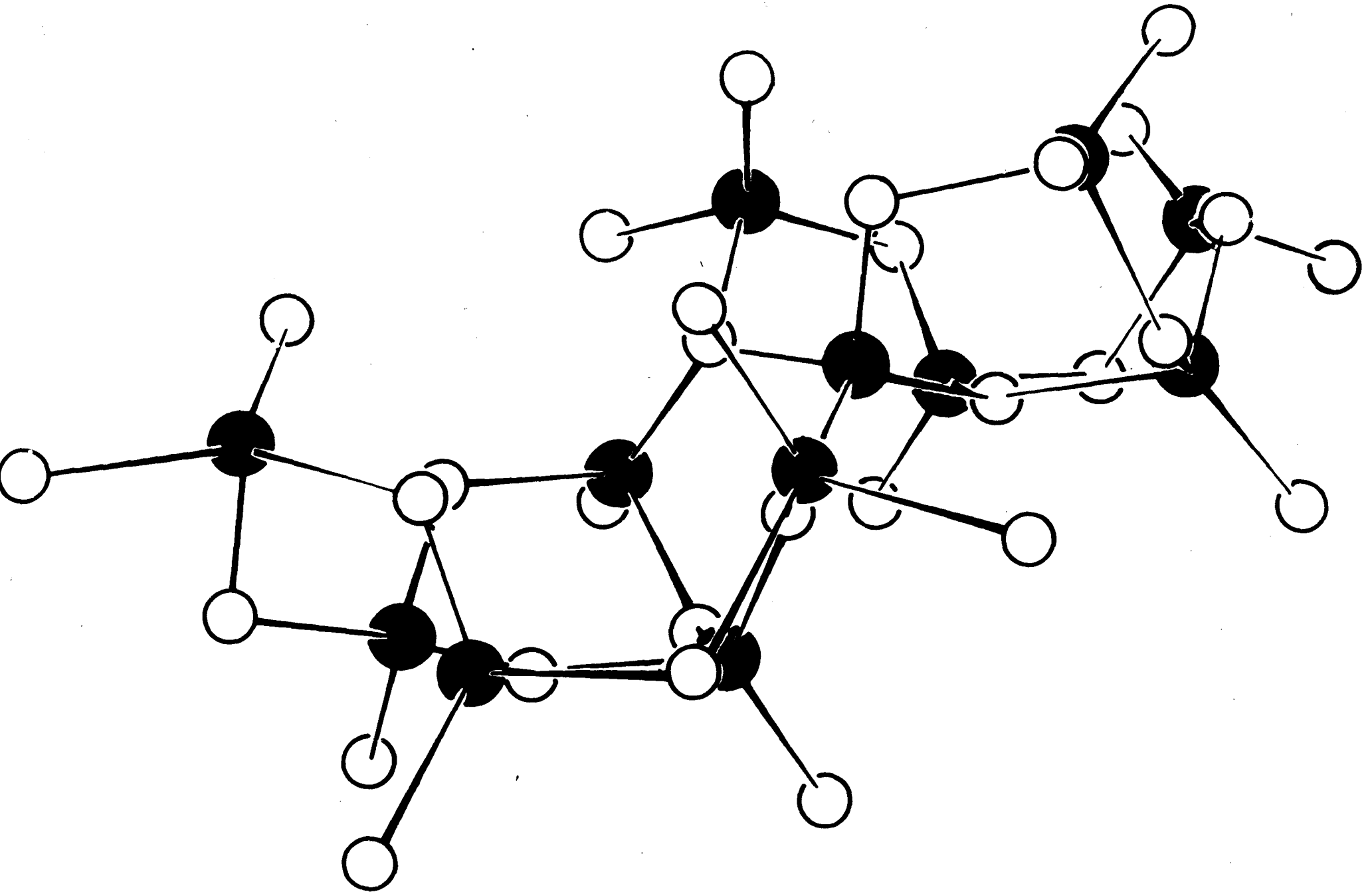

Figure II.2 Structure of α-silicon nitride

Table II.1 Unit cell data of silicon nitride in Å

(after Cutler & Croft, 1974)

α-phase		β-phase		
a	c	a	c	
7.748 ± 0.001	5.617 ± 0.001	7.608 ± 0.001	2.9107 ± 0.0005	Hardie & Jack (1957)
7.753 ± 0.004	5.618 ± 0.004	7.606 ± 0.003	2.909 ± 0.002	Ruddelsden & Popper (1958)
7.752 ± 0.003	5.619 ± 0.001	7.604 ± 0.001	2.907 ± 0.001	Suzuki (1963)
7.755 ± 0.005	5.616 ± 0.005	7.606 ± 0.005	2.709 ± 0.003	Thompson & Pratt (1967)
7.7520± 0.0007 (wool)	5.6198± 0.005	7.608 ± 0.005	2.911 ± 0.001	Wild, Grieveson & Jack (1972)
7.7533± 0.008 (needles)	5.6167 ± 0.006			
7.760 ± 0.001	5.613 ± 0.001			Priest, Burns & Skáar (1973)

The probability that α-silicon nitride had a defect structure in which a few nitrogen atoms are replaced by oxygen suggested that more nitrogen might be similarly replaced, without changing the structure, by applying the simple principles of silicate chemistry. In all silicates and in the various forms of silica itself, the fundamental building unit is the SiO_4 group carrying four negative charges. The tetrahedra may occur separately, or may be joined together by sharing oxygen corners into rings, chains, two dimensional sheets, or three-dimensional net-works. Aluminium plays a special role in the silicate structures because the AlO_4 tetrahedron - with five negative charges - is about the same size as SiO_4 and can replace it in the rings, chains and net-works provided that valency or charge compensation is made elsewhere in the structure. It is possible to replace N^{3-} by O^{2-} in silicon nitride if at the same time Si^{4+} is replaced by Al^{3+}, charge compensation might also be feasible by introducing other metal atoms like Mg^{2+} and Li^{+}. It was predicted by Wild, Grieveson & Jack (1968) that a variety of new materials, vitreous as well as crystalline, could be obtained built up of silicon-aluminium-oxygen-nitrogen tetrahedra in the same way that the almost infinite range of silicates is built up of silicon-aluminium-oxygen units; see Table II.2.

Aluminium nitride has a wurtzite-type structure which is discussed in Chapter IX. The many AlN-polytypes

Table II.2 Structural units in some nitrogen ceramics

phase	structural unit
β-Si_3N_4	SiN_4
α-$Si_{11.5}N_{15}O_{0.5}$	$SiN_{3.9}O_{0.1}$
Si_2N_2O	SiN_3O
Sialon	$(Si,Al)(O,N)_4$
AlN	AlN_4
$MgSiN_2$	$MgN_4 : SiN_4$
$LiSi_2N_3$	$LiN_4 : 2SiN_4$

observed in Si-Al-O-N and Mg-Si-Al-O-N systems are discussed elsewhere (Chapter IX). There is also an extensive range of metal-silicon nitrides all of which have structures based on that of AlN. Just as AlN is built up of AlN_4 tetrahedra, in $MgSiN_2$ there are equal numbers of MgN_4 and SiN_4 tetrahedra (Table II.2), and in $LiSi_2N_3$ there are twice as many SiN_4 tetrahedra as LiN_4 units. Figure II.3 and Table II.3 show that the structures of $MgSiN_2$, $LiSi_2N_3$ and LiSiON can be regarded as orthorhombic superlattices of the hexagonal AlN.

II.2 Preparation of silicon nitride

Silicon nitride was formed first by Deville & Wöhler (1857) by heating silicon in nitrogen at high temperature and has since been prepared in the following ways:

(1) Forgeng & Decker (1958) obtained α-Si_3N_4 by nitriding high purity silicon at 1200-1300°C and β-Si_3N_4 by nitriding above 1450°.

(2) Parr (1966) and Thompson & Pratt (1966) produced Si_3N_4 by nitriding silicon compacts using a two-stage heating process, first at 1200°C where acicular growth of α-Si_3N_4 occurred, and then above 1450°C to give a granular mixture of α and β.

(3) Evans & Davidge (1970) found that the ratio of α to β depended upon the time and temperature of heat

Table II.3 Orthorhombic unit-cell dimensions of metal-silicon nitride and oxynitride structures

	$a = \sqrt{3}a'$	$b = 2a'$	$c = c'$
AlN	5.39	6.22	4.98
$MgSiN_2$	5.275	6.455	4.978
LiSiNO	5.194	6.394	4.742
		$b = 3a'$	
Li_2SiO_3	5.395	9.360	4.675
$LiSi_2N_3$	5.303	9.196	4.780
Si_2N_2O	5.498	8.877	4.853
$(Si,Al)_2(O,N)_3$	5.498	8.913	4.856

a' and c' are the dimensions of the equivalent wurtzite-type hexagonal cell

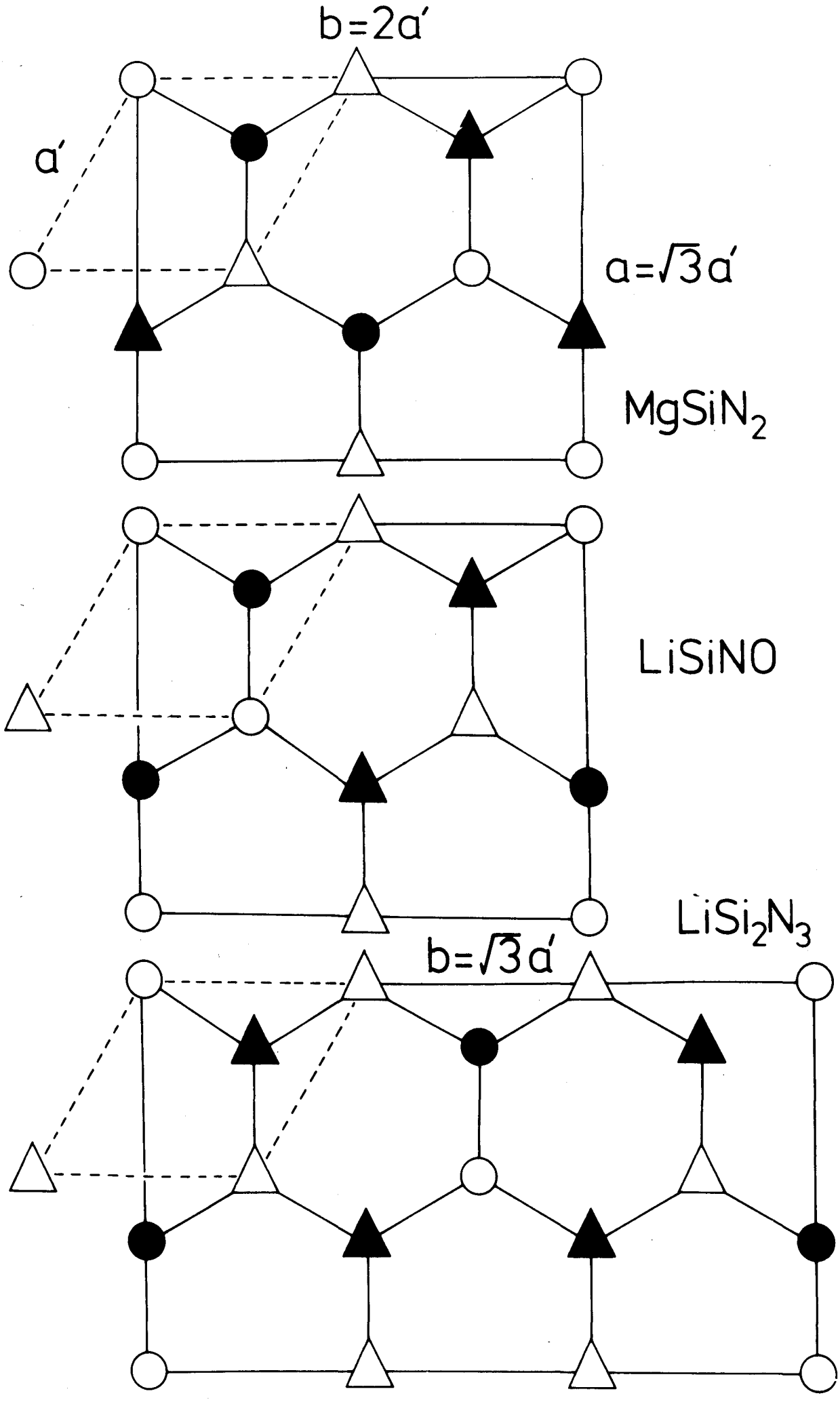

Figure II.3 Typical metal-silicon nitride and

treatment at each stage.

II.3 Hot-pressed and reaction-bonded silicon nitride

Deeley, Herbert & Moore (1961) hot-pressed α-Si_3N_4 with MgO and their method was improved by Lumby & Coe (1970) who hot-pressed α-Si_3N_4 with 1^w/o MgO at temperatures up to 1750^{o}C. In their investigation of the role of MgO in hot-pressing, Wild et al (1972) added 10^w/o MgO and showed that it reacts at 1000-1400^{o}C with the surface silica always present on Si_3N_4 particles to give forsterite

$$2\ MgO + SiO_2 = Mg_2SiO_4$$

and above 1400^{o}C, Mg_2SiO_4 reacts with any "combined SiO_2" in α-Si_3N_4 and also further surface SiO_2 to give a liquid of enstatite composition

$$SiO_2 + Mg_2SiO_4 = 2\ MgSiO_3$$

Some nitrogen is incorporated in this liquid and cools to give a magnesium silicon oxynitride glass as shown by subsequent divitrification; which gives silicon oxynitride and enstatite. The grain boundary glass phase[(A)] can be seen in Figure II.4 in the transmission electron micrograph of hot-pressed silicon nitride.

Gazza (1973) hot pressed Si_3N_4 with yttria and obtained higher hot-strength than with MgO even with impure, commercial silicon nitride powder. Rae et al (1975) showed that this superiority of yttria is due to the formation of a refractory yttrium-silicon oxynitride

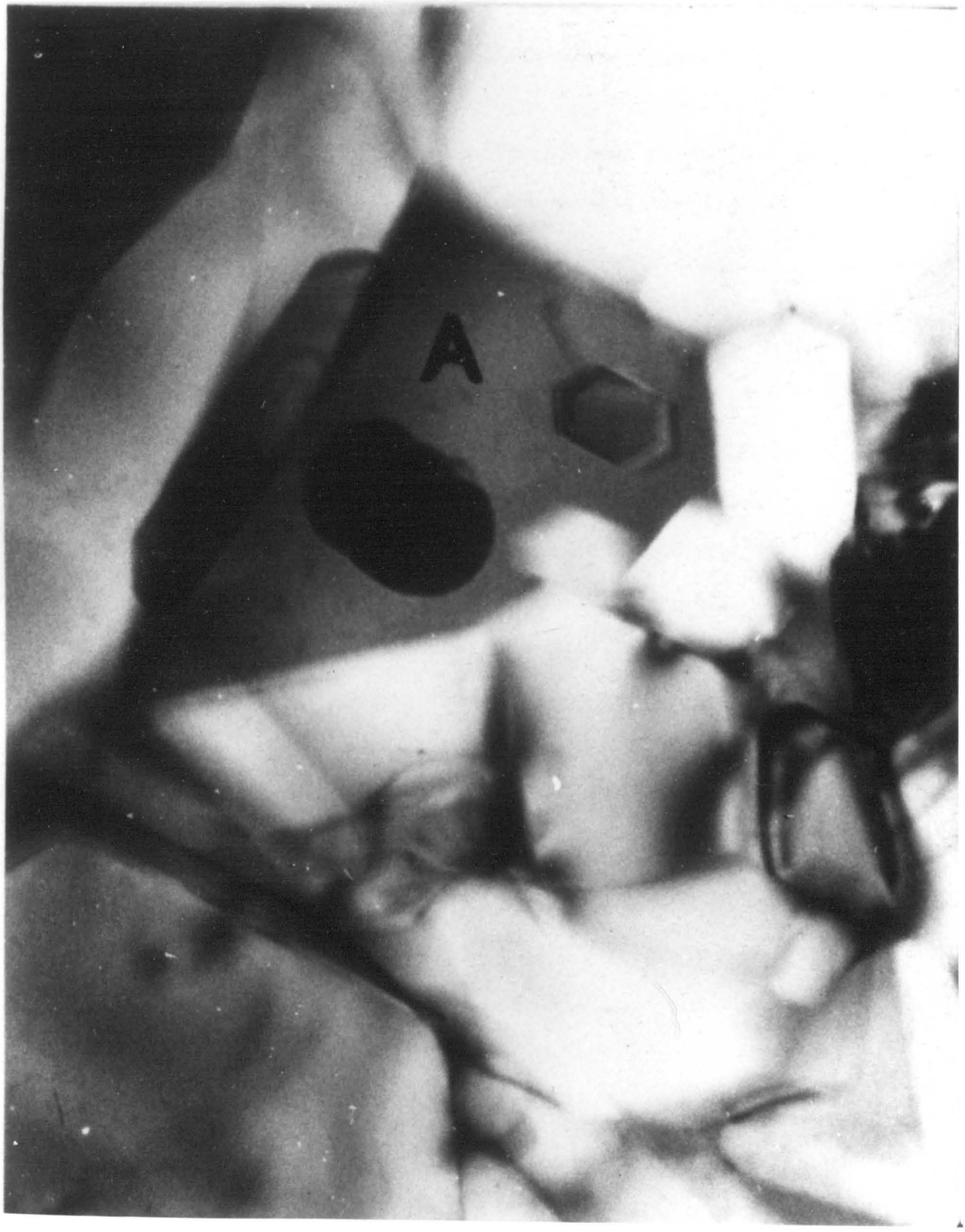

Figure II.4 Transmission electron micrograph of hot-pressed Si_3N_4 (after Nuttall & Thompson, 1974)

$Y_2Si\,[Si_2O_3N_4]$ with the structure of a melilite $Ca_2Mg\,[Si_2O_7]$ and which can accommodate calcium and other impurities which would otherwise form a low softening-temperature glass.

Complex shapes in silicon nitride may be fabricated by reaction-bonding because there are negligible dimensional changes during the nitriding reaction

$$3\ Si + 2\ N_2 = Si_3N_4$$

A powdered silicon compact is made into the required shape by any of the usual ceramic techniques, such as slip casting, dough moulding or extrusion, and then partially nitrided. This form is then machined to the required shape and dimensions and is then nitrided at $\sim 1400^{\circ}C$ to give a fully-reacted ceramic whose dimensions are usually within 0.05% of the machined preform. The main disadvantage of this method is the high porosity (15-30%).

II.4 Sialons

Although Al_2O_3 was added to Si_3N_4 to aid sintering by Deeley et al (1961) and Saito et al (1966) and observed no change in the unit cell of β-Si_3N_4, an extensive examination of the Si_3N_4-Al_2O_3 system made independently by Oyama & Kamigaito (1972) and Jack & Wilson (1972) showed otherwise. Work done at Newcastle by the latter authors showed that, up to 65 w/o Al_2O_3 was accommodated in Si_3N_4 when mixtures of α-Si_3N_4 and Al_2O_3 were hot-pressed at $1700^{\circ}C$. X-ray analysis of

the product showed at least 90% of a compound having the β-Si_3N_4 structure but with lattice parameters increasing with increasing amounts of Al_2O_3 in the starting mixes. Hot-pressing at 2000°C gave a homogeneous product with Al_2O_3 concentrations up to 74 w/o. This expanded β-Si_3N_4 structure was β'-sialon.

The following alternative compositions for β' were considered:

(1) β Si_6^{24} $N_8^{\overline{24}}$

$\downarrow$

β' $Si_{6-0.75x}^{24-3x}$ $Al_{0.67x}^{2x}$ $O_x^{\overline{2x}}$ $N_{8-x}^{\overline{24-3x}}$

$\downarrow$

$Al_{5.33}^{16}$ $O_8^{\overline{16}}$ $\equiv$ Al_2O_3

(2) β Si_6^{24} $N_8^{\overline{24}}$

$\downarrow$

β' Si_{6-z}^{24-4z} Al_z^{3z} $O_z^{\overline{2z}}$ $N_{8-z}^{\overline{24-3z}}$

$\downarrow$

Al_6^{18} $O_6^{\overline{12}}$ $N_2^{\overline{6}}$ $\equiv$ $Al_2O_3.AlN$

On the basis of limited chemical analysis and the observation of only one single-phase crystalline product

on X-ray photographs it was concluded that the composition (1) represented the reactions between Si_3N_4 and Al_2O_3. Doubts about the homogeneity range for β' were raised by Lumby, North & Taylor (1975) and subsequent work at Newcastle (see Jack, 1976) and Stuttgart (Gauckler, Lukas & Petzow, 1975) has shown that Si_3N_4 reacts with equi-molecular mixtures of Al_2O_3 and AlN (that is the equivalent of the spinel $Al_3O_3N \equiv Al_2O_3.AlN$). It is concluded that the β'-phase field extends along the join Si_3N_4-Al_3O_3N and not along the join Si_3N_4-Al_2O_3 as previously supposed. The initial incorrect interpretations are due to:

(1) volatilisation of silicon monoxide and nitrogen in the reducing environment of the graphite die during hot-pressing;

(2) volatilisation of silicon and carbon monoxides; and

(3) simultaneous formation of a silica-rich glass.

Thus, possible reactions to produce β'-sialon with $Z = 4$ are:

$$4\ Si_3N_4 + 6\ Al_2O_3 = 3\ Si_2Al_4O_4N_4 + 6\ SiO + 2\ N_2 \quad - (1)$$

$$Si_3N_4 + 2\ Al_2O_3 + C = Si_2Al_4O_4N_4 + SiO + CO \quad - (2)$$

$$Si_3N_4 + 2\ Al_2O_3 = Si_2Al_4O_4N_4 + SiO_2 \quad - (3)$$

β'-sialon phases were obtained by reacting silicon nitride with lithium aluminium spinel, $LiAl_5O_8$ and also with magnesium-aluminium spinel, $MgAl_2O_4$. The metal:non-metal

atom—ratio 3M:4X in the spinels is the same as that in the silicon nitride and, as described previously, $AlN.Al_2O_3$ also has a 3M:4X ratio. It is concluded that β' extends along the join Si_3N_4-Al_3O_3N with a composition range $Si_{6-Z}Al_ZO_ZN_{8-Z}$ where Z extends from 0 to about 4.2.

The investigation of β'-sialon has been extended at Newcastle by considering the whole Si-Al-O-N aystem, the representation of which is discussed in detail in Chapter V. Phase relationships and homogeneity ranges deduced from the results of hot-pressing appropriate mixtures of Si_3N_4, AlN, Al_2O_3, SiO_2 and Si_2N_2O at high temperature in a graphite die are shown by Figure II.5; this must be regarded as a behaviour diagram and does not necessarily represent thermodynamic equilibrium.

The β'-phase has a homogeneity range along the 3M:4X line as discussed above. The other phases 8H, 15R, 12H, 21R, 27R, $2H^{\delta}$ are all AlN polytypes and extend along directions of constant M:X ratio, i.e. 4M:5X, 5M:6X, 6M:7X, 7M:8X, 9M:10X, > 10M:11X respectively; the O'-sialon phase extends along 2M:3X and occurs when silicon oxynitride is reacted with alumina; it has slightly larger unit-cell dimensions than Si_2N_2O. The phase "X", so-called initially because its structure could not be determined (Jack & Wilson, 1972) is now known to have a monoclinic unit cell with dimensions a, 9.728; b, 8.404; c = 9.572 Å; β, 108.96° (Thompson, 1975).

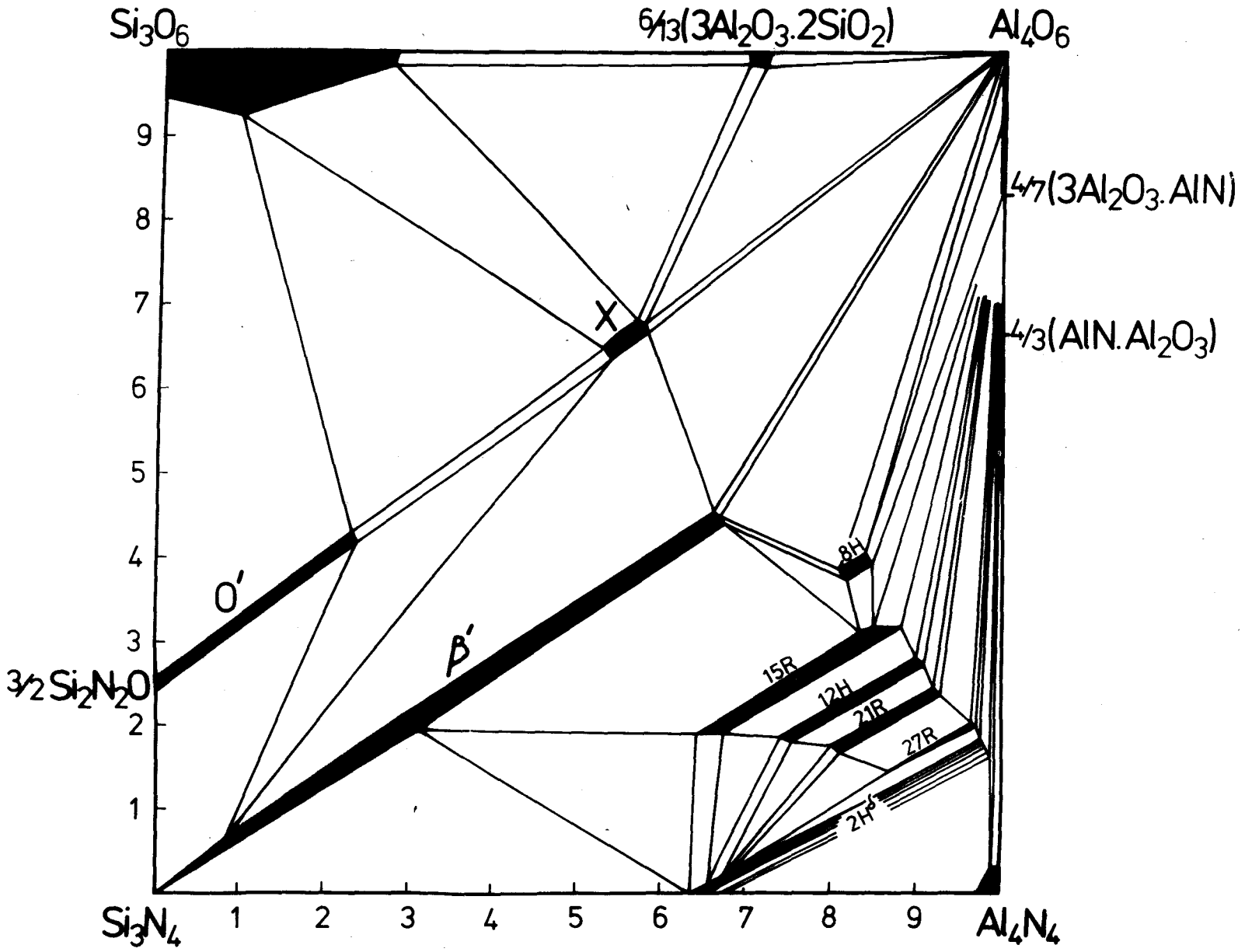

Figure II.5 The Si_3N_4-AlN-Al_2O_3-SiO_2 system

II.5 Properties of β'-sialon

β'-sialon is similar to β-silicon nitride in its physical and mechanical properties but, chemically depending upon its composition, is closer to Al_2O_3. The coefficient of thermal expansion for a composition $z = 3$ is $2.7 \times 10^{-6}/^{\circ}C$ (Jack, 1973) and is less than that of β-Si_3N_4 ($3.5 \times 10^{-6}/^{\circ}C$). Thus its thermal shock properties are at least as good as hot-pressed silicon nitride. Oxidation resistance at 1200-1400°C is better than for silicon nitride, probably because a coherent and protective layer of mullite is formed on the surface. Compatibility with molten metals is good; aluminium and copper at 1200°C and pure iron and cast iron at 1600°C kept molten in sialon crucibles for 30 minutes showed no signs of attack (Jack, 1973). Sialon prepared glass-free has a higher creep resistance and a higher room-temperature impact strength than β-Si_3N_4 (Arrol, 1974).

One potential advantage of β'-sialon over silicon nitride is in fabrication. The usual techniques of extrusion, pressing and slip-casting can be used to produce shapes of the mixed components (e.g. Si_3N_4, Al_2O_3, AlN) and then these can be fired to near theoretical density in an inert atmosphere at about 1600°C. Densifying agents such as MgO which promote liquid-phase sintering increase the density of the fired product. The properties of pressureless sintered and hot-pressed β'-sialon are compared with silicon nitride in Table II.4.

Table II.4 Some physical properties of silicon nitrides and β'-sialons

Property	hot-pressed Si_3N_4	hot-pressed sialon*	reaction-bonded Si_3N_4	sintered sialon*
Density g cm^{-3}	3.18	3.2		
Coeff. of thermal expansion: $^{o}C^{-1}$ (0-1000°C)	4.1	3.0	2.5	2.7
Thermal conductivity watts m^{-1} $^{o}K^{-1}$	20	21	15.5	-
Modulus of rupture (20°C) Mn m^{-2}	855	827	207	336
Elastic modulus 10^4 Mn m^{-2}	29	30	5.5	-
Hardness VPN	1600	1600	1100	-

* z = 1.0 - 3.0

II.6 Metal nitrides

The common refractory ceramic nitride other than silicon nitride is aluminium nitride. Taylor & Lennie (1960) first produced dense AlN bodies by hot-pressing pre-sintered powders at 2000°C in graphite dies at 5000 p.s.i. (34.5Mn m^{-2}). AlN hydrolyses readily to give Al_2O_3 and NH_3, and at 700-800°C reacts with oxygen to give a surface coating of alumina. AlN sublimes at 2400°C and is slightly anisotropic with a mean expansion coefficient of 4.8×10^{-6} $^oC^{-1}$.

Ternary nitrides of the type $MSiN_2$ have been reported where M is Be, Mg, Ca, Ba and Mn. $MnSiN_2$ and $MgSiN_2$ were prepared by Wild et al (1972) and David et al (1970). Magnesium silicon nitride was prepared by nitriding compacts of magnesium and silicon (2:1 ratio) at 1000-1200°C, and also by hot-pressing equal moles of Si_3N_4 and Mg_3N_2 at 1700°C. The $MgSiN_2$ X-ray diffraction pattern was indexed in terms of an orthorhombic cell with dimensions *a*, 5.28; *b*, 6.46; *c*, 4.98 Å, and containing four formula units of $MgSiN_2$; it is pseudohexagonal with an AlN-type structure.

Lithium silicon nitride was produced by the Carborundum Company in 1969 by hot pressing mixtures of Li_3N and Si_3N_4 at 1350-1850°C for one hour. The correct structure was reported by Taylor & Thompson (1972) and Devid et al (1973) who showed that $LiSi_2N_3$ is

orthorhombic with Space Group $Cmc2_1$. There are four formula units per unit cell the dimensions of which are: a, 9.186; b, 5.302; c, 4.776 Å. The nitrogen atoms build a slightly distorted hexagonal close packing and the lithium and silicon atoms are ordered among one half of the tetrahedral sites in the structure. A quaternary nitride of composition $MgAlSiN_3$ with a similar structure to $LiSi_2N_3$ is reported in the present work in Chapter X.

III. Scope of the Present Investigation

In the hot pressing of α-Si_3N_4 with MgO additions the nature of the vitreous phase formed at grain boundaries was not studied in detail. Even though the Si_3N_4-MgO join had been investigated briefly, phase relationships in the complete Mg-Si-O-N system were almost unknown. As discussed in Chapter I earlier work on β'-magnesium sialon involved only a study of the Si_3N_4-$MgAl_2O_4$ join and the range of homogeneity of the β'-magnesium sialon was not determined. The first detailed attempt to study this was made by Bell & Wilson (1973), who investigated the system MgO-Al_2O_3-Si_3N_4. Several new phases were observed in this system but were not characterized. Therefore a detailed investigation of the complete Mg-Si-Al-O-N system was considered necessary in order to gain an understanding of the phase relationships in the system, particularly those involving the phases observed previously.

The Mg-Si-Al-O-N system may be represented, for ease of investigation by Janeck's (1907) triangular prism, with $6MgO$, $2Mg_3N_2$, Si_3N_4, $4AlN$, $2Al_2O_3$, $3SiO_2$ at the corners and the method of representation is discussed in detail in Chapter V. To simplify the investigation selected sections were studied which would broadly cover

the whole prism; the two quasi-ternary sections (other than Si-Al-O-N which is now well known, see Jack, 1976) and the two pseudo ternary sections are fundamental to this study. The quasi-ternary sections Mg-Al-O-N and Mg-Si-O-N are described in Chapter VI. The pseudo-ternary system $MgO-Al_2O_3-SiO_2$ has been done previously (Osborn & Muan, 1960) and was not repeated.

In the Si-Al-O-N system β'-sialon and AlN-polytypes are formed along lines of constant M:X composition, and therefore it is expected that magnesium sialon analogue of these polytypes and the β'-phase will form on planes of constant M:X ratio. The constant M:X planes 3:4, 1:1 and 5:4 were investigated and in the 1M:1X plane a new phase of composition $MgAlSiN_3$ was observed and its crystal structure determination is given in Chapter X. Even though the main part of the work involves the characterization of new phases and the determination of phase relationships another important aspect is the assessment of the physical and mechanical properties of particularly the new phases. In the Si-Al-O-N system, β'-sialon shows a most promising combination of properties for high-temperature engineering applications. It is therefore of interest to compare the properties of β'-magnesium sialon with those of β'-sialon, bearing in mind that the properties of the magnesium phase will vary with composition, and also be dependent on the starting materials and the

preparative techniques involved. The β'-magnesium sialon formation and some property measurements on selected β'-magnesium sialons are described in Chapter VII.

IV. Experimental Methods

IV.1 Raw materials

Two types of silicon nitride powder were used:

(i) HS 130 supplied by Joseph Lucas Limited has an $\alpha : \beta$ ratio of 9:1 and a silica content of $\sim 4^{w}/o$; the particle size is $< 8\ \mu m$ and impurities are about $0.8^{w}/o$ of mainly Ca, Fe, Si and Al.

(ii) H.C. Starck Berlin silicon nitride which according to the supplier has the analysis:

Si	min.	60.4 $^{w}/o$
N	min.	38.1 $^{w}/o$
C	max.	0.2 $^{w}/o$
Fe	max.	0.3 $^{w}/o$

particle size 1.5 - 2.5 μ m

The alumina used was low-soda Alcoa A17 and XA16 both of which have mean particle size of 3.5 μm and a purity of $99.85^{w}/o$. In some cases where high reactivity was required, submicron grade Baikowski alumina, $99.99^{w}/o$ purity, was used.

Magnesia was B.D.H. Analar grade with a purity of $99.2^{w}/o$ and a loss on ignition of $3^{w}/o$ (confirmed by thermogravimetric analysis). Any added MgO was therefore precalcined at 700°C for 2 hours (Shelly & Nicholson, 1971) before use.

Aluminium nitride was of two types:

(i) Koch-Light Laboratories Ltd., 99^{w}/o pure and particle size $< 50\ \mu m$

(ii) H.C. Starck Berlin, specified as:

Al	min.	65.3 ^{w}/o	particle size 3 - 8 μm
N	min.	33.5 ^{w}/o	
C	max.	0.08^{w}/o	
Fe	max.	0.15^{w}/o	

Both had about 6^{w}/o alumina and larger particle sizes than specified.

Magnesium nitride was supplied by H.C. Starck Berlin with the following chemical analysis:

Mg	min.	71.0 ^{w}/o	particle size - 100 mesh
N	min.	27.0 ^{w}/o	
Fe	max.	0.08^{w}/o	

It was stored under nitrogen and all additions to powder mixtures were made in nitrogen in a dry-box; X-ray analysis showed a trace of MgO .

Silica was added as B.D.H. precipitated amorphous silica, submicron grade, or as quartz crystal powder - 80 mesh supplied by Thermal Syndicate Limited.

Spinels (e.g. $MgAl_2O_4$ or other compositions) were prepared by hot-pressing mixtures of MgO and Al_2O_3 at 1700^{o}C for 1 hour and powdering the compacted product in a tungsten carbide percussion mortar and sieving to -300 mesh. Similarly forsterite (Mg_2SiO_4) was prepared by hot-pressing mixtures of MgO and silica at 1500^{o}C for 1 hour, powdering, and sieving to -300 mesh.

IV.2 Powder preparation

The powders were vacuum dried (using anhydrone as a desiccant) at 100°C for 24 hours, mixed in the required proportions and wet-milled in *n*-butanol using 3" diameter polythene jars on a vibro-mill (Triton Engineering Co. Ltd.) for 30 minutes. Alumina balls were used to achieve efficient mixing with a weight ratio of 3 balls : 1 powder : 1 liquid. The alumina contamination from the balls was found to be negligible ($< 0.002\%$). After mixing the butanol was evaporated on a hot plate with magnetic stirring.

IV.3 Cold compaction

According to Price (1974) the presence of moisture increases the bulk density of a compact for a given applied pressure (Figure IV.1), but water cannot be used with silicon nitride and aluminium nitride powders as they are hydrolysed, therefore powders were compacted with 5-10$^{w}/_{o}$ butanol in a steel die. A pressure of 4000 p.s.i. (27.6Mn m^{-2}) was applied by means of a hydraulic press. This uniaxial pressure has an inherent disadvantage compared to isostatic pressing (see Figure IV.2) because of density contours developed in the pellet. To minimise this effect, the thickness of the pellet was not more than its diameter. Two sizes of pellets were pressed, 2.5cm diameter x 2cm thickness and 1cm diameter x 1cm thickness. Pellets were vacuum

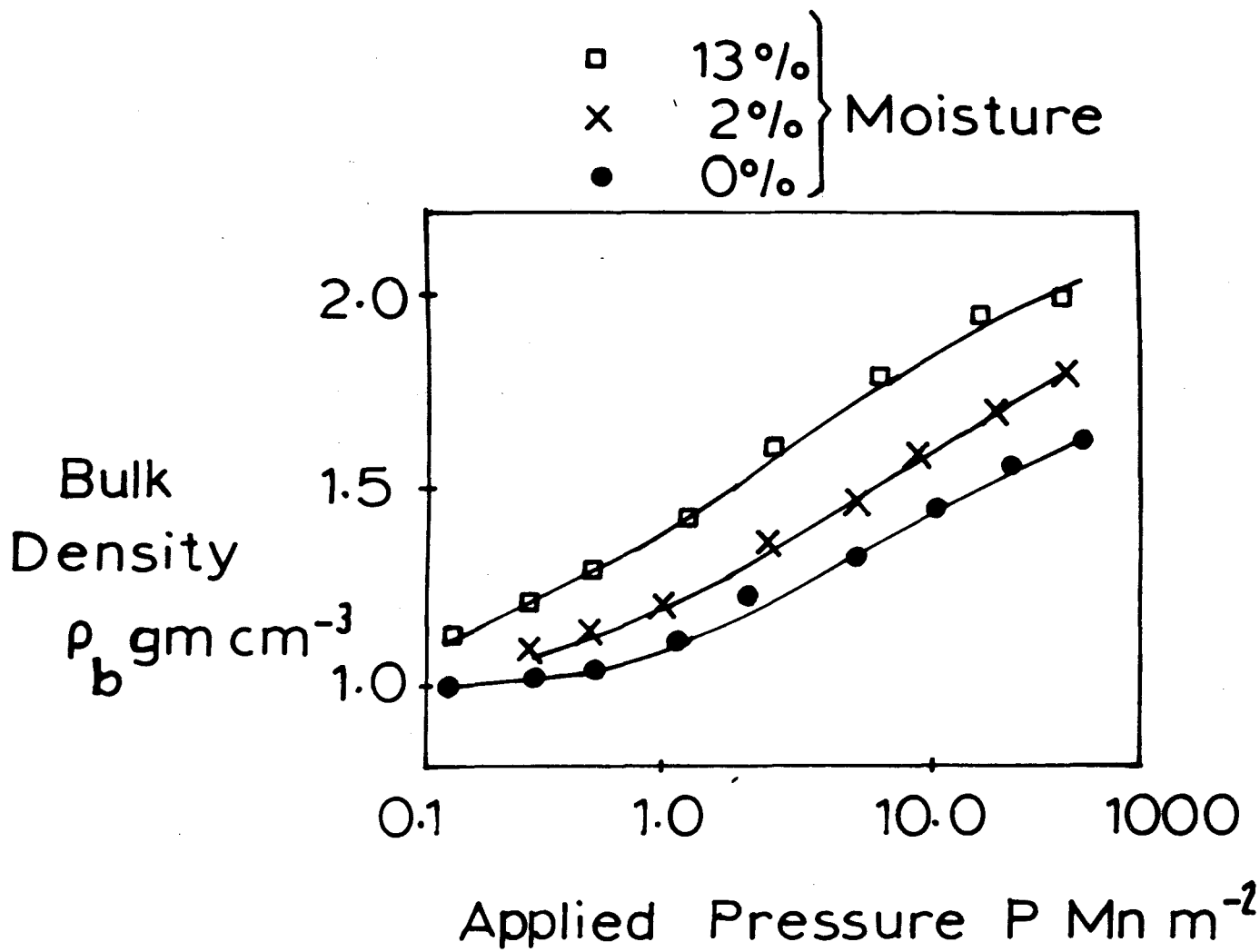

Figure IV.1 The effect of pressure on the dry bulk density of compacted powder (after Price, 1974)

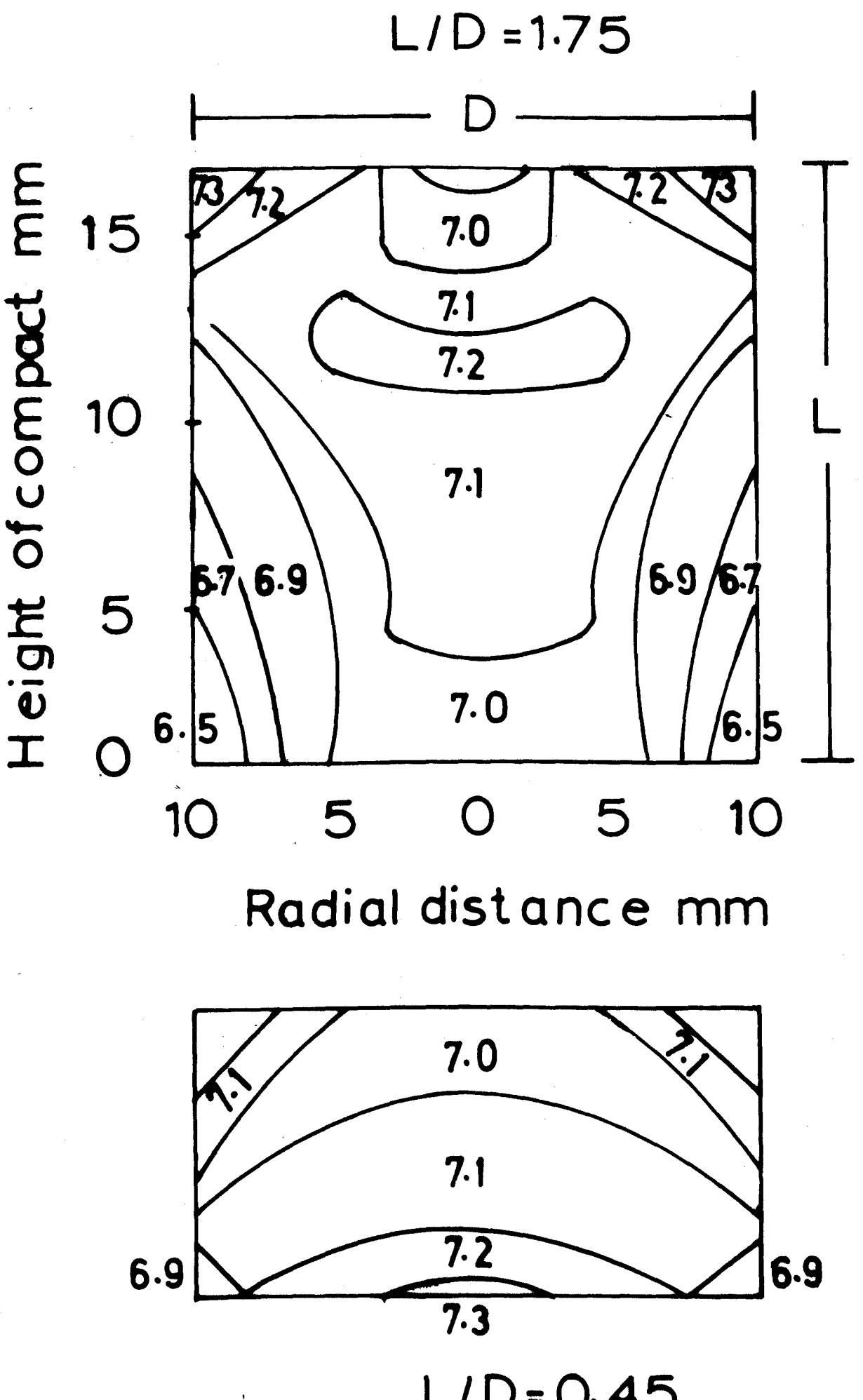

Figure IV.2 Density distribution in the sample prepared by pressing from one side (after Perelman & Roman, 1974)

dried at 100°C over anhydrone before hot-pressing.

IV. Hot-pressing

High frequency induction heating was used with the power supplied by a Radyne R150E generator operating at 450KHZ with a maximum output of 15KW. Power to the generator was fed via a saturable reactor to maintain operating stability and was controlled by a hand operated voltage regulator which varied the supply voltage to the oscillator high tension transformer.

A graphite die was used as the susceptor and was placed centrally inside a water cooled copper coil (see Figure IV.3) fed by the generator. The die and the coil were placed in a sindanyo box with a thin sheet of asbestos paper between the die and the coil so as to retain an insulating layer of fused stabilized zirconia powder.

The graphite die was about 8" long and 3" diameter with a 1.5" hole bored axially inside which was placed a graphite annular liner of 0.25" wall thickness. Two 1" diameter plungers were ground to a sliding fit with liner and inside the latter the pellet, embedded in boron nitride, was located between the two graphite plungers. Pressure was transmitted to the pellet via a silicon nitride plunger, placed on top of the graphite plunger (Figure IV.3) using an Apex A24 hand-operated hydraulic press. The temperature at the centre of the die was

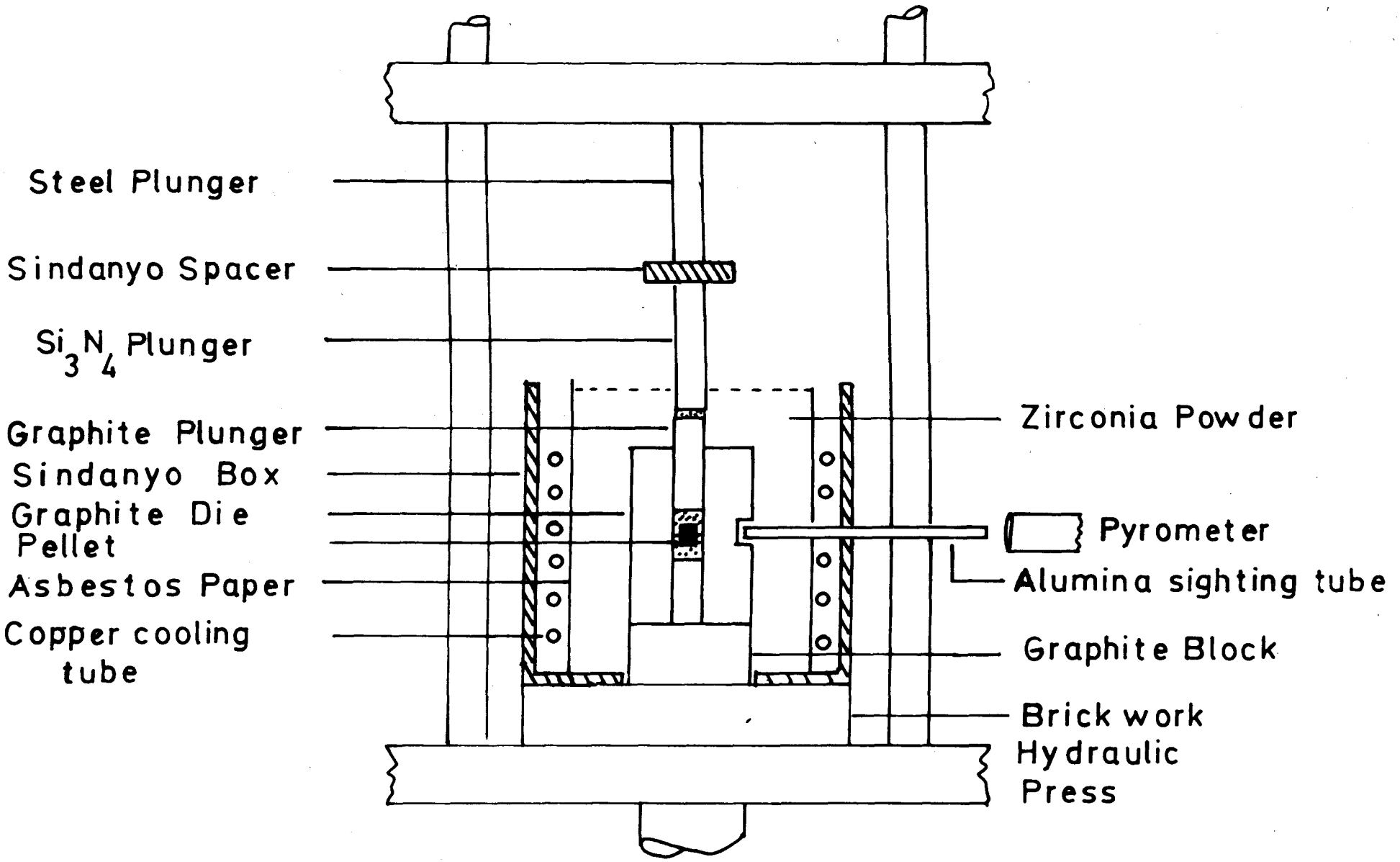

Figure IV.3 Pressure application on the pellet at high temperature

measured by a disappearing filament pyrometer (± 5%) with a short focus objective lens sighted on to the die down an open-ended alumina tube protruding into the wall of the die to a depth of ¼". The rate of heating was 50-100°C min^{-1} and pressure was gradually increased from 500 to 6000 p.s.i. (3-41Mn m^{-2}). After reaction, the die was cooled under pressure to about 200°C over a period of 3 hours.

IV.5 Sintering in a nitrogen atmosphere

Compacts were placed in an alumina crucible fitting over the end of a thermocouple sheath which was pushed slowly into a vertical molybdenum wound furnace. The molybdenum winding was protected from oxidation by passing a nitrogen-hydrogen gas mixture over it. Nitrogen gas was passed through a purification train as illustrated in Figure IV.4 and then through the reaction tube at 135$cm^3 min^{-1}$. The operating temperature (maximum 1680°C) was measured by a Pt-Pt-13%Rh thermocouple.

IV.6 X-ray techniques

X-ray investigation was carried out using powder methods because the products obtained were always microcrystalline. Phase identification and unit-cell dimensions were obtained from diffraction patterns using a Hägg-Guinier focussing camera with monochromatic Cu $K\alpha_1$ radiation. Potassium chloride was used as an internal

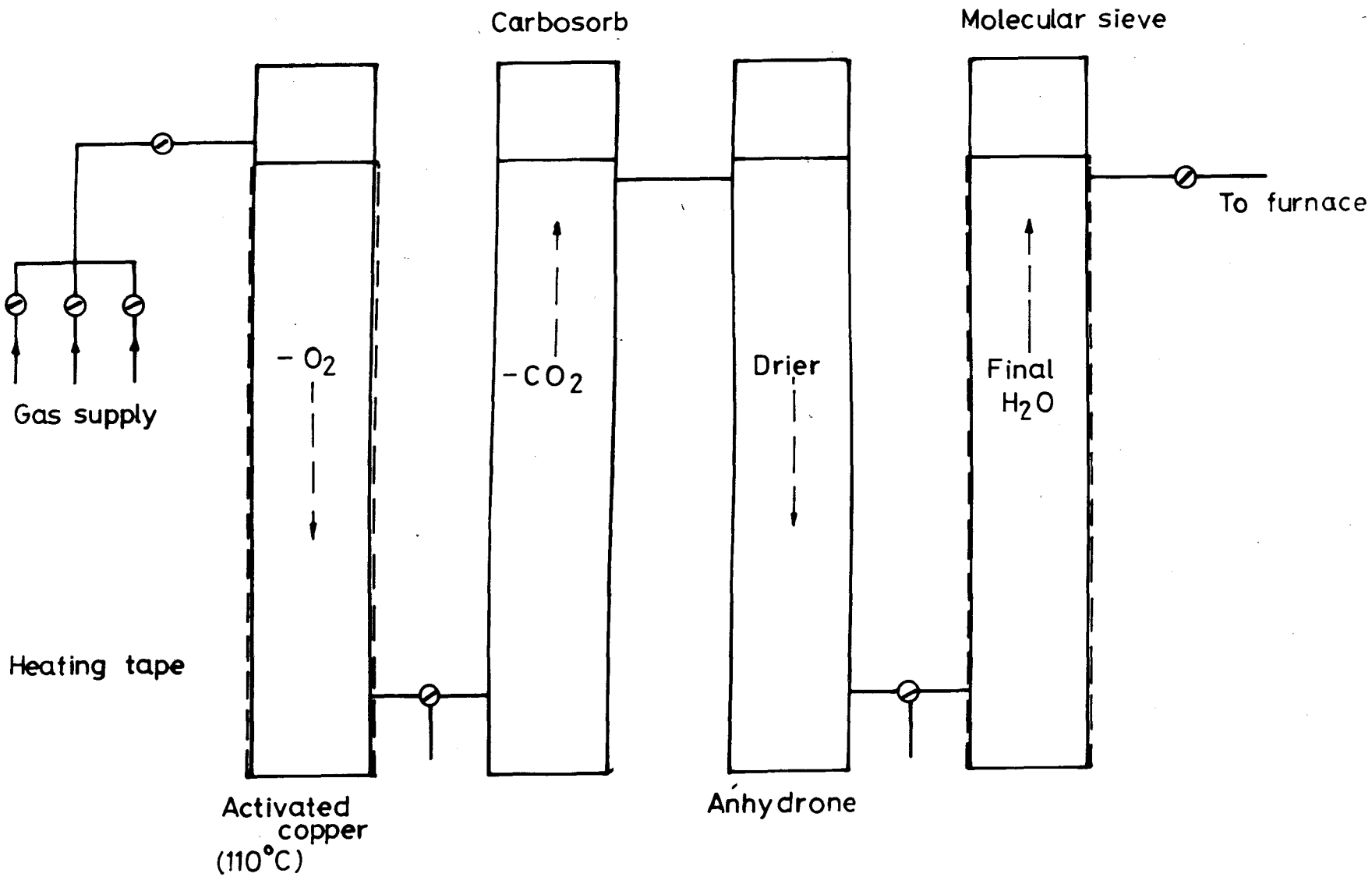

Figure IV.4 Gas Purification Train

standard. Accurate lattice parameter determinations were obtained from Unicam 19cm X-ray photographs taken with Fe Kα radiation with a LiF monochromator. The positions of the X-ray reflextions were measured with a vernier scale (Hilger & Watts Ltd.).

The intensities of reflexions were measured on a manual direct-reading X-ray microdensitometer designed by Taylor (1951) which compares the density of powder lines on a film against a linear optical wedge. The intensity profiles of the reflexions were plotted as large scale graphs and the areas under the curves were planimetered. For structure determination two sets of photographs were used: the intensities of each film were scaled and their mean values were taken as the "observed intensities".

IV.7 Structure determination

Having measured the intensity, observed structure amplitudes (F^{obs}_{hkl}) for overlapped reflexions were calculated using the formula

$$F^{obs}_{hkl} = \sqrt{\frac{I_{obs}}{I_{calc}}} \cdot \left| F^{calc}_{hkl} \right|$$

where F^{calc}_{hkl} = calculated structure amplitude for plane hkl

and $I_{calc} = \sum_{m} \left| F^{calc}_{hkl} \right|^2$

(summation of all overlapped reflexions in the particular I_{obs})

in which m = multiplicity of reflecting planes

This equation was applied by computer program to all overlapped reflexions in each I_{obs} in order to obtain a list of F^{obs} values.

Structure refinement was carried out using the SHELL-X computer programs (Sheldrick, 1975) modified to run on the Newcastle University IBM370 computer by Dr. W. Clegg in the Department of Inorganic Chemistry, University of Newcastle on Tyne. The program calculated structure factors from input coordinates, indices and scattering factors and then carried out least squares refinement on the F_{obs} and F_{calc} values. The program had the following advantages:

(1) It is often convenient to tie together various parameters in a refinement. Thus if a particular atomic site consists of Al_xSi_{1-x} (say), it is desirable to refine only one occupation factor (x) rather than both x and $1-x$. Using "free-variables" this program enables parameters, occupation number and temperature factor constraints to be included in the refinement.

(2) Three cycles of least squares refinement using

100 planes can be done in 3-4 seconds

(3) Fourier maps can be obtained as part of the same output

(4) Accurate scattering factors are used taking into account anomalous dispersion effects.

IV.8 Thermal expansion

Coefficients of thermal expansion were determined by X-ray methods using a 19cm Unicam S150 high-temperature Debye-Scherrer camera and Cu Kα radiation from a graphite monochrometer. The unit-cell dimensions were measured at approximately 200° intervals in the range 20-1000°C.

IV.9 Density and porosity

Bulk density, material density and apparent porosity were determined by the water displacement method. Discs were boiled in pure water for 2 hours, left to cool and weighed suspended in water (w_2). The excess surface water was removed using blotting paper and the sample re-weighed (w_3). Then the samples were dried in an air oven at 110°C for 24 hours and weighed again after cooling in a desiccator (w_1). Density and porosity were then calculated:

$$\text{Bulk density} = \frac{w_1}{w_3 - w_2}$$

$$\text{Material density} = \frac{w_1}{w_1 - w_2}$$

$$\% \text{ Apparent porosity} = \frac{w_3 - w_1}{w_3 - w_2} \times 100$$

For accurate density determinations, the flotation method was used (Knight, 1945). A "clean" hot-pressed sample was crushed and sieved to -300 mesh, the powder was added to methylene iodide of density 3.325g cm^{-3}, and floated on top. Toluene was added dropwise from a burette to the methylene iodide solution and stirred. Finally a mixture was achieved in which the powder remained suspended for about twenty four hours at a constant temperature. This solution was then filtered and the density determined.

Theoretical density was determined from the formula:

$$\text{Density} = \frac{M}{N_o . V}$$

where M is the molecular weight of total formula units in the unit-cell,

N_o is the Avogadro's number and

V is the unit-cell volume determined from unit-cell dimensions.

V. The Representation of the Mg-Si-Al-O-N System

To discuss the phase relationships in the Mg-Si-Al-O-N system a three-dimensional representation is necessary. If Si, Al, O and N are represented by the vertices of a regular tetrahedron (Figure V.1) any point within the tetrahedron is the equivalent of one atom of composition $Si_aAl_bO_cN_{1-(a+b+c)}$ but if in any phase the combining elements have their accepted valencies Si^{IV}, Al^{III}, O^{II} and N^{III}, one degree of freedom is lost and it is easily shown that the composition is given by $Si_a\ Al_b\ O_{3-7a-6b}\ N_{6a+5b-2}$. The system is then a pseudo-ternary one. If the tetrahedron of Figure V.1 is described in terms of three orthogonal axes x, y and z with corners:

oxygen at co-ordinates	0, 0, 0
silicon at	1, 0, 1
aluminium at	0, 1, 1
and nitrogen at	1, 1, 0

the compositions of all solid phases then lie on the irregular quadrilateral plane $(01\bar{6})$ shown in Figure V.2 the corners of which represent $(1/7)Si_3N_4$, $(1/2)AlN$, $(1/5)Al_2O_3$ and $(1/3)SiO_2$. The simplest representation is obtained by expressing concentrations in equivalents and just as in a reciprocal salt pair (see Zernike, 1955),

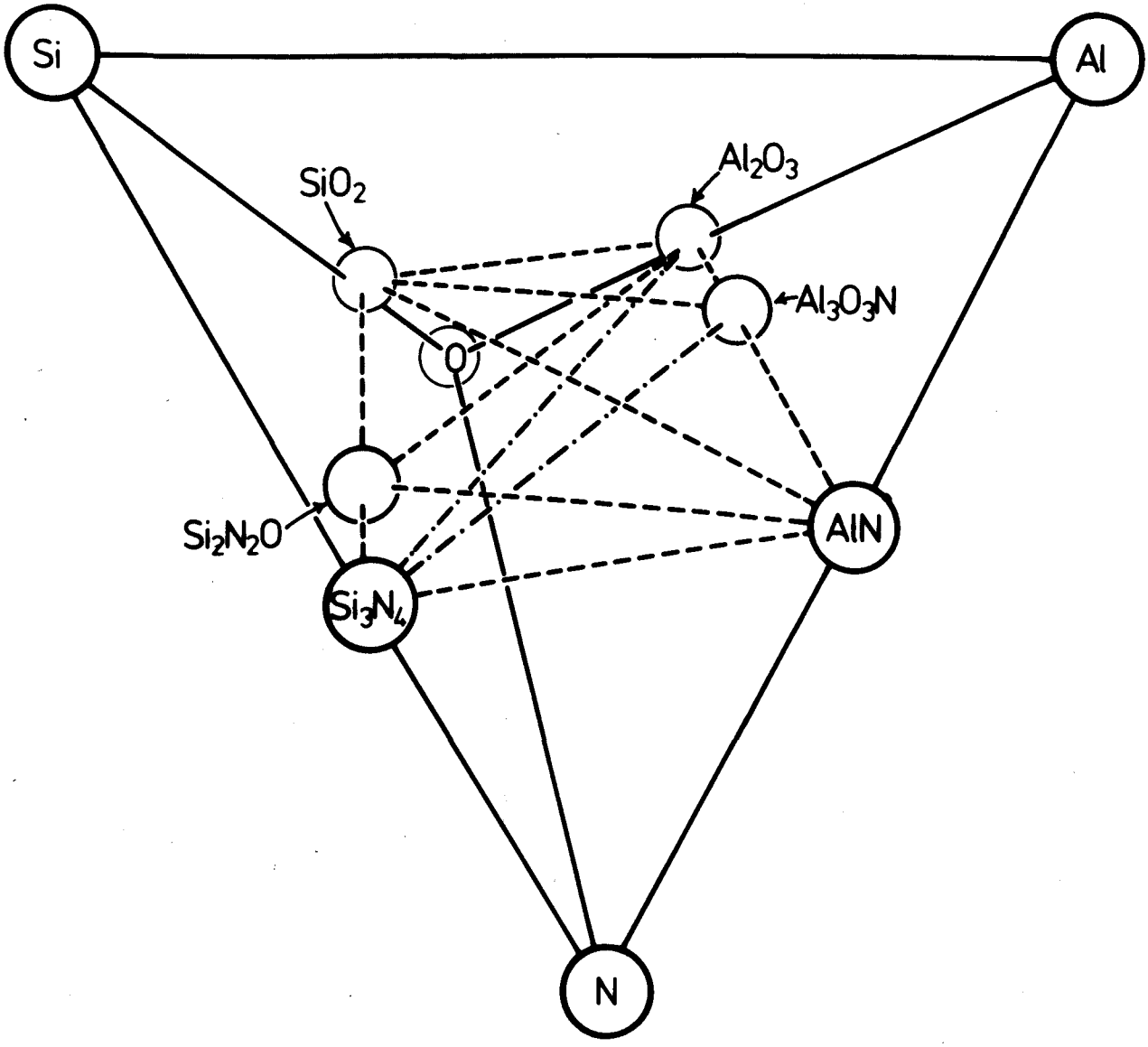

Figure V.1 The tetrahedral representation of the Si-Al-O-N system

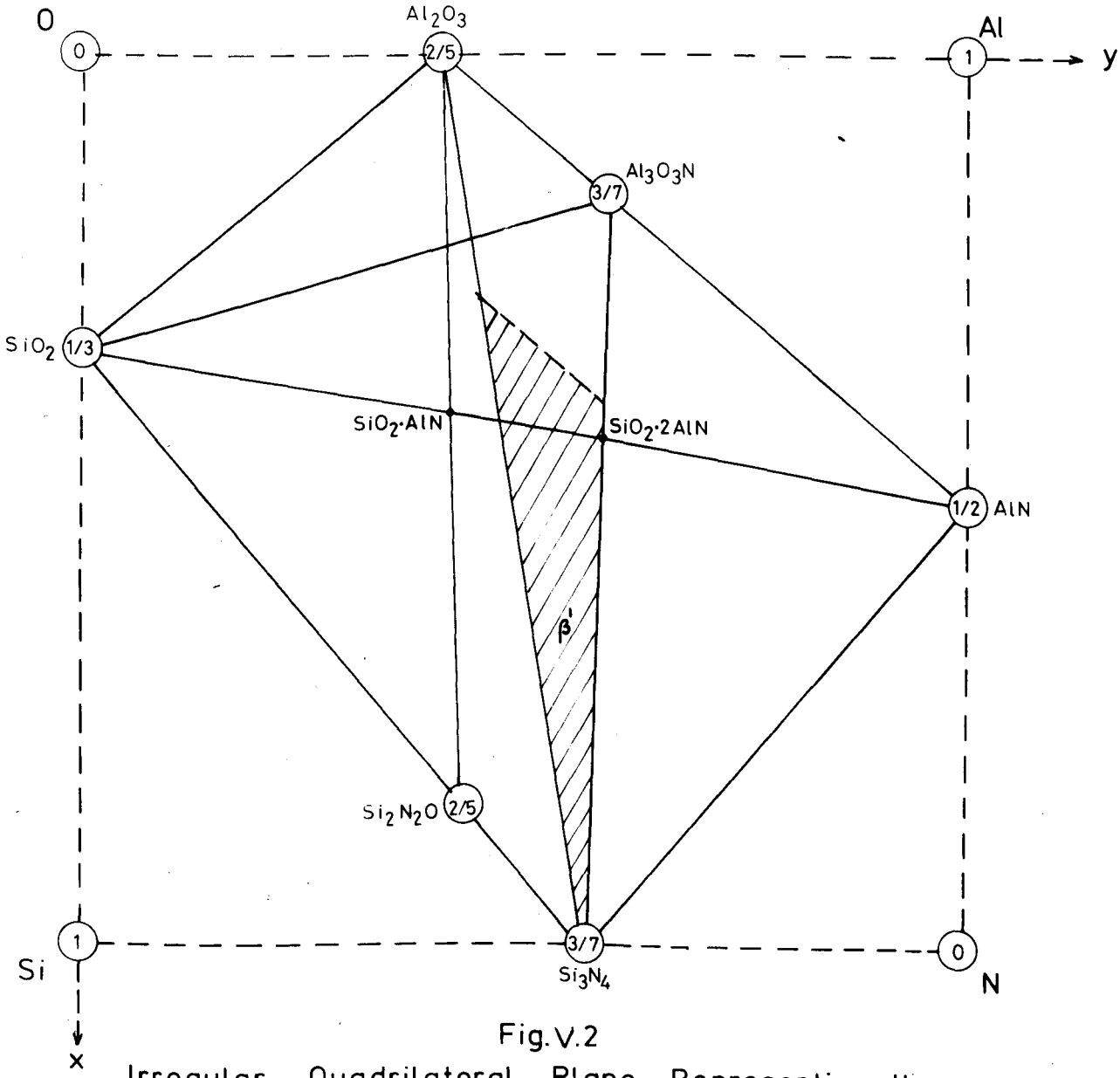

Fig. V.2

Irregular Quadrilateral Plane Representing the $Si_3N_4 - AlN - Al_2O_3 - SiO_2$ System.

(Figures within circles are heights above the plane of the paper along the cube axis z.)

the composition of any mixture can be characterized by two quantities

$$\frac{3(Al)}{4(Si) + 3(Al)} \quad \text{and} \quad \frac{2(O)}{3(N) + 2(O)}$$

When these ratios are plotted perpendicular to each other a square is obtained; see Figure V.3. It is convenient to let the bottom left-hand corner of the square represent one mole of Si_3N_4; the other three corners then represent Al_4N_4, Al_4O_6 and Si_3O_6. It should be noted that all possible phases or mixtures of phases in which the combining elements Si, Al, O and N have their normal valencies lie within this diagram. It is the same as the irregular quadrilateral plane of Figure V.1 except that concentrations are expressed in equivalents instead of atomic units. Any point in the square of Figure V.3 is a combination of 12+ve and 12-ve valencies, i.e. it is convenient to regard compounds in ionic terms even though the interatomic bonding is predominantly covalent. In going from the left-hand to the right-hand side of the diagram, $3Si^{4+}$ is replaced by $4Al^{3+}$; and from bottom to top, $4N^{3-}$ is replaced by $6O^{2-}$. The centre of the square represents a composition $Si_{1.5}Al_2O_3N_2$; note that the number of atoms changes with change in position but the number of equivalents remains constant. Because of the constant 12+:12- "composition" it is often convenient

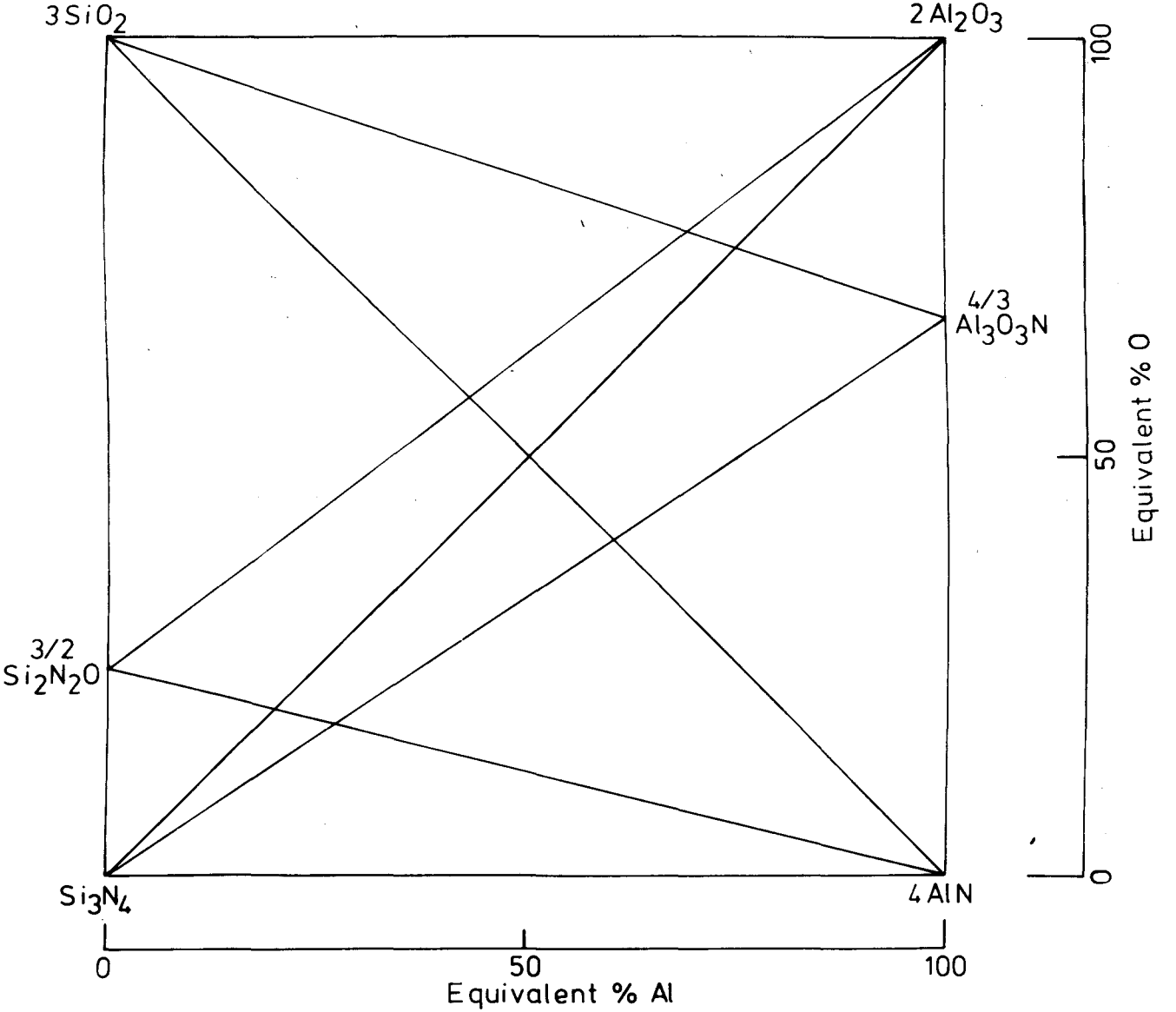

Fig. V.3

The Square Representation of the Si–Al–O–N System using Equivalent Concentrations

to scale the sides of the square 0-12 ; each unit is then one valency.

In the Mg-Si-Al-O-N system it is unlikely that any solid phases, vitreous or crystalline, contain atoms of variable valency and is what Zernicke (1955) describes as a "quaternary system of the third kind". This is represented by Jäneck's (1907) triangular prism in which all edges are equal. Figure V.4(a) outlines this representation for magnesium-sialon system; it is based on the standard Si_3N_4 - Al_4N_4 - Al_4O_6 - Si_3O_6 square with Mg in equivalent units along a third dimension. The front triangular face of the prism represents nitrides and the rear face oxides. Any composition in this prism may be projected onto the base plane and onto a triangular end plane simultaneously. From the square plane the relative concentrations of O and N can be read, and from the triangular projection the Mg, Si and Al contents can be read (Figure V.4(b).

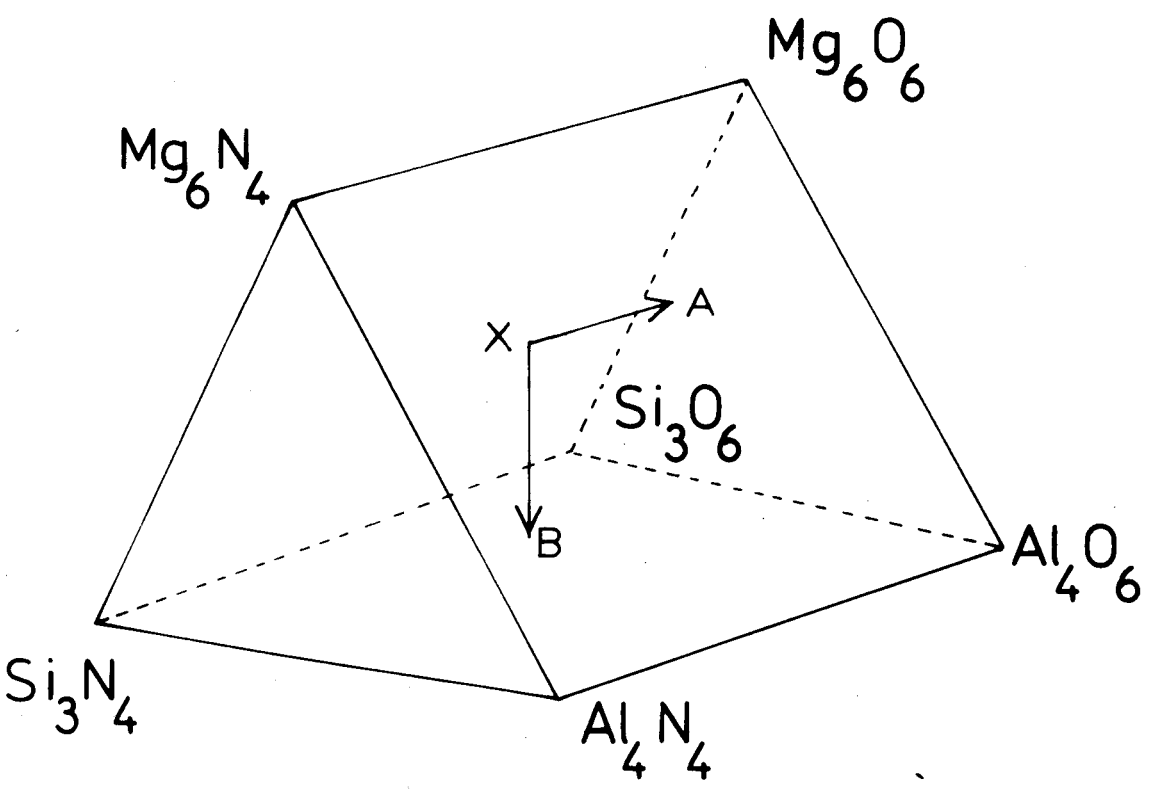

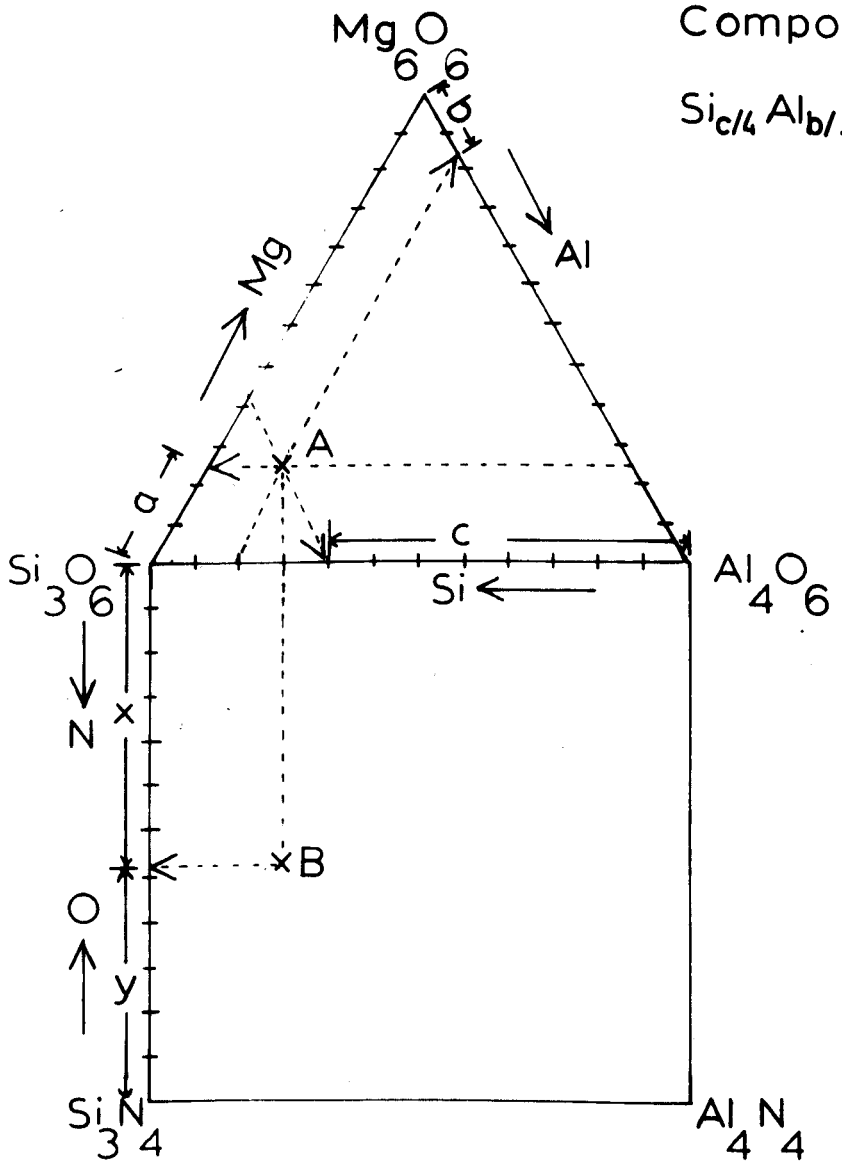

Composition X :

$Si_{c/4}Al_{b/3}Mg_{a/3}O_{y/2}N_{x/3}$

Figure V.4(a) The magnesium sialon representation
(b) Composition X projected to a square plane and a triangle

VI. Quasi-Ternary Systems in the Mg-Si-Al-O-N System

VI.1 Introduction

The Si-Al-O-N has previously been investigated and is discussed in Chapter II. The other two quasi-ternary systems Mg-Al-O-N and Mg-Si-O-N have not been investigated before the present work. These are represented by the squares $2Mg_3N_2 - 6MgO - 2Al_2O_3 - 4AlN$ and $6MgO - 2Mg_3N_2 - Si_3N_4 - 3SiO_2$. The end members are readily available raw materials and compositions inside the squares can be formulated by taking any three appropriate end members.

The binary joins $MgO-Al_2O_3$, Al_2O_3-AlN, $MgO-SiO_2$ of these quasi-ternary systems have been extensively investigated and are discussed in the literature, while $Mg_3N_2-Si_3N_4$ and $SiO_2-Si_3N_4$ are only reported briefly.

The $MgO-Al_2O_3$ binary system has been investigated by Roy, Roy & Osborn (1953) and Alper et al (1962); its phase equilibrium diagram is given in Figure VI.1. The homogeneity range of the single phase spinel solid solution at 1800°C is from 53-75 m/o Al_2O_3, with the upper limit in equilibrium with corundum.

The Al_2O_3-AlN join has been investigated by Lejus (1967) and the phase equilibrium diagram is given in Figure VI.2. The single phase nitrogen-containing

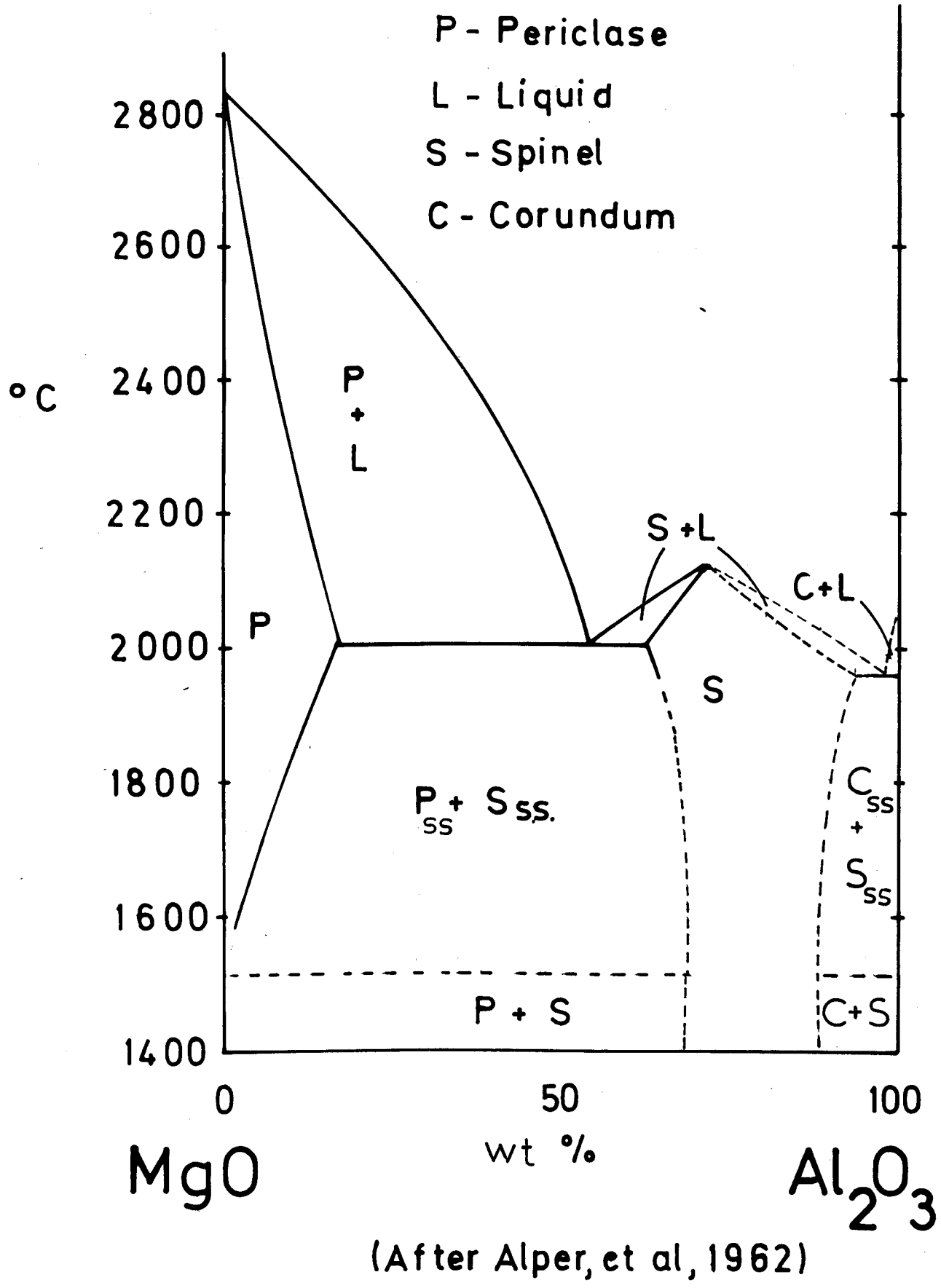

Figure VI.1 The $MgO-Al_2O_3$ system

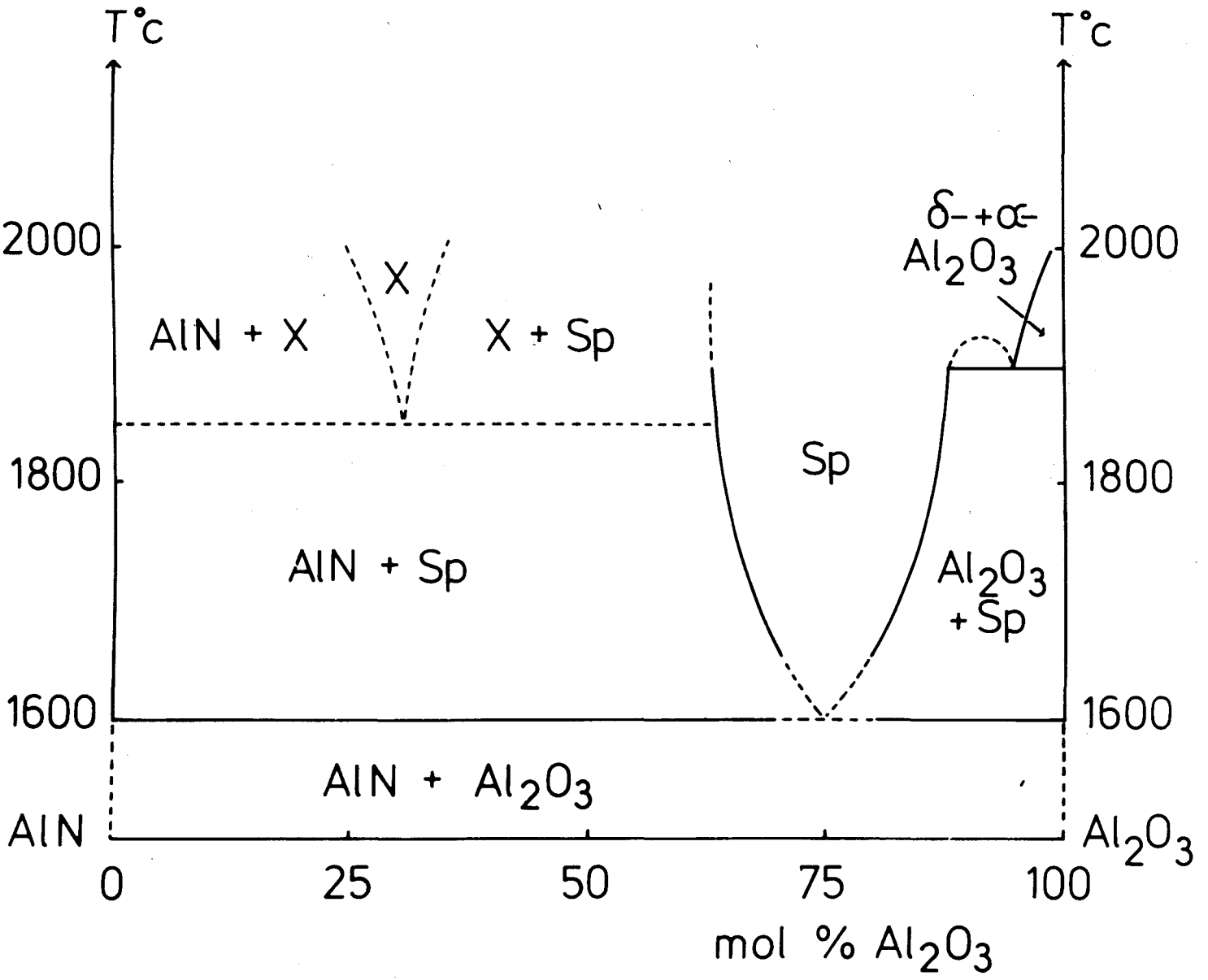

Figure VI.2 The Al_2O_3-AlN system (after Lejus, 1967)

spinel extends from 16 to 33 m/o AlN at 1800°C and its range of homogeneity may be expressed as $Al_{\frac{8+x}{3}} \square_{\frac{1-x}{3}} O_{4-x} N_x$ where x, the number of nitrogen atoms replacing oxygen in a total of four non-metals, varies from x=0.22 to 0.57. When x=1, the composition Al_3O_3N corresponds to a spinel without metal or non-metal atom vacancies and when x=0, the composition $Al_{8/3} \square_{1/3} O_4$ represents the spinel, γ-Al_2O_3.

The MgO-SiO_2 system has been investigated by Bowen & Anderson (1914) and Greig (1927) and the phase equilibrium diagram is given in Figure VI.3. Any liquid composition in this does not produce a glass.

A limited investigation of the Mg_3N_2-Si_3N_4 system has been carried out by David & Lang (1965) who reacted mixtures of Si_3N_4 and Mg_3N_2 at 1200°C under N_2 from x=0.25 to x=2 where x is the molar ratio Si_3N_4/Mg_3N_2; they obtained $MgSiN_2$ over a homogeneity range extending from x=0.6 to 1.22.

VI.2 Homogeneous spinel phase-field

The range of spinel formation between the joins MgO-Al_2O_3 and Al_2O_3-AlN was investigated in the present work by hot-pressing the compositions within the triangle MgO-Al_2O_3-AlN. MgO was added to pre-prepared spinel of composition $3Al_2O_3$.AlN and hot pressed at

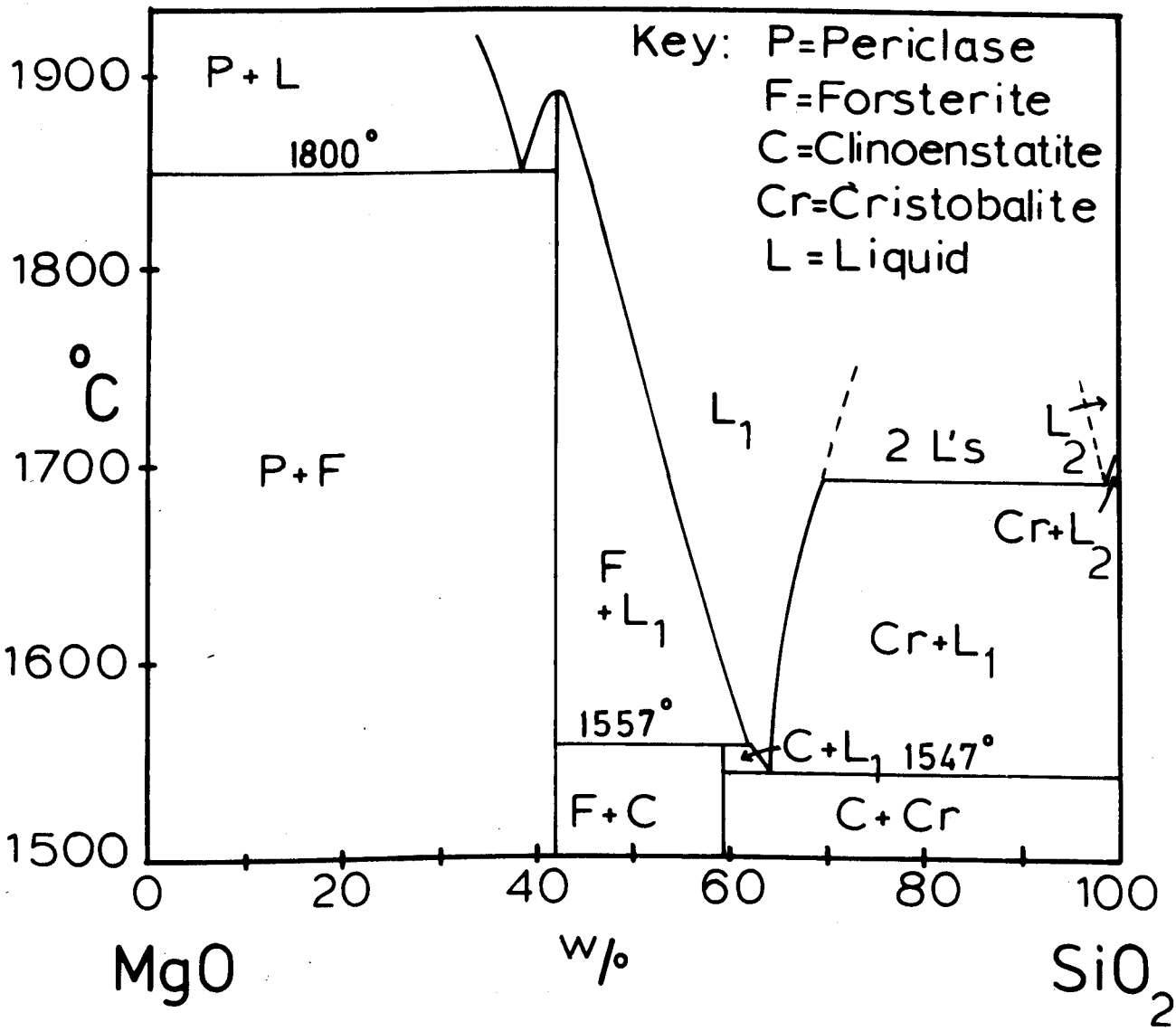

Figure VI.3 The MgO-SiO_2 system
(after Grieg, 1927)

1800°C as described in Chapter IV. AlN was also added to pre-prepared $MgAl_2O_4$ and similarly hot pressed. Other compositions were made from the end members. All hot-pressed compositions are shown in Figure VI.4; weight losses on pressing were less than 1w/o.

The spinel-producing compositions have been reproduced by starting with different raw materials to produce the same fired composition. The material density and the unit-cell dimension of these spinels are listed in Table VI.1 from which it is seen that irrespective of the method of production the material density and unit-cell dimension agree within experimental error.

The variation of unit-cell dimension and density with composition for Mg-Al-O-N spinel and Mg-Al-O spinel are compared in Table VI.2 and the variation of unit-cell dimension ($\underline{a}$) and density (ρ) with M:X atom-ratio is plotted in Figure VI.5. The smooth variation shows a discontinuity above the ratio 3:4 and a comparison of material density with X-ray density is consistent with vacancies in non-metal atom sites rather than with a structure containing excess interstitial metal atoms for M:X $>$ 3:4. Thus at M:X $<$ 3:4 the spinels have vacant metal sites and at $>$ 3:4 they have vacant non-metal sites. This is not unexpected because there are numerous examples in the literature of oxide and sulphide structures showing a

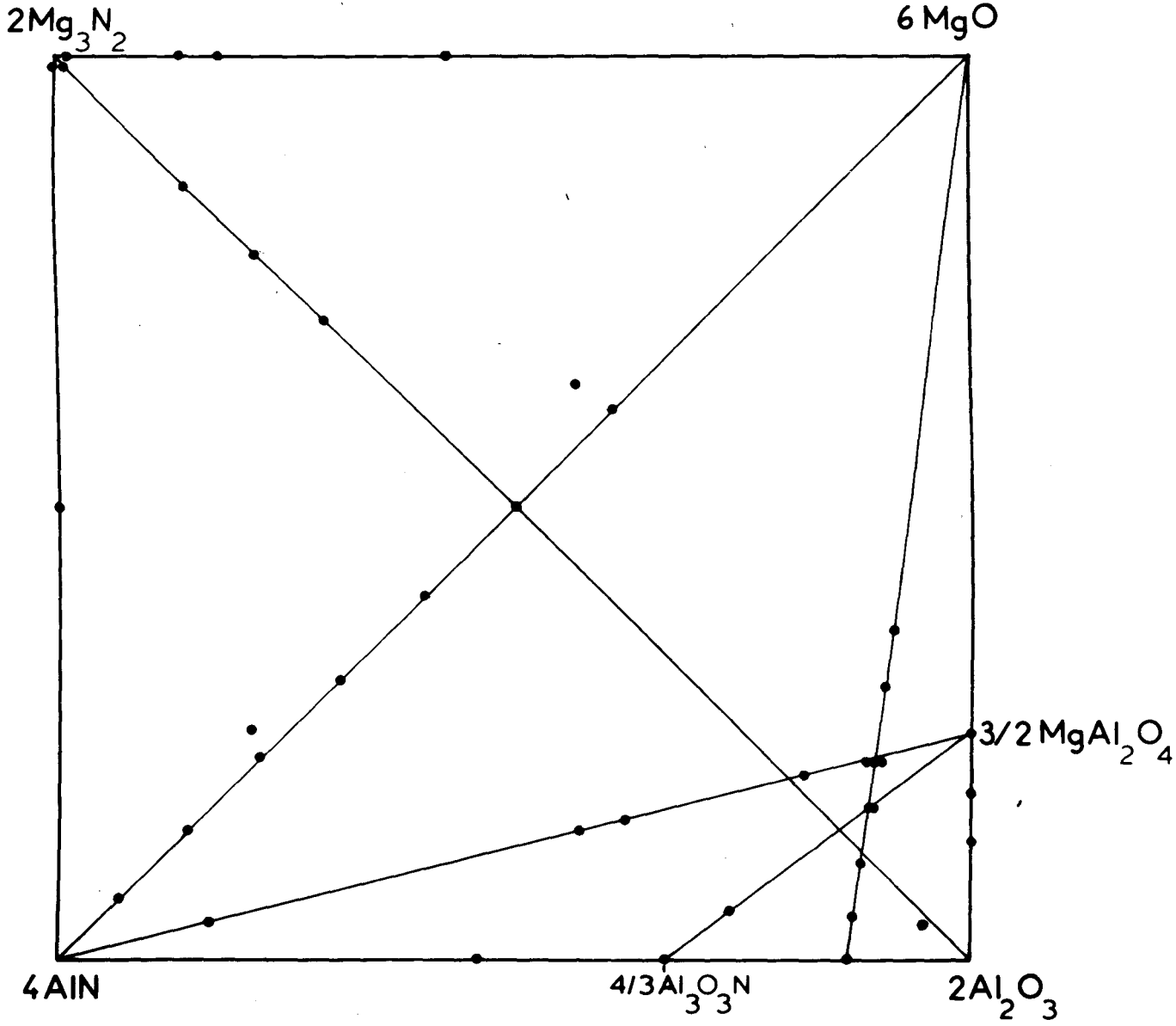

Figure VI.4 Hot-pressed compositions in the $MgO-Al_2O_3-AlN-Mg_3N_2$ system

Table VI.1 Different Mg-Al-O-N spinel producing routes

specimen no.	components	conditions of preparation	material density $g\ cm^{-3}$	unit-cell dimension Å	N-spinel composition
1.	MgO, Al_2O_3, AlN	dry mixed, 1800°C, 1h H.P.	3.59	8.054	$Al_3O_3N.2MgAl_2O_4$ (X-ray density av. 3.62)
2.	MgO, Al_2O_3, AlN	wet mixed, 1800°C, 1h H.P.	3.59	8.054	
3.	$MgO, 3Al_2O_3, AlN(\delta)$	dry mixed, 1800°C, 1h H.P.	3.61	8.053	
4.	MgO, Al_2O_3, AlN	dry mixed 1800°C, 1h H.P.	3.53	8.076	$Al_3O_3N.2MgAl_2O_4.MgO$ (X-ray density av. 3.54)
5.	MgO, Al_2O_3, AlN	wet mixed, 1800°C, 1h H.P.	3.53	8.077	
6.	$MgO, 3Al_2O_3, AlN(\delta)$	dry mixed 1800°C, 1h H.P.	3.53	8.076	
7.	$AlN, MgAl_2O_4$	dry mixed, 1800°C, 1h H.P.	3.51	8.072	

Table VI.2 Variation of unit-cell dimension and density for spinels

composition	X-ray density g. cm^{-3}	material density g. cm^{-3}	a_0 Å	M:X atom-ratio
$\square_{0.21}Al_{2.79}O_{3.63}N_{0.37}$	3.689	3.669	7.934	0.698
$\square_{0.14}Al_{2.66}Mg_{0.20}O_{3.62}N_{0.38}$	3.680	3.672	7.960	0.715
$\square_{0.07}Al_{2.49}Mg_{0.44}O_{3.64}N_{0.36}$	3.655	3.642	8.000	0.733
$Al_{2.31}Mg_{0.69}O_{3.69}N_{0.31}$	3.621	3.607	8.054	0.750
$Al_{2.09}Mg_{0.91}O_{3.63}N_{0.28}\square_{0.09}$	3.541	3.528	8.077	0.767
$Al_{2.14}Mg_{0.93}O_{3.71}N_{0.29}$	3.623			
$\square_{0.16}Al_{2.32}Mg_{0.52}O_4$	3.609	3.580	8.002	0.710
$\square_{0.09}Al_{2.18}Mg_{0.73}O_4$	3.597	3.493	8.036	0.728
Al_2MgO_4	3.582	3.543	8.081	0.750
$Al_{1.86}Mg_{1.14}O_{3.93}\square_{0.07}$	3.532	3.521	8.082	0.763
$Al_{1.89}Mg_{1.16}O_4$	3.602			

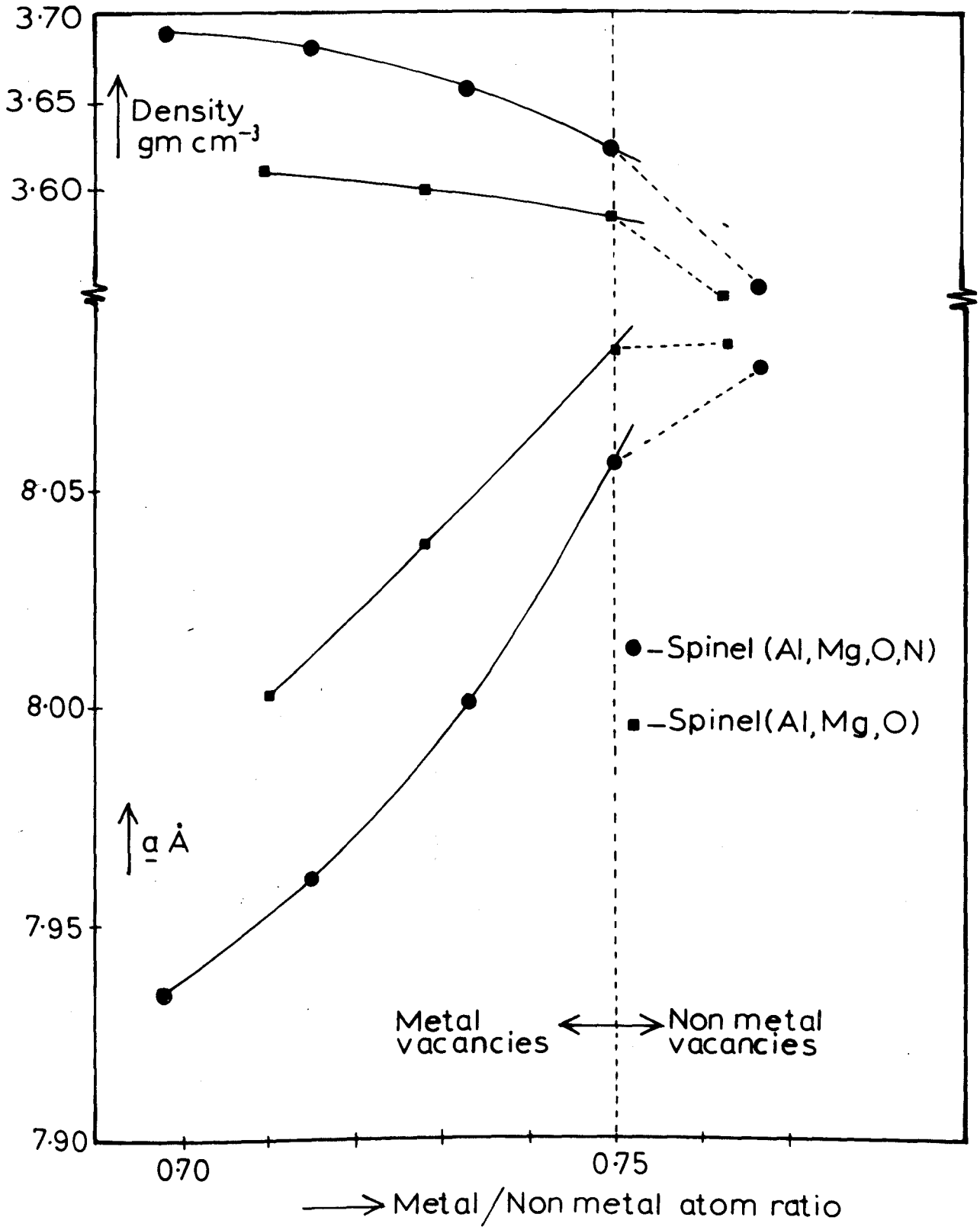

Figure VI.5 Variation of density and unit-cell dimension with metal:non:metal atom radio for spinels

smooth transition from cation vacancies to anion vacancies with composition (Greenwood, 1968).

VI.3 Properties of Mg-Al-O-N spinel

Magnesium aluminium spinel is a useful ceramic material in that it is a good low-loss insulating material (Smoke, 1954; Keer et al, 1974) and has good resistance to basic slags and coal ash (Singer & Singer, 1963). It can be fabricated in translucent shapes by adding 0.25-1^{w}/o CaO (Bratton, 1974) and, like other transluscent oxides, is potentially useful for such engineering applications as arc-enclosing envelopes at very high temperatures, alkali-metal vapour discharge devices and antenna windows.

The spinel of composition $Al_3O_3N.2MgAl_2O_4$ (specimen 1, Table VI.1) was investigated briefly. It had vickers hardness of 1510 using a 5kg load and survived 15 cycles of rapid heating and cooling from 1000°C to 20°C. The coefficient of thermal expansion for Mg-Al-O-N spinels deduced from X-ray methods in the range 20-1000°C is given below and the variation of unit-cell dimension $\underline{a}$ with temperature plotted in Figure VI.6.

$Al_3O_3N.2MgAl_2O_4$: $= 7.0 \times 10^{-6}\ ^{o}C^{-1}$

$Al_3O_3N.2MgAl_2O_4.MgO$: $= 7.6 \times 10^{-6}\ ^{o}C^{-1}$

(specimen 4, Table VI.1)

$MgAl_2O_4$: $= 8.8 \times 10^{-6}\ ^{o}C^{-1}$ (Bayer, 1973).

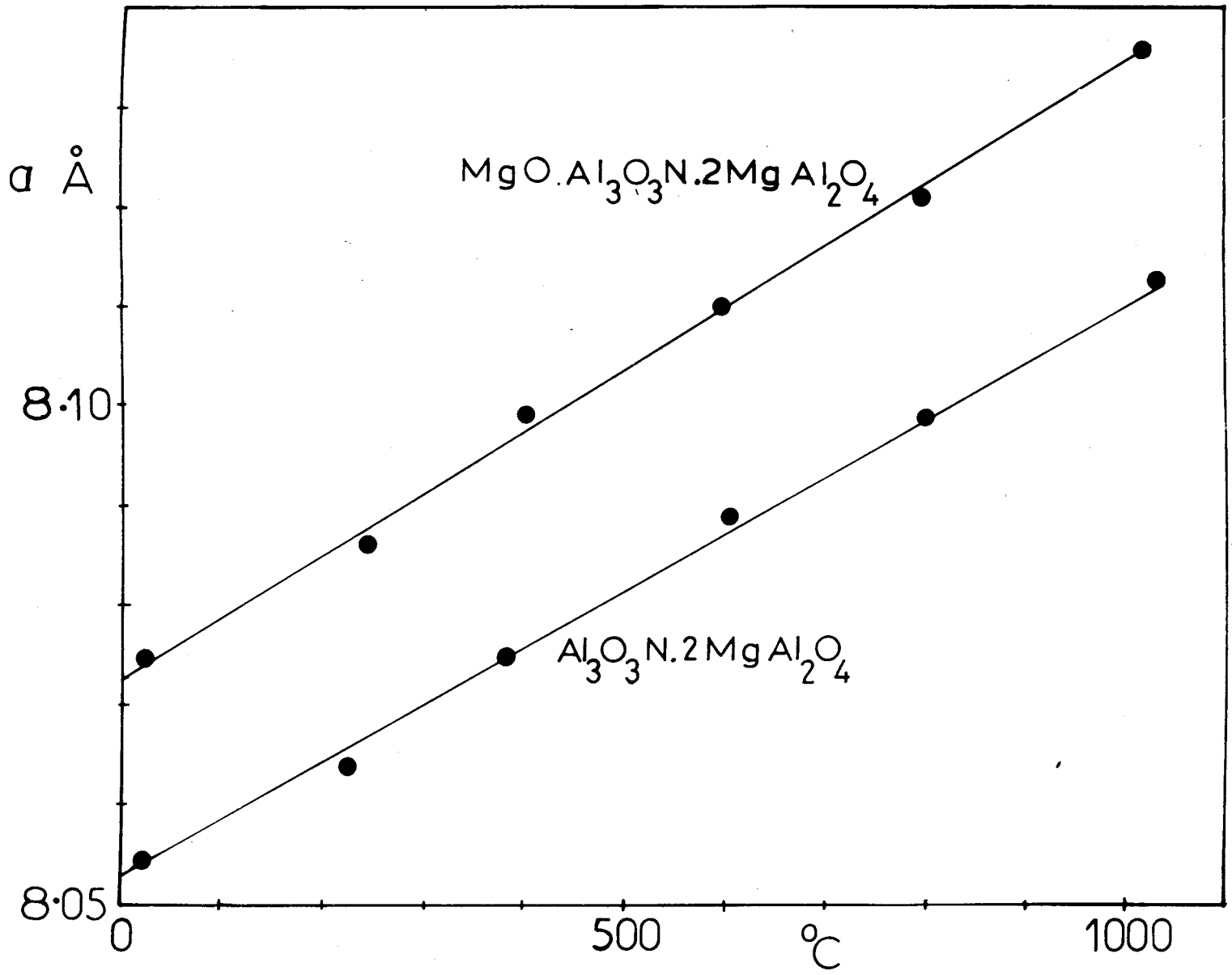

Figure VI.6 Variation of unit-cell dimension with temperature for Mg-Al-O-N spinel

The coefficient of expansion for Mg-Al-O-N spinels is lower than for $MgAl_2O_4$.

This brief investigation suggests the possibility, that Mg-Al-O-N spinel may have better ceramic properties than $MgAl_2O_4$ and needs detail examination.

VI.4 Phase relationships in the Mg-Al-O-N system

The diagram in Figure VI.7 has been constructed from the results of hot-pressing mixtures of MgO, AlN and Al_2O_3 at 1800°C for one hour. It is not an equilibrium phase diagram but an idealised behaviour diagram. The phase designated as R has a $2H^S$ structure (i.e. AlN type isotropically expanded along c, Ramsdell symbol used, see Chapter IX) according to its unit-cell dimensions, but its X-ray reflexions are broad suggesting a range of homogeneity. In all preparations involving magnesium and nitrogen at high temperatures, Mg_3N_2 is lost by volatilisation and the fired composition is shifted from the starting composition in a direction away from Mg_3N_2. Any initial composition between AlN and MgO therefore reduces its final M:X ratio from the original 1:1 .

The maximum amount of 21R phase was observed along the AlN-Al_2O_3 join at a composition corresponding to 7M:8X . This is an AlN polytype phase and probably accommodates only a small concentration of magnesium. It was also observed when the composition which gave R

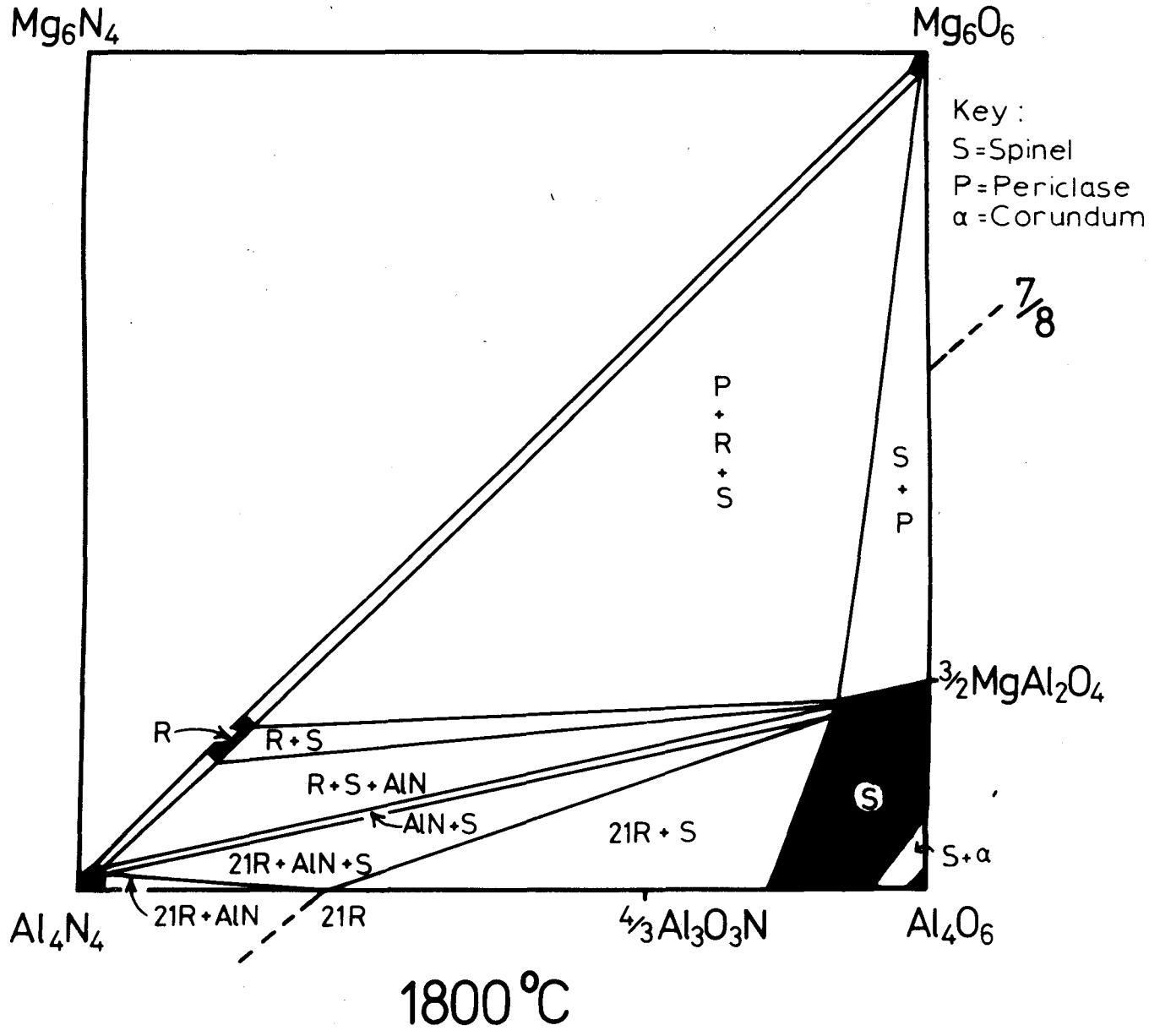

Figure VI.7 The $MgO-Al_2O_3-AlN-Mg_3N_2$ behaviour diagram

phase was hot pressed at 1950°C; clearly this is due to the volatilisation of Mg_3N_2 at the high temperature. Crystallographic data for these phases are given in Chapter IX.

Any composition in the $2Mg_3N_2$ - 6MgO - 4AlN triangle hot-pressed between 1400-1800°C gives a mixture of AlN and MgO with a weight loss. For example if Mg_3N_2 and Al_2O_3 are reacted together the product is AlN and MgO according to the equation:

$$Mg_3N_2 + Al_2O_3 = 2AlN + 3MgO$$

and any weight loss corresponds to the volatilisation of excess Mg_3N_2. AlN can accommodate some MgO to give a slightly distorted AlN (see Chapter VIII). Reactions between Mg_3N_2 and MgO are discussed later.

VI.5 The use of Mg_3N_2 as a reactant

All compositions with Mg_3N_2 must be mixed in a dry inert atmosphere, because of its rapid hydrolysis in air. Therefore mixtures were made up in an airtight dry-box in a flowing stream of carefully dried nitrogen. Mg_3N_2 hydrolyses to MgO and NH_3 and volatilises above 800°C to Mg vapour and N_2 (Soulen, Sthapitanoda & Margrave, 1955) and so a special study had to be undertaken to estimate the extent of hydrolysis and volatilisation of Mg_3N_2 under hot-pressing conditions; Table VI.3 summarises this experimental work.

Table VI.3 Conversion and volatilisation of Mg_3N_2

No.	conditions (Mg_3N_2 pellets)	weight change w/o	visual estimation of phases from X-ray powder photographs+ %			total MgO estimated w/o
			MgO	Mg_3N_2	6H polytype	
1.	Pellet covered with BN; 4h at 20°C	1.5	6*	94	-	6
2.	H.P. 800°C, 1 min.	0	2	98	-	2
3.	H.P. 800°C, 30 min.	0	2	98	-	2
4.	H.P. 1000°C, 30 min.	2	20	80	-	20
5.	H.P. 1100°C, 30 min.	6	30	70	-	35
6.	H.P. 1200°C, 30 min.	-5	35	65	-	35
7.	H.P. 1200°C, 60 min.	-5	35	65	-	35
8.	H.P. 1300°C, 30 min.	-6	30	50	20	36
9.	H.P. 1400°C, 30 min.	-6	10	-	90	37
10.	H.P. 1450°C, 30 min.	-20	20	-	80	44
11.	30%Mg_3N_2, 70%BN pellet sintered at 1400°C, 30 min.	-5	10	90%BN	-	10
12.	50%Mg_3N_2, 50%BN pellet sintered at 1400°C, 30 min.	-6	20	80%BN		20

+ neglecting any C

* calculated from weight change

Figure VI.8, which plots $^{w}/_{o}Mg_3N_2$ converted to MgO against temperature, shows that the conversion is rapid between 800 and 1200°C after which the reaction slows down at 1200-1450°C. The increase in MgO content cannot be attributed to hydrolysis, as seen from experiment 1 in Table VI.3, because the amount of MgO formed after 4 hours is only 6$^{w}/_{o}$ due to hydrolysis by atmospheric moisture. Therefore the MgO formation must be due to high temperature oxidation of Mg_3N_2 by CO in the die.

Above 800°C Mg_3N_2 dissociates into Mg gas and N_2, and the magnesium reacts with CO which is present in the die at elevated temperatures.

$$Mg_3N_2 + 3CO = 3MgO + 3C + N_2$$

$$\Delta G_{1100°C} = -87 \pm 4 \text{ k cal mol}^{-1}$$

$$\Delta G_{1300°C} = -68 \pm 4 \text{ k cal mol}^{-1}$$

In some runs carbon was observed on X-ray photographs of the products and examination of the pellets indicated that the reaction was initiated at the surface and spread to the centre with increasing time. Above 1400°C the entire pellet had reacted and the 6H phase which forms by reaction between MgO and Mg_3N_2 had started to melt.

The proportions of Mg_3N_2 converted to MgO and volatilised depend on the temperature, the amount of

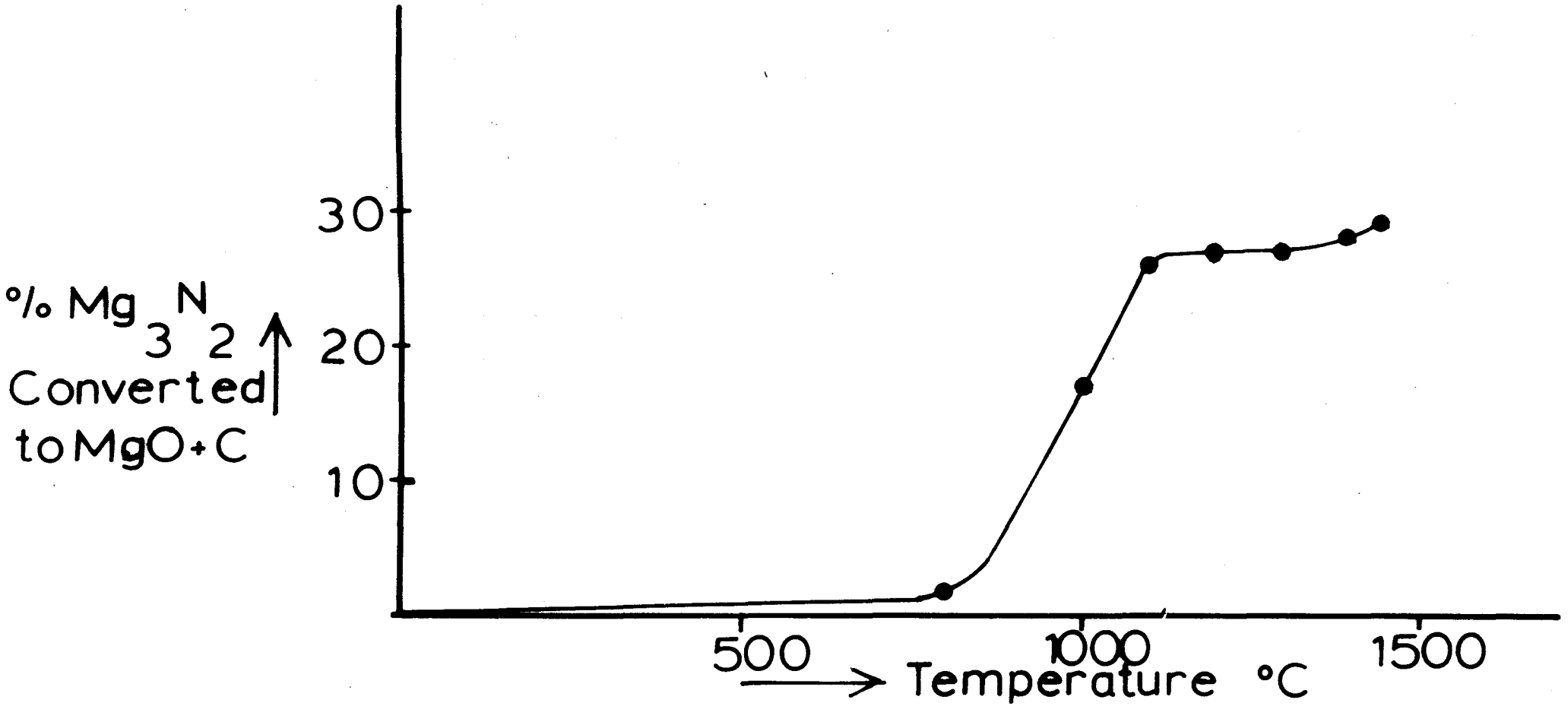

Figure VI.8 The variation of % Mg_3N_2 converted to MgO with temperature

Mg_3N_2 and to a lesser extent on time. From the weight change it is possible to calculate approximately the % conversion to MgO and % volatilisation for a particular temperature. At 1450°C 25^w/o Mg_3N_2 is converted to MgO and 25^w/o is volatilised. Since this depends on the amount of Mg_3N_2 present in the sample (see Table VI.3, experiment numbers 11 and 12) a linear relationship was assumed for this variation; see Figure VI.9. When Mg_3N_2 was used as a starting material, this graph was used to estimate the MgO produced and the extent of volatilisation for the appropriate composition.

VI.6 Phase relationships in the Mg-Si-O-N system

The investigation of phase relationships in this system was in two parts:

(1) compositions made from MgO, SiO_2 and Si_3N_4, hot-pressed or sintered at 1700°C;

(2) compositions made from MgO, Si_3N_4 and Mg_3N_2, hot-pressed at 1400-1550°C.

Figure VI.10 shows the starting compositions and Figure VI.11 has been constructed on the basis of X-ray examination of the products cooled to room temperature over about 4 hours. The isothermal phase equilibrium diagrams at 1700°C and at 1300°C are given for the Mg-Si-O-N system below and above the $MgO-MgSiN_2$ join respectively in Figures VI.12 and VI.13.

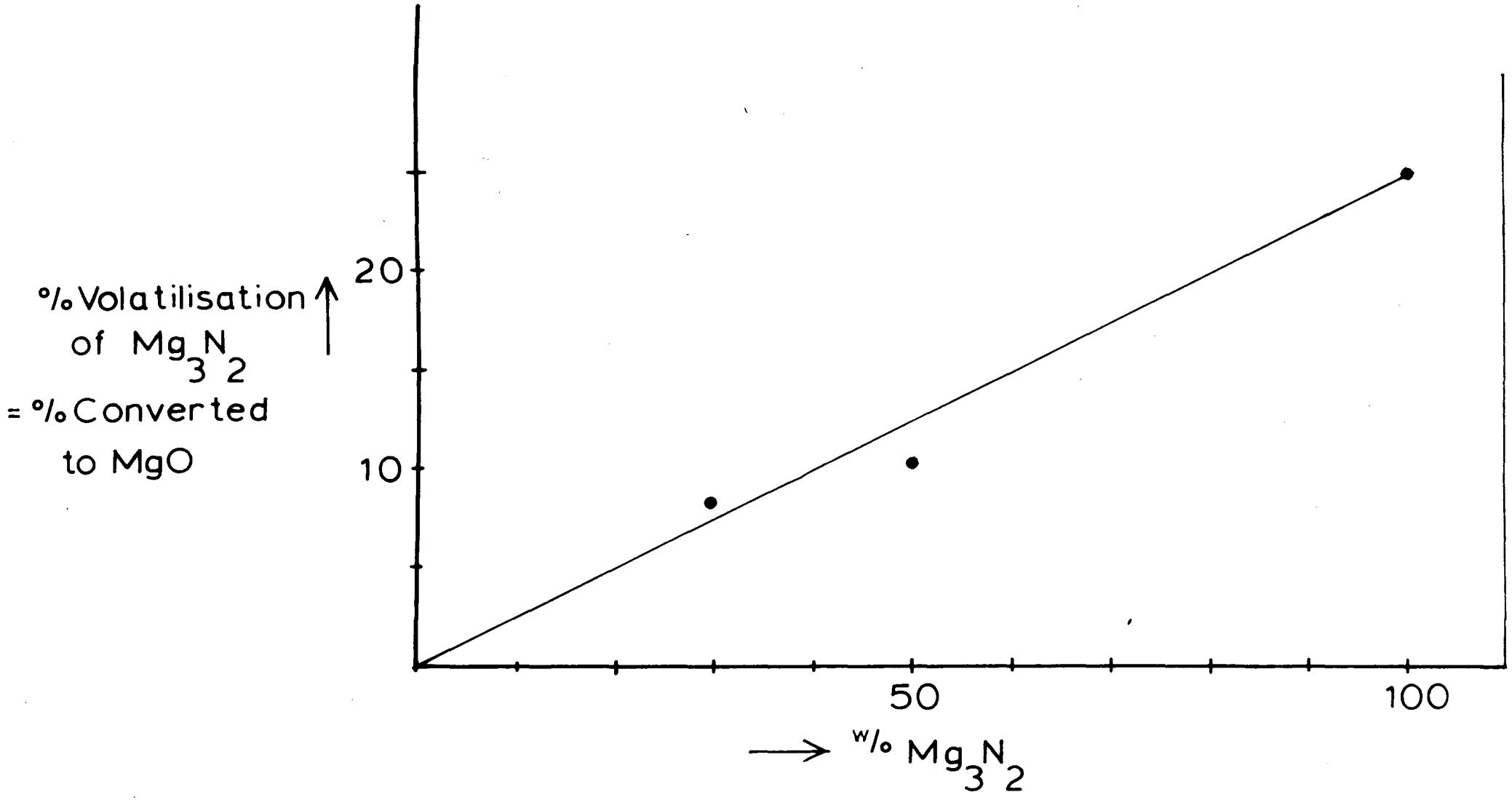

Figure VI.9 The calibration curve for Mg_3N_2

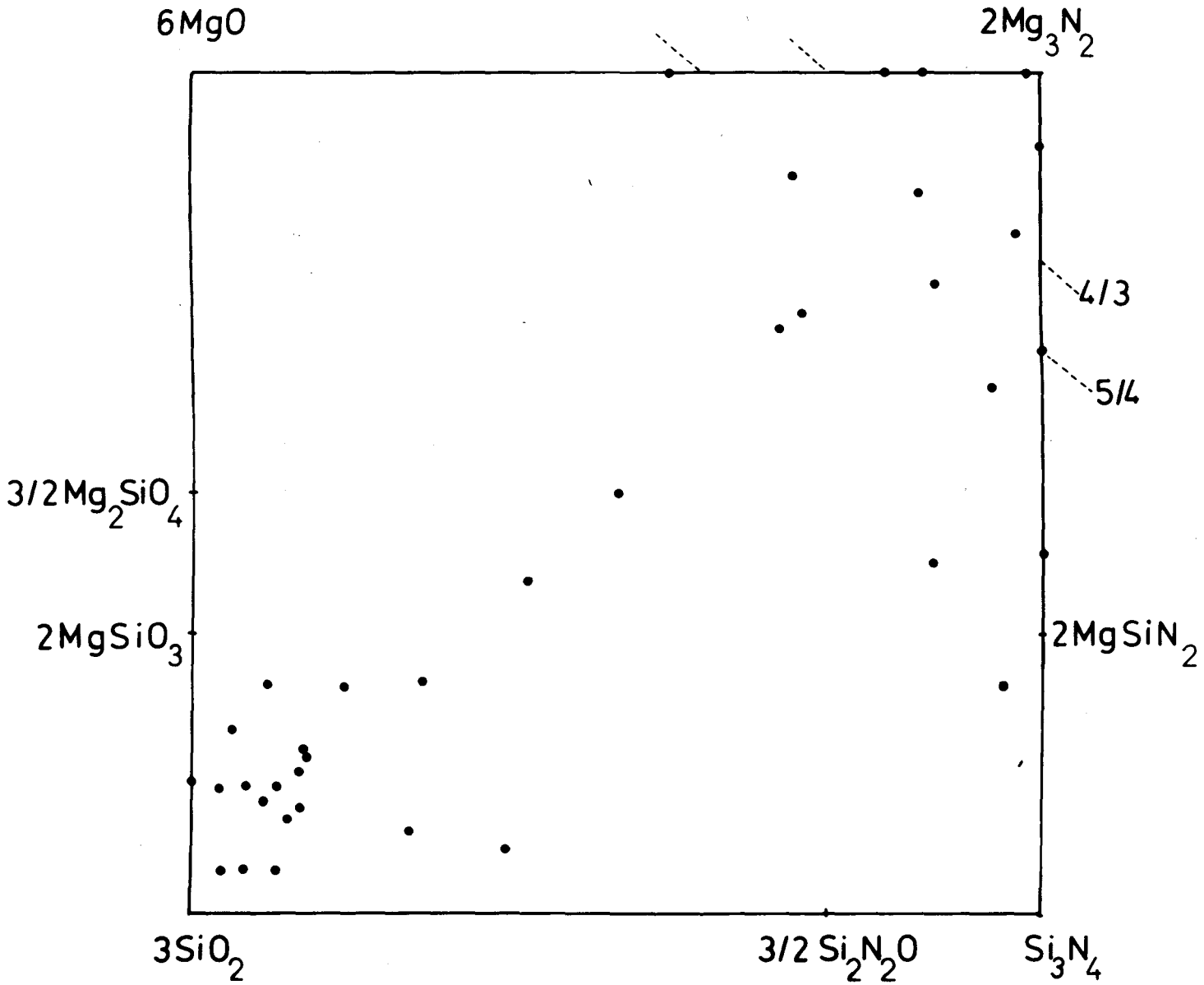

Figure VI.10 Hot-pressed compositions in the $MgO-Mg_3N_2-Si_3N_4-SiO_2$ system

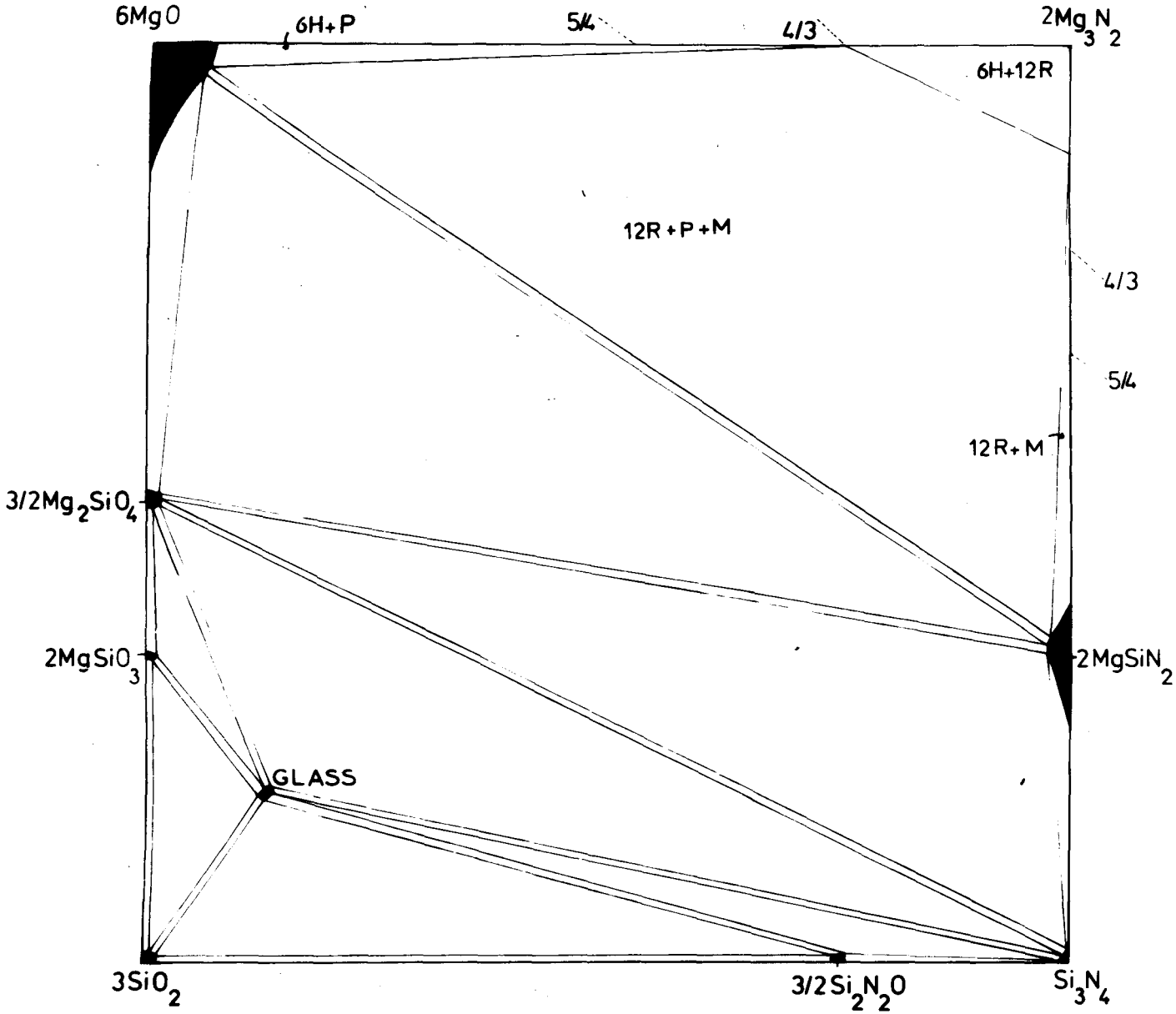

Figure VI.11 The $MgO-Mg_3N_2-Si_3N_4-SiO_2$ behaviour diagram

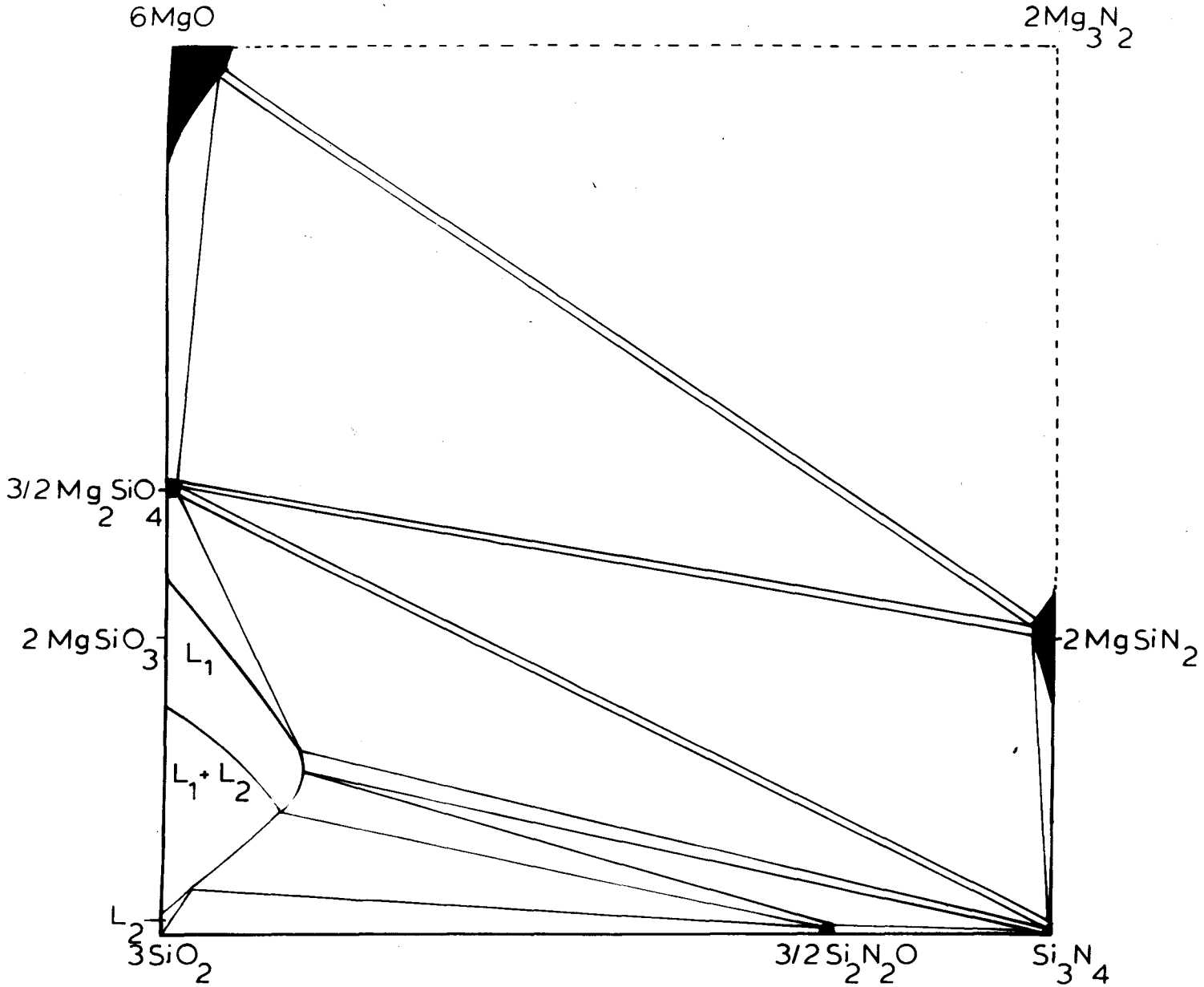

Figure VI.12 1700°C isothermal phase diagram for the sub-system $MgO-MgSiN_2-Si_3N_4-SiO_2$

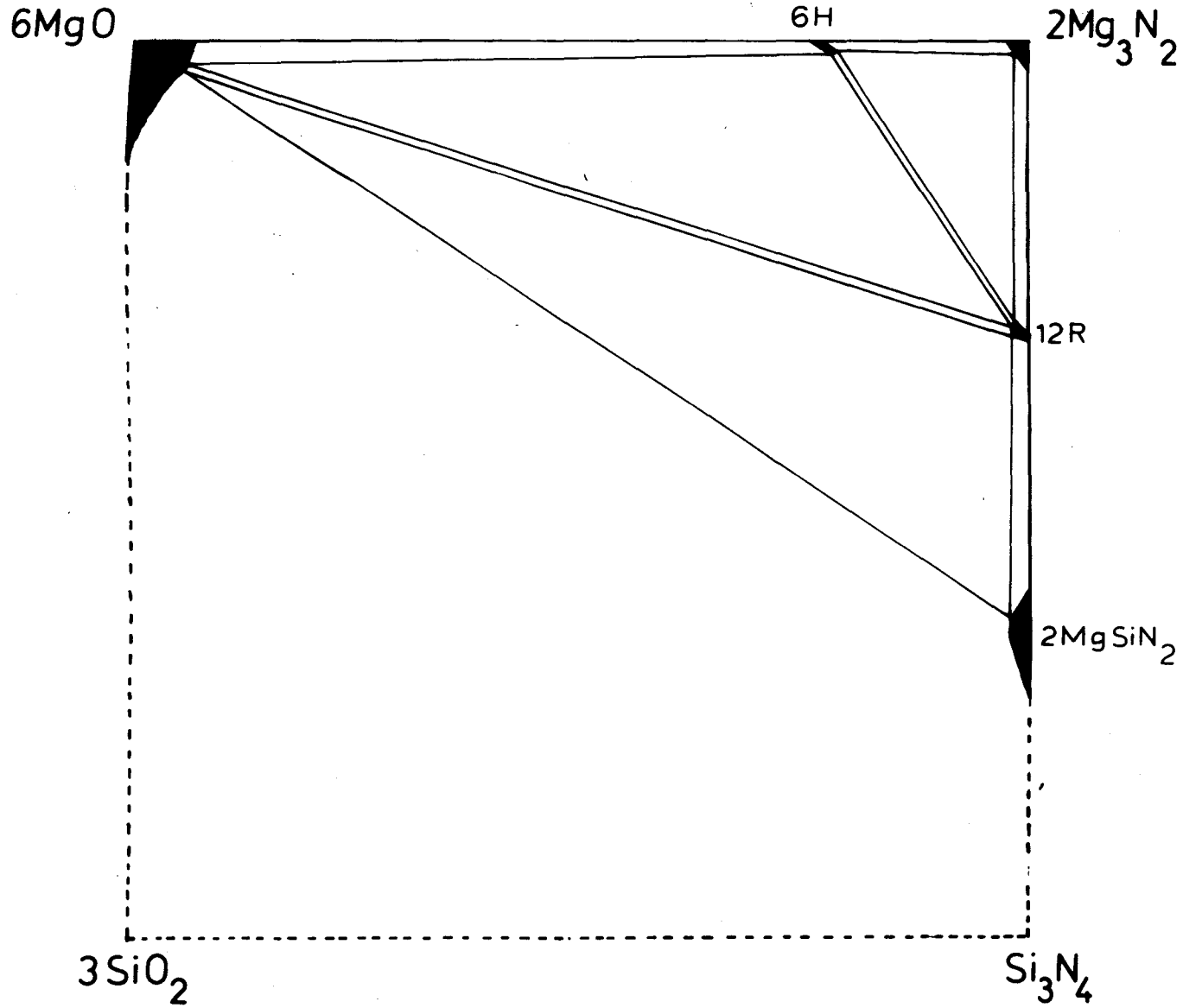

Figure VI.13 1300°C isothermal phase diagram for the sub-system $MgO-Mg_3N_2-Si_3N_4$

In the $6MgO - 2Mg_3N_2 - 2MgSiN_2$ sub-section of the diagram two new polytype phases observed with Ramsdell symbols 6H and 12R are discussed in Chapter VIII. These phases were not observed pure, because the MgO produced by addition of Mg_3N_2 was always in excess of the amount required to form them. By analogy with Be-Si-O-N system (Huseby, Lukas & Petzow, 1975) it is probable that 6H and 12R will form pure in the Mg-Si-O-N system if suitable conditions are maintained to prevent conversion of Mg_3N_2 to MgO. Under these assumed conditions the probable phase diagram is given in Figure VI.13.

VI.7 $MgO-Si_3N_4$ binary join

Magnesia was added to silicon nitride as a sintering aid by Deeley, Herbert & Moore (1961) but a systematic investigation of the system was carried out only fairly recently by Oyama (1972) and Wilson (1974). In the present work the previous work at Newcastle was repeated by hot-pressing mixtures of MgO and Si_3N_4 at 1700°C and 1810°C. There were a few discrepancies with earlier results which may be due to difficulties in reaching equilibrium. The results are plotted schematically in Figures VI.14 and VI.15 along with the weight loss at 1810°C. The weight loss at 1700°C varied from 0-7% with increase of MgO.

Forsterite and magnesium silicon nitride ($MgSiN_2$)

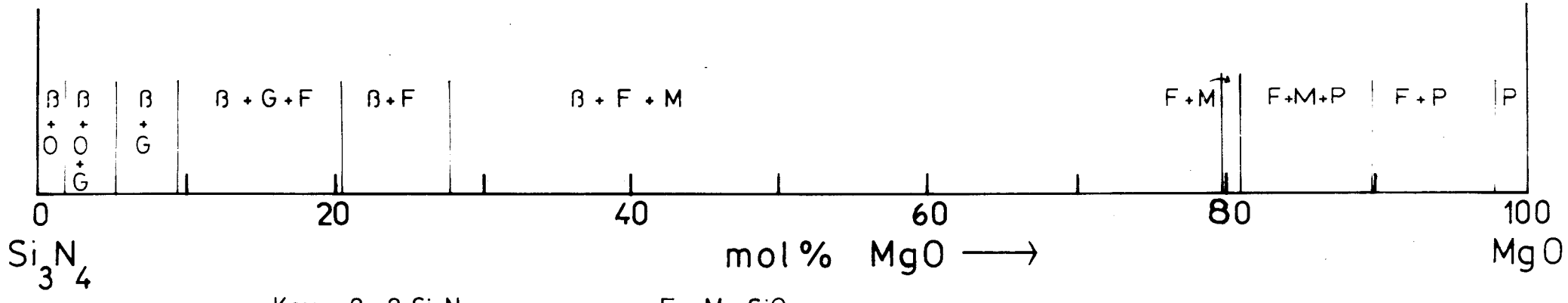

Key : β = β Si_3N_4 F = Mg_2SiO_4

O = Si_2N_2O M = $MgSiN_2$

G = Glass(Mg,Si,O,N) P = Periclase

Figure VI.14 A schematic representation of the behaviour of Si_3N_4-MgO system at 1750°C

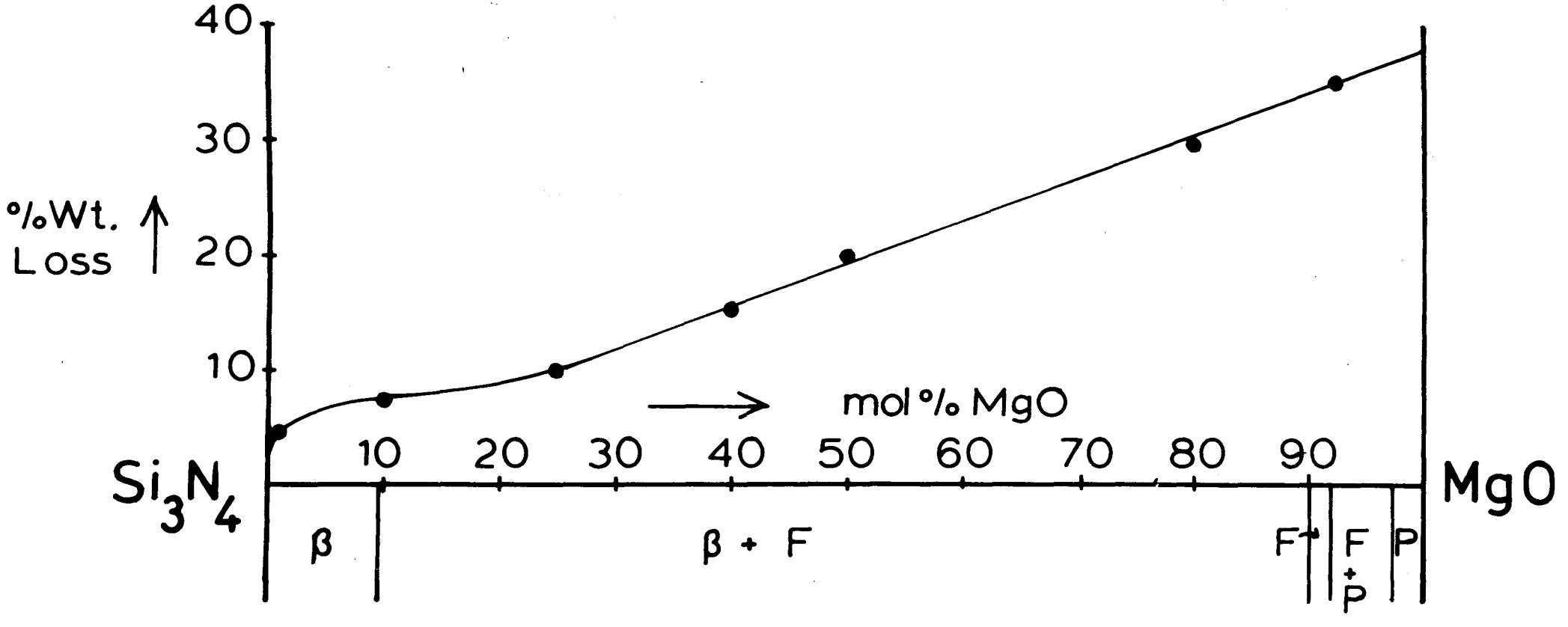

Figure VI.15 A schematic representation of the behaviour of Si_3N_4-Mgo system at 1810°C along with weight loss

were observed at 80^{m}/o MgO in the 1700°C hot-pressing which is formed according to the reaction:

$$4MgO + Si_3N_4 = 2MgSiN_2 + Mg_2SiO_4$$

To understand the phase assemblages in this system it is better to refer to the Mg-Si-O-N prism face (Figure VI.11). Since Si_3N_4 contains SiO_2 impurity the line joining 6MgO to Si_3N_4 is displaced slightly towards SiO_2. The first phases to appear are β-Si_3N_4 and Si_2N_2O and with increase of MgO the 3-phase region of β-Si_3N_4, Si_2N_2O and glass (liquid at 1700°C) is reached. Experimentally it is difficult to observe the two phase regions glass + β-Si_3N_4, forsterite + β-Si_3N_4, and forsterite + $MgSiN_2$ because they have such narrow ranges of compositional variation.

Above 1810°C there is a gradual increase in volatilisation of Mg_3N_2 with increase of MgO, according to the reaction:

$$Si_3N_4 + 12MgO = 2Mg_3N_2 + 3Mg_2SiO_4$$

At 92^{m}/o MgO, the only observed phase is forsterite and the weight loss is 35%. According to the above equation complete volatilisation of Mg_3N_2 gives a weight loss of 32%. Above 1800°C Si_2N_2O is not the first phase to appear because it decomposes and the behaviour diagram simplifies to $\beta \longrightarrow \beta$ + forsterite $\longrightarrow$ forsterite $\longrightarrow$ forsterite + MgO $\longrightarrow$ MgO (Figure VI.15.

This observation is compatible with the prism face Mg-Si-O-N along the join Si_3N_4-6MgO if the volatilisation of Mg_3N_2 is assumed.

According to Oyama (1972) up to 20^m/o MgO goes into solid solution in β-Si_3N_4 but he observed no increase in unit-cell dimensions although there were changes in intensities on a diffractometer trace. With increasing MgO concentrations forsterite and magnesium silicon nitride were formed along with β-Si_3N_4. In the present work no evidence of any solid solubility between Si_3N_4 and MgO was obtained.

VI.8 Glass formation

The initial investigation was carried out along the join 20^w/oMgO:80^w/oSiO_2-Si_3N_4, by adding varying amounts of Si_3N_4 to a pre-sintered (1700°C) mix of MgO and SiO_2. The results are tabulated in Table VI.4 and X-ray photographs of the products shown in Figure VI.16 and optical micrographs in Figure VI.17. It is seen that 10^w/oSi_3N_4 forms a glass and no trace of crystalline phases. According to the starting composition, $Si_{28}Mg_9O_{57}N_6$, the glass contains about 6^a/oN and this was confirmed by chemical analysis. It is greyish-black in colour and not transparent in bulk. On divitrification of the glass in a nitrogen atmosphere at 1500°C for 8 hours, the X-ray powder photograph (see Figure VI.16) showed a mixture of Si_2N_2O, clinoenstatite

Table VI.4 Mg-Si-O-N glass formation

run	reactants	conditions	products	weight loss %
A	$20^{w}/oMgO, 80^{w}/oSiO_2$	1700°C, H.P. 10 min.	80% cristobalite 20% protoenstatite	8
B	$4^{w}/oSi_3N_4, 96^{w}/oA$	1700°C, H.P. 10 min.	10% (cristobalite & protoenstatite) 90% glass	0
C	$10^{w}/oSi_3N_4, 90^{w}/oA$	1700°C, H.P. 10 min.	no diffraction pattern blackening near d=4.0 Å 100% glass	0
D	$15^{w}/oSi_3N_4, 85^{w}/oA$	1700°C, H.P. 10 min.	10% Si_2N_2O, 5% cristobalite 85% glass	2
E	$10^{w}/oSi_3N_4, 24^{w}/oMgO,$ $66^{w}/oSiO_2$	1700°C, H.P. 10 min.	as in C	10
F	as in E	sintered in N_2 in Mo. furnace for 30 min. 1600°C	glass and trace Si_2N_2O	2
G	as in C	sintered in graphite die 1700°C, 10 min.	as in C	3

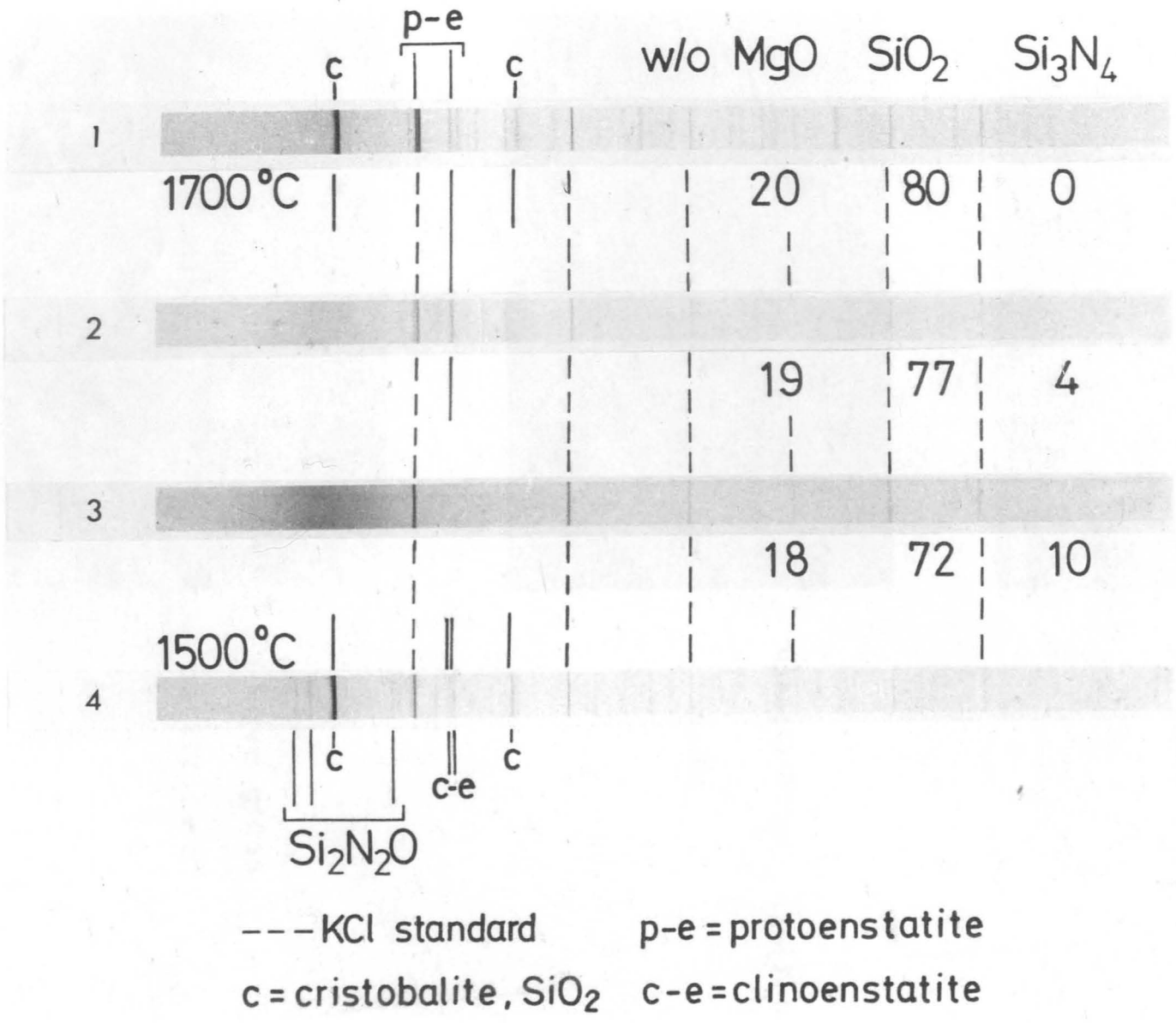

Figure VI.16 X-ray photographs of runs which lead to glass formation

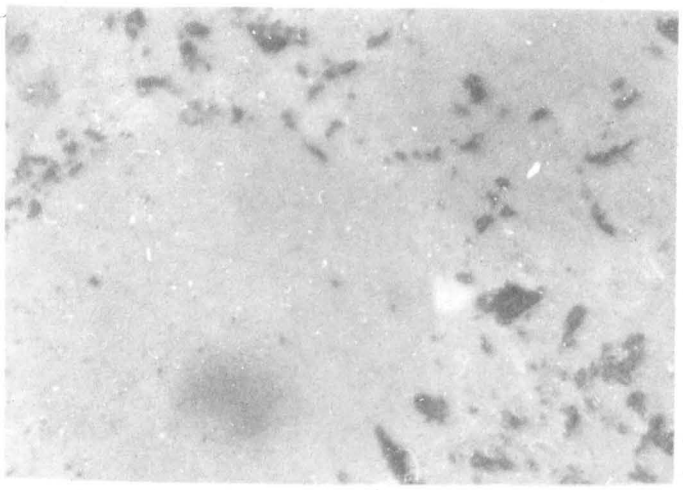

19 $MgO:77\,SiO_2:4\,Si_3N_4$ (wt%)

Partially vitrified

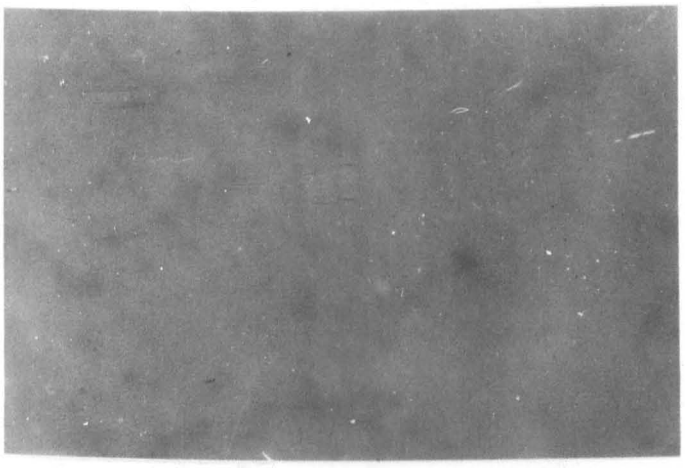

18 $MgO:72\,SiO_2:10\,Si_3N_4$ (wt%)

Glass

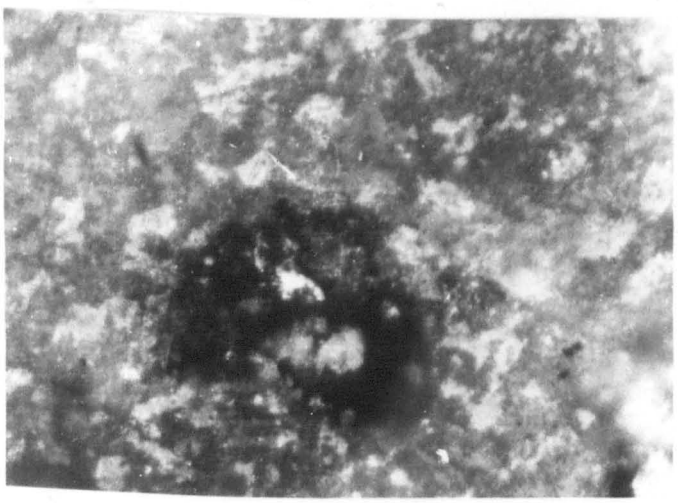

Above glass

devitrified

Figure VI.17

Optical micrographs of glass containing samples (x400)

and cristobalite as expected from the equilibrium diagram (Figure VI.12). The weight loss in some runs may be due to volatilisation of some silica as SiO due to reduction by carbon

$$SiO_2 + C \rightleftharpoons SiO + CO$$

The range of glass formation is more limited than would be expected from a glass forming region; this may be due to the temperature and the rate of cooling for a particular composition. In the present work the temperature was not varied with composition.

The chemical solubility of nitrogen in silicate glasses were first reported by Müfinger & Meyer (1963). Elmer & Nordberg (1965) have shown that oxide glasses with less than 1 w/o nitrogen have better physical properties than similar non-nitrogen containing glasses. The water solubility and coefficient of thermal expansion is lower while hardness, DC resistivity, and resistance to divitrification by electrolysis increases. If in the tetrahedral net-work of a glass the nitrogen is co-ordinated by three ligands the structure should be more rigid and hence have a higher viscosity than for silicate glasses.

In the hot-pressing of silicon nitride with magnesium oxide it has already been mentioned that a phase, liquid at higher temperature, cools to give a glass. Divitrification of this glass gives enstatite

and silicon oxynitride after heat-treatment at 1350°C Wild et al, 1972). Both the original high-temperature liquid and the glass which forms on cooling must, therefore contain nitrogen. The prospect of producing glasses more refractory and more resistant to divitrification than vitreous silica is worth further exploration.

In the Mg-Si-Al-O-N system glasses were formed at the compositions:

(i) $Si_{29}Al_3Mg_3O_{62}N_3$ (by sintering at 1700°C for 15 minutes a mixture of $6.7^{w}/o Al_2O_3$, $6.2^{w}/o MgO$, $4.8^{w}/o Si_3N_4$ and $82.2^{w}/o SiO_2$)

and

(ii) $Si_{21}Al_8Mg_{10}O_{52}N_9$ (by sintering at 1650°C for 30 minutes a mixture of $17.3^{w}/o AlN$, $22.1^{w}/o MgO$ and $61.6^{w}/o$ quartz)

Analysis of glass (i) by EPMA gave results similar to the starting composition. The range of glass formation is more extensive in the Mg-Si-Al-O-N system than suggested by the preliminary observation in the Mg-Si-O-N but both system need further investigation.

VII. β'-Magnesium Sialon

VII.1 Introduction

Bell & Wilson (1973) hot-pressed magnesium spinel ($MgAl_2O_4$) with α-Si_3N_4 at 1700°C, and obtained a phase with an expanded β-Si_3N_4 structure the unit-cell dimensions of which increased up to 30 m/o spinel (Figure VII.1). Because of the absence of any other crystalline phases, and the gradual increase of unit-cell dimensions with increase of spinel, it was concluded that the structure was that of magnesium containing β'-sialon. Japanese workers have also sintered α-Si_3N_4-$MgAl_2O_4$ mixtures at 1700-1800°C in inert atmospheres and obtained single-phase β'-sialon (German patent no. 235093 Oct. 1973, Toyota, Japan).

Bell & Wilson (1973) also reacted MgO with mixtures of equal weights of Si_3N_4 and Al_2O_3 and obtained β'-magnesium sialon and X-phase. Other workers have also added MgO to mixtures of Al_2O_3 and Si_3N_4. Terwilliger & Lange (1975) added 0-5 w/o MgO to different mixtures of Si_3N_4 and Al_2O_3 and observed sintering and densification of the resultant sialons. Work at the Joseph Lucas Group Research Centre also confirms this.

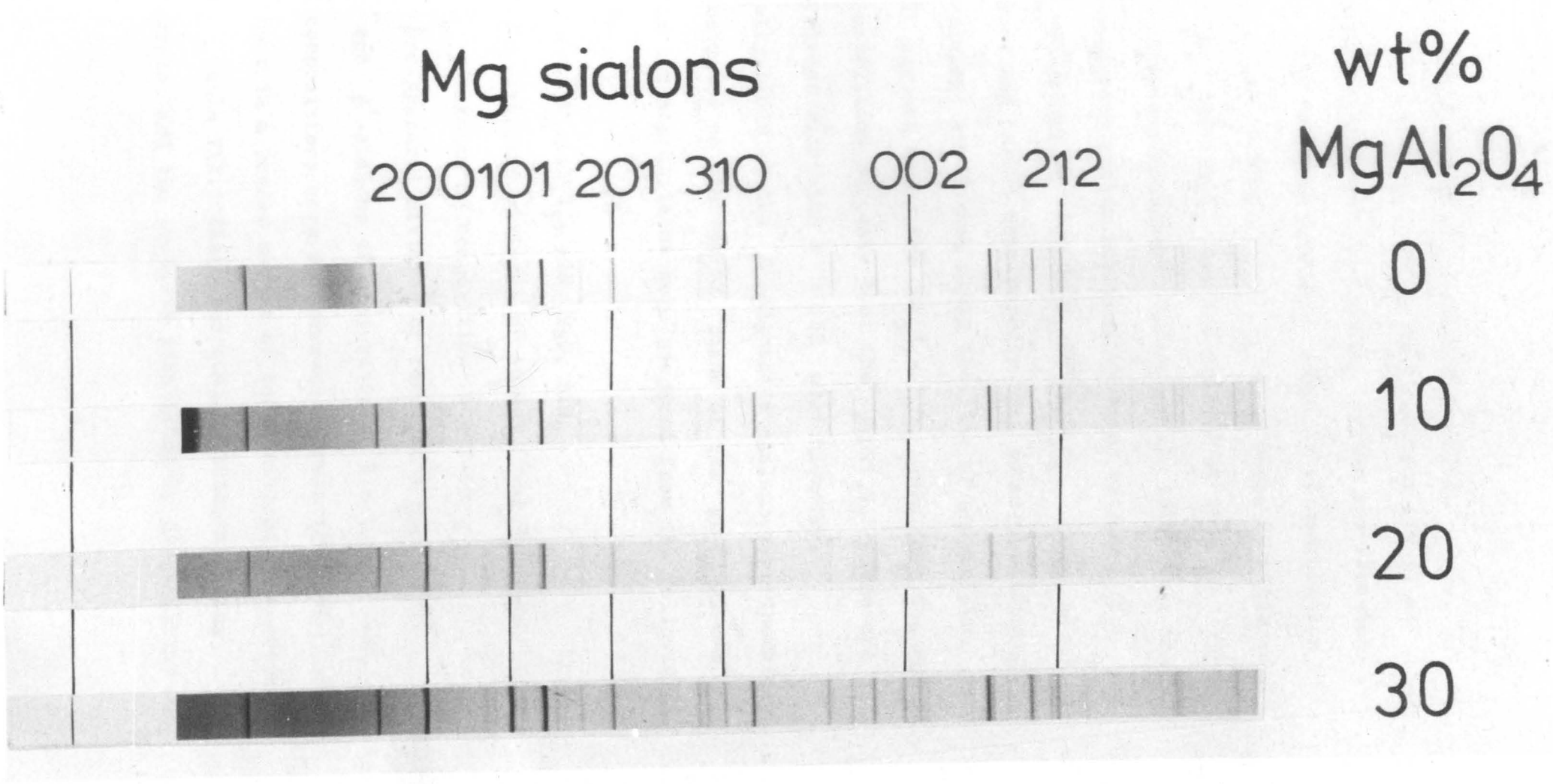

Figure VII.1 X-ray photographs of magnesium sialons

VII.2 Formation of β'-magnesium sialons

The previous work by Bell & Wilson (1973) at Newcastle on the $MgO-Al_2O_3-Si_3N_4$ system was repeated in the present investigation. Spinels of composition $MgAl_2O_4$ and $0.31MgO.0.69Al_2O_3$ were added to mixtures of Si_3N_4 and Al_2O_3 and hot-pressed at 1800°C. It was erroneously concluded (Hendry et al, 1974) that the β'-magnesium sialon homogeneity range extended from Si_3N_4-30$^m/_o MgAl_2O_4$ to Si_3N_4-80$^m/_o Al_2O_3$. More recent evidence has proved conclusively that non-Mg containing β'-sialons are formed along the line of composition 3M:4X and not along the $Si_3N_4-Al_2O_3$ join (see Chapter II). This conclusion suggests that the β-Si_3N_4 structure type always maintains a 3M:4X stoichiometry. Investigations of the β'-magnesium sialons were therefore concentrated on the 3M:4X plane of the Mg-Si-Al-O-N system and compositions were prepared from the following mixes:

(1) α-Si_3N_4, Al_2O_3, AlN, MgO, SiO_2 .

(2) Pre-prepared mixtures of spinel ($MgAl_2O_4$) and β'-sialon of composition $z = 1.85$.

(3) Pre-prepared mixtures of forsterite (Mg_2SiO_4) and β'-sialons of compositions $z = 1.14$ & 1.85.

All compositions were hot-pressed between 1700-1800°C for one hour in a powder medium of boron nitride in a graphite die. Table VII.1 lists the compositions, starting materials, and the products identified by Hägg-Guinier

Table VII.1 Composition of mixtures hot-pressed at 1800°C of -magnesium sialon products

run	composition I	composition II	reactants	X-ray* analysis minor phase (0-3%)
1	$Si_{2.79}Al_{0.21}Mg_{0.10}O_{0.41}N_{3.72}$	$Si_{5.40}Al_{0.41}Mg_{0.19}O_{0.79}N_{7.21}$	s+Sp	-
2	$Si_{2.57}Al_{0.43}Mg_{0.21}O_{0.86}N_{3.43}$	$Si_{4.79}Al_{0.82}Mg_{0.39}O_{1.60}N_{6.40}$	s+Sp	-
3	$Si_{2.48}Al_{0.52}Mg_{0.26}O_{1.06}N_{3.30}$	$Si_{4.56}Al_{0.96}Mg_{0.48}O_{1.92}N_{6.08}$	s+Sp	15R
4	$Si_{2.33}Al_{0.67}Mg_{0.33}O_{1.33}N_{3.11}$	$Si_{4.21}Al_{1.20}Mg_{0.59}O_{2.38}N_{5.62}$	s+Sp	15R,Sp
5	$Si_{2.08}Al_{1.15}Mg_{0.12}O_{1.38}N_{3.08}$	$Si_{3.73}Al_{2.06}Mg_{0.21}O_{2.48}N_{5.52}$	z=1.85+Sp	15R
6	$Si_{1.93}Al_{1.29}Mg_{0.21}O_{1.71}N_{2.86}$	$Si_{3.38}Al_{2.25}Mg_{0.37}O_{2.99}N_{5.01}$	z=1.85+Sp	15R,Sp
7	$Si_{2.50}Al_{0.56}Mg_{0.16}O_{0.87}N_{3.42}$	$Si_{4.68}Al_{1.02}Mg_{0.30}O_{1.62}N_{6.38}$	z=1.14+Fo	15R
8	$Si_{2.22}Al_{0.96}Mg_{0.12}O_{1.2}N_{3.2}$	$Si_{4.03}Al_{1.76}Mg_{0.21}O_{2.18}N_{5.82}$	z=1.85+Fo	15R
9	$Si_{2.20}Al_{0.93}Mg_{0.21}O_{1.34}N_{3.10}$	$Si_{3.97}Al_{1.65}Mg_{0.33}O_{2.41}N_{5.56}$	z=1.85+Fo	15R,Sp

contd next page

Table VII.1 contd.

run	composition I	composition II	reactants	X-ray* analysis minor phase (0-3%)
10	$Si_{2.5}Al_{0.6}O_{0.6}N_{0.6}$	$Si_{4.86}Al_{1.14}O_{1.14}N_{6.86}$	s+A+A'	-
11	$Si_{2.25}AlON_{3.33}$	$Si_{4.15}Al_{1.85}O_{1.85}N_{6.15}$	s+A+A'	-
12	$Si_{2.18}Al_{1.09}O_{1.09}N_{3.27}$	$Si_4Al_2O_2N_6$	s+A+A'	-
13	$Si_{2.03}Al_{1.30}O_{1.30}N_{3.13}$	$Si_{3.65}Al_{2.35}O_{2.35}N_{5.65}$	s+A+A'	-
14	$Si_{2.28}Al_{0.91}Mg_{0.09}O_{1.09}N_{3.27}$	$Si_{4.16}Al_{1.68}Mg_{0.16}O_2N_6$	s+A+A'+M	tr.SiC
15	$Si_{2.37}Al_{0.72}Mg_{0.18}O_{1.09}N_{3.27}$	$Si_{4.33}Al_{1.34}Mg_{0.33}O_2N_6$	s+A+A'+M	SiC,Sp
16	$Si_{2.46}Al_{0.54}Mg_{0.27}O_{1.09}N_{3.27}$	$Si_{4.49}Al_{1.02}Mg_{0.49}O_2N_6$	s+A+A'+M	SiC,Sp
17	$Si_{2.13}Al_{1.10}Mg_{0.10}O_{1.30}N_{3.13}$	$Si_{3.83}Al_{1.99}Mg_{0.18}O_2.N_6$	s+A+A'+M	15R
18	$Si_{2.23}Al_{0.90}Mg_{0.20}O_{1.30}N_{3.13}$	$Si_{4.01}Al_{1.63}Mg_{0.36}O_{2.35}N_{5.65}$	s+A+A'+M	15R
19	$Si_{2.33}Al_{0.70}Mg_{0.30}O_{1.30}N_{3.13}$	$Si_{4.19}Al_{1.27}Mg_{0.54}O_{2.35}N_{5.65}$	s+A+A'+M	15R

contd next page

Table VII.1 contd.

Notes: I ≡ $Si_{3-x/4-y/2}\ Al_y\ Mg_{(x-y)/2}\ O_x\ N_{4-2x/3}$

II ≡ $Si_{6-z+m/2}\ Al_{z-m}\ Mg_{m/2}\ O_z\ N_{8-z}$

15R is the magnesium sialon with the 15R polytype structure

≡ major phase β', 97-100%

Key: s = α-Si_3N_4

A = Al_2O_3

A' = AlN

M = MgO

Sp = spinel, $MgAl_2O_4$

Fo = Forsterite, Mg_2SiO_4

X-ray powder photographs of all mixtures that give 97-100% β'-magnesium sialon while Figure VII.2 shows all the compositions hot-pressed in the 3:4 plane. The phase assemblages that are formed in this plane are discussed in Chapter VIII.

In the Mg-Si-Al-O-N representation by Jänecke's triangular prism, at any composition the total metal or non-metal valencies equals 12. On this basis any composition in the 3:4 plane can be represented by the formula:

$$Si_{3-x/4-y/2}\ Mg_{(x-y)/2}\ Al_y\ O_x\ N_{4-2x/3}$$

In sialon compositions the formula $Si_{6-z}\ Al_z\ O_z\ N_{8-z}$ has been widely adopted, and on this basis compositions in the 3:4 plane may be represented by:

$$Si_{6-z+m/2}\ Mg_{m/2}\ Al_{z-m}\ O_z\ N_{8-z}$$

The values x, y, z and m are related by:

$$z = \frac{8\,(O)}{(O)+(N)} = \frac{24x}{12+x}$$

$$m = \frac{6\,(Mg)}{(Si)+(Al)+(Mg)} = \frac{24\,(x-y)}{12+x}$$

Compositions have been expressed according to both formulae.

α-Si_3N_4 powder has about 4 w/o SiO_2 as impurity

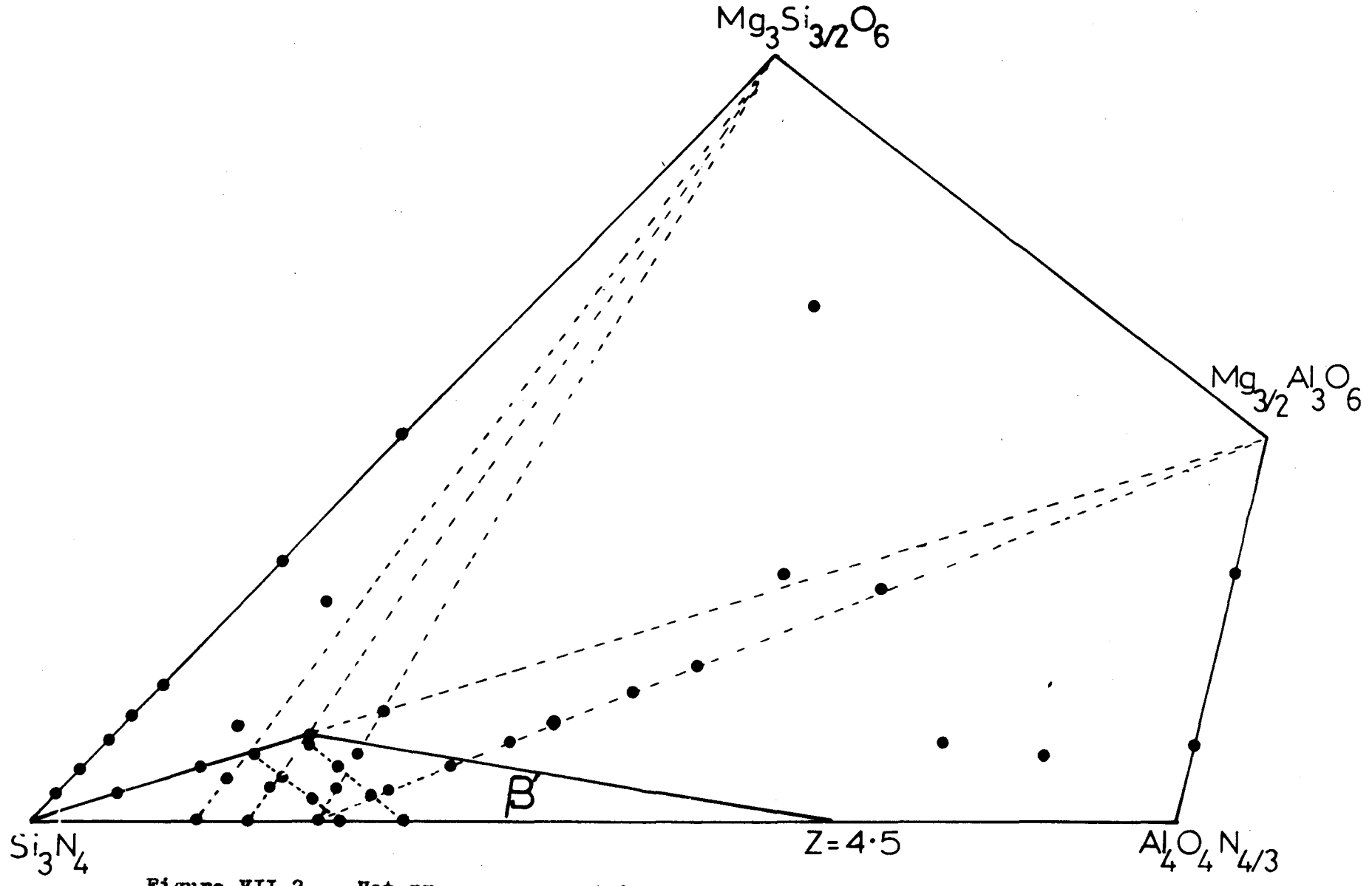

Figure VII,2 Hot-pressed compositions in the 3M:4X compositional plane

and AlN has $6^{W}/_{O}Al_2O_3$. A composition made up from Si_3N_4 and AlN powders therefore has a slightly smaller M:X atom-ratio than the same mixture prepared from pure nitride powders. When a composition was prepared the oxide impurities were compensated so that the overall composition was 3M:4X. β'-magnesium sialon has an advantage over the β'-sialon because, in the presence of MgO, the silica impurity of silicon nitride forms magnesium silicate which reacts with some silicon nitride to produce a liquid which aids densification by liquid-phase sintering and is subsequently incorporated into solid solution to give a single-phase β'.

Table VII.1 shows that there are minor impurities such as 15R, spinel or silicon carbide in β'-magnesium sialons due to one or more of the following:

(i) some volatilisation in the graphite die (see section II.5);

(ii) localised preferential reaction in forming 15R or spinel prior to β' and these remaining unaltered during subsequent heat-treatment;

(iii) incorrect estimation of the oxide impurities in the Si_3N_4 and AlN so that the composition does not lie exactly on the 3M:4X plane.

The work done by Messier & Gazza (1975) on the thermal decomposition of sialon mixtures in reducing atmospheres shows the decomposition product to be AlN or AlN-polytypes. For example the reactions:

$$Si_3N_4 + Al_2O_3 = 2AlN + 3SiO + N_2$$

and $$Si_3N_4 + 2Al_2O_3 + C = \underset{(15R\text{-sialon})}{SiAl_4O_2N_4} + 2SiO + 2CO$$

can take place in the graphite die to form 15R-sialon with disappearance of the volatile products. If the oxide impurities in Si_3N_4 and AlN are overestimated the composition of the mix will be slightly above the 3M:4X plane in the phase diagram. For example the product of run 7 in Table VII.1 contains 2% 15R; this hot-pressed sample was powdered and mixed with 3 w/o SiO_2 and after hot-pressing again the product was β'-magnesium sialon and spinel.

VII.3 Homogeneity of β'-magnesium sialons

The area of β'-magnesium sialon homogeneity is plotted in Figure VII.2 using the results of hot-pressed compositions. The same composition produced by different reactants gives a product with the same unit-cell dimensions. The formation of β'-magnesium sialon from starting composition of 3M:4X, would be expected to have the same structure as β-Si_3N_4 or β'-sialon and a range of homogeneity. To maintain electrical neutrality when magnesium is incorporated into the structure of the β'-phase it is necessary to adjust the oxygen:nitrogen ratio accordingly.

It is difficult to determine whether magnesium

is incorporated in the β'-sialon structure by chemical analysis or electron-micro-probe-analysis or by any one method conclusively. Therefore several methods had to be used.

The unit-cell dimensions of β'-magnesium sialons were determined and the infra-red absorption spectrum of β'-magnesium sialons was studied by Dr. S. Wild at the Polytechnic of Wales. He found that all the peaks in the β-Si_3N_4 spectrum were broadened and shifted systematically with increasing z value. In particular, the line at $580cm^{-1}$ showed a linear variation of wave-number with unit-cell dimensions as shown in Figure VII.3. Table VII.2 lists unit-cell dimensions, wave-number, differences in unit-cell dimensions and wave-number, z-value and magnesium content. The differences in unit-cell dimensions (Δ a, Δ c) and wave-number (ν) between β'-magnesium sialon and the equivalent β'-sialon of the same z-value as a function of Mg content are plotted out in Figure VII.4. It can be seen that there is a smooth variation with increase in magnesium content. This is because any β'-magnesium sialon is derived from the corresponding β'-sialon for the same oxygen:nitrogen ratio by replacing one aluminium by half each of magnesium and silicon (see formula 2, in section VII.2).

Table VII.3 lists X-ray density, powder density

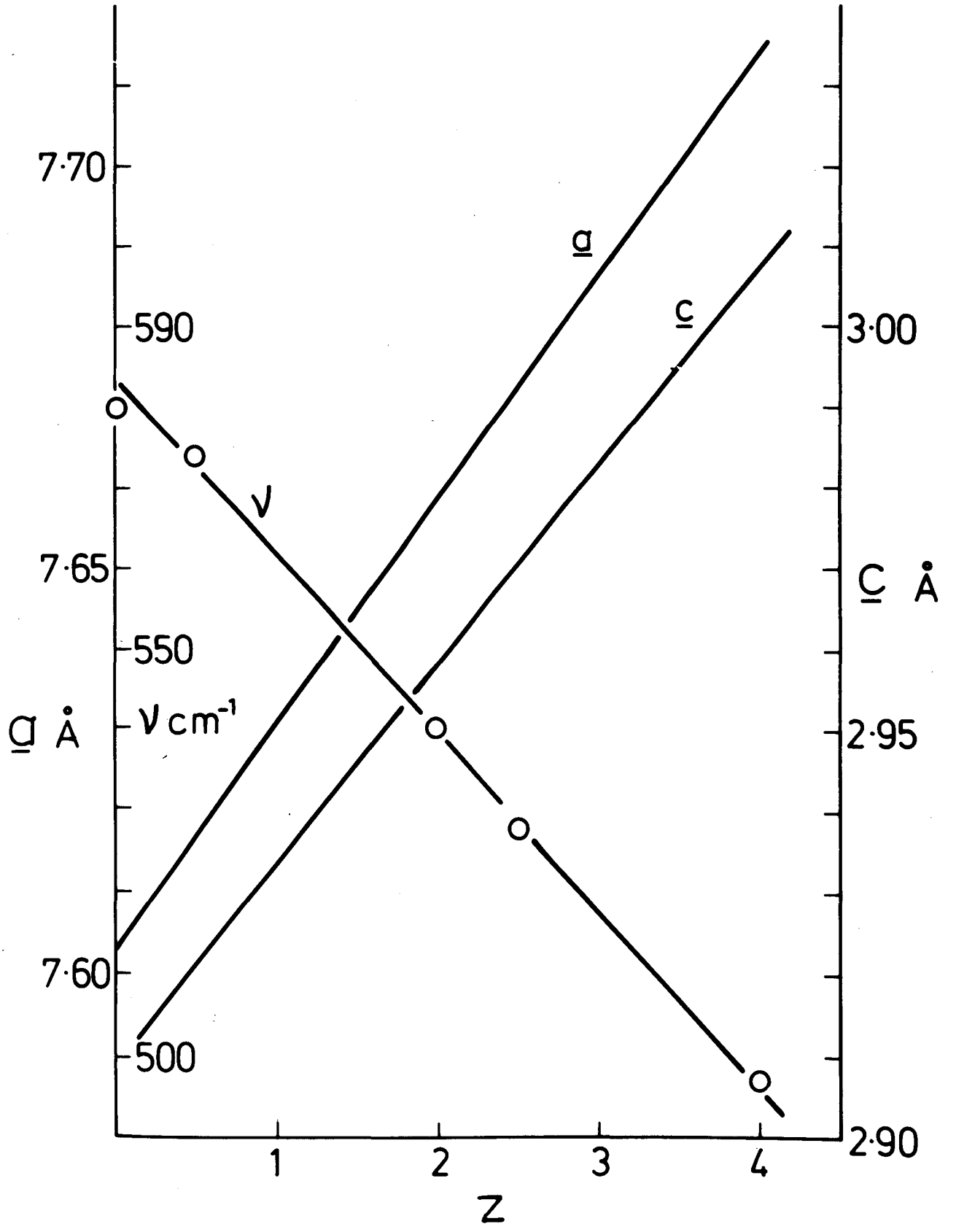

Figure VII.3 Variation of unit-cell dimensions and wave-number with z-value for β'-sialon

Table VII.2 Unit-cell dimensions and wave-numbers (I.R.) of β'-magnesium sialons

run*	a Å	c Å	ν cm^{-1}	$\frac{Z}{8(O)/(O+N)}$	$-\Delta a$ $\times 10^3$ Å	$-\Delta c$ $\times 10^3$ Å	$\Delta\nu$ cm^{-1}	Mg + (m/2)
β-Si_3N_4	7.603	2.909	580.0	0	0	0	0	0
14	7.655	2.951	545.5	2.00	3	7	5.0	0.16
17	7.663	2.961	-	2.35	5	6	-	0.18
1	7.617	2.918	575.5	0.79	8	10	8.5	0.19
5	7.663	2.961	-	2.48	9	9	-	0.21
15	7.644	2.943	554.5	2.00	14	15	14.0	0.33
18	7.655	2.947	-	2.35	13	20	-	0.36
9	7.655	2.947	-	2.41	15	19	-	0.38
2	7.623	2.922	572.0	1.60	24	26	23.0	0.39
3	7.632	2.928	-	1.91	24	28	-	0.48
16	7.632	2.929	565.5	2.00	26	29	25.0	0.49
19	7.638	2.933	-	2.35	30	34	-	0.54
20	7.638	2.933	563.5	2.39	32	35	31.5	0.59

* Run refers to same runs as in Table VII.1

+ m as in $Mg_{m/2}\ Si_{6-z+m/2}\ Al_{z-m}\ O_z\ N_{8-z}$

Table VII.3 Density measurements of β'-magnesium sialons

run[+]	X-ray density	powder density	sealed porosity
	g cm^{-3}	g cm^{-3}	%
12	3.119	3.119	0
14	3.126	3.124	0.1
15	3.139	3.125	0.4
16	3.164	3.161	0.1
13	3.105	3.106	-
17	3.113	3.115	-
18	3.131	3.131	0
19	3.157	3.151	0.2

[+] Run refers to same run as in Table VII.1

NOTE: % sealed porosity = % true porosity (as apparent porosity = 0)

$$= 100 \left(1 - \frac{\text{powder density}}{\text{X-ray density}}\right)$$

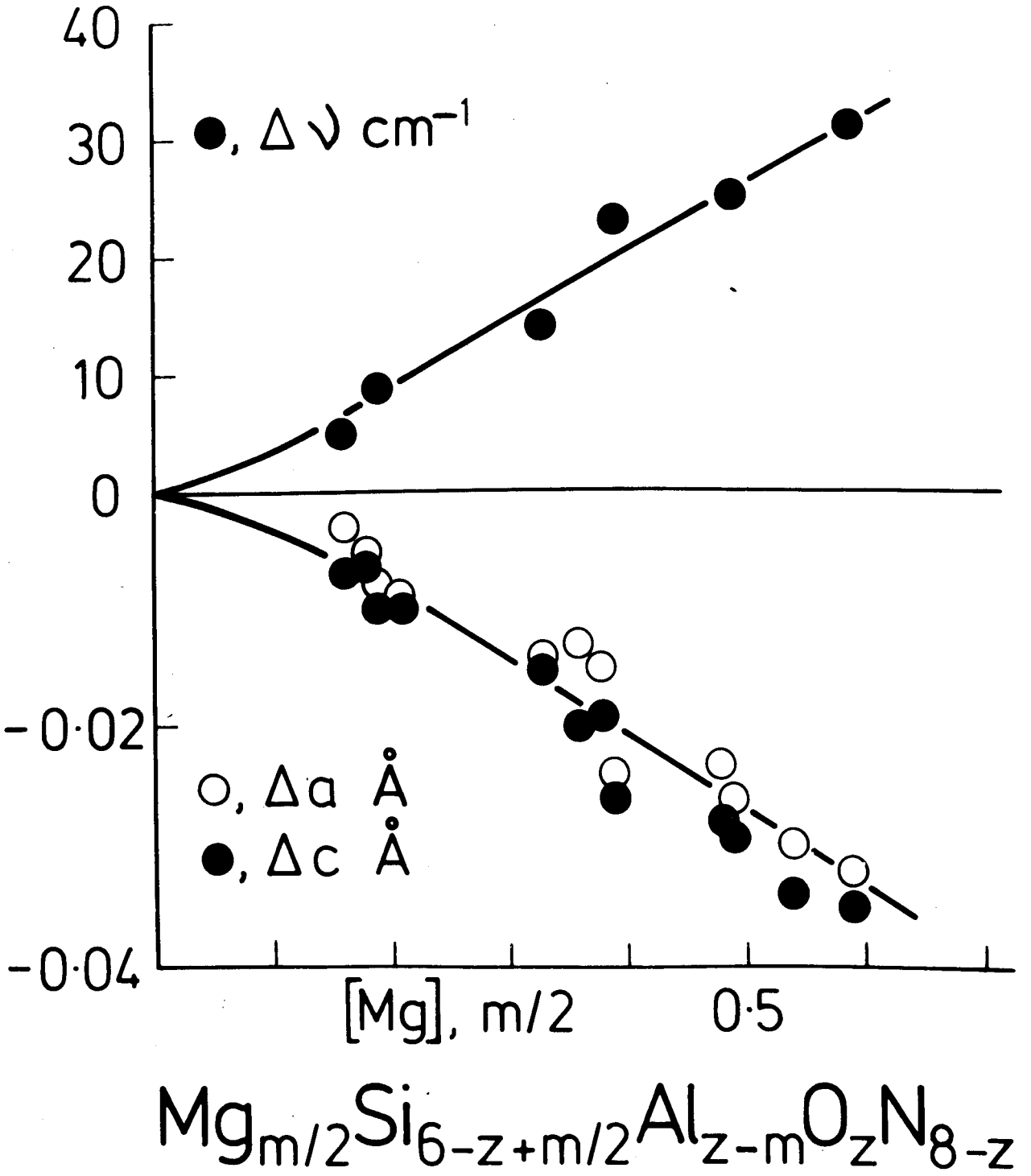

Figure VI.4 Variation of difference in unit-cell dimensions and wave-number with Mg content

and sealed porosity for some β'-magnesium sialons and the agreement between X-ray density and powder density is good and discounts the possibility of having a vitreous magnesium sialon phase, which would invariably reduce the powder density.

The self consistency of results namely, the absence of any second crystalline phase, correlation between X-ray and infra-red measurements and the density measurements all provide convincing evidence that magnesium is incorporated in the structure.

VII.4 Properties of β'-magnesium sialon

VII.4(i) Density and porosity

The density and porosity of some β'-magnesium sialons are listed in Table VII.3. The theoretical density of the specimens are in close agreement with measured density, which suggest that the assumed structure is correct and β'-magnesium sialons are nearly single-phase. The sealed porosity measurements show that β'-magnesium sialons can be produced easily by hot-pressing with near zero porosities.

VII.4(ii) Coefficient of thermal expansion

For the β'-magnesium sialon of composition $Si_{3.46}Al_{2.26}Mg_{0.28}O_{2.83}N_{5.17}$ the variation of unit-cell dimensions with temperature is plotted in

Figure VII.5 and the coefficient of expansion was found to be almost isotropic and equal to $2.7\pm0.2\times10^{-6}$ $^{o}C^{-1}$. This value compares well with that of β'-sialon (z=3) where $\alpha = 2.7\times10^{-6}$ $^{o}C^{-1}$ (Wilson, 1974) and β-Si_3N_4 $\alpha_a = 3.3\times10^{-6}$, $\alpha_c = 3.8\times10^{-6}$ $^{o}C^{-1}$ (Berkbile, 1970).

VII.4(iii) Thermal shock resistance

When ceramic materials are subjected to very high transient temperature-gradients, substantial stresses develop; resistance to "cracking" under these conditions is called thermal shock resistance. The simplest method of testing the resistance to thermal shock is by heating a thin 1" diameter hot-pressed disc weighing about 10g in a furnace at 1200°C and rapidly dropping into a beaker of water at 20°C. This is repeated and the number of cycles survived by the disc is taken as a measure of thermal shock resistance. The β'-magnesium sialon of composition $Si_{4.19}Al_{1.27}Mg_{0.54}O_{2.35}N_{5.65}$, specimen 20, Table VII.1 (referred to later as z=2.35 β'-magnesium sialon) survived 18 cycles - an average from 6 samples tested.

VII.4(iv) Chemical resistance

Hot-pressed blocks of β'-magnesium sialon of composition z=2.35 weighing about 1g were subjected to 6N sulphuric acid at 90°C, 6N hydrochloric acid at 70°C, 2N sodium hydroxide at 100°C and 6N hydrofluoric

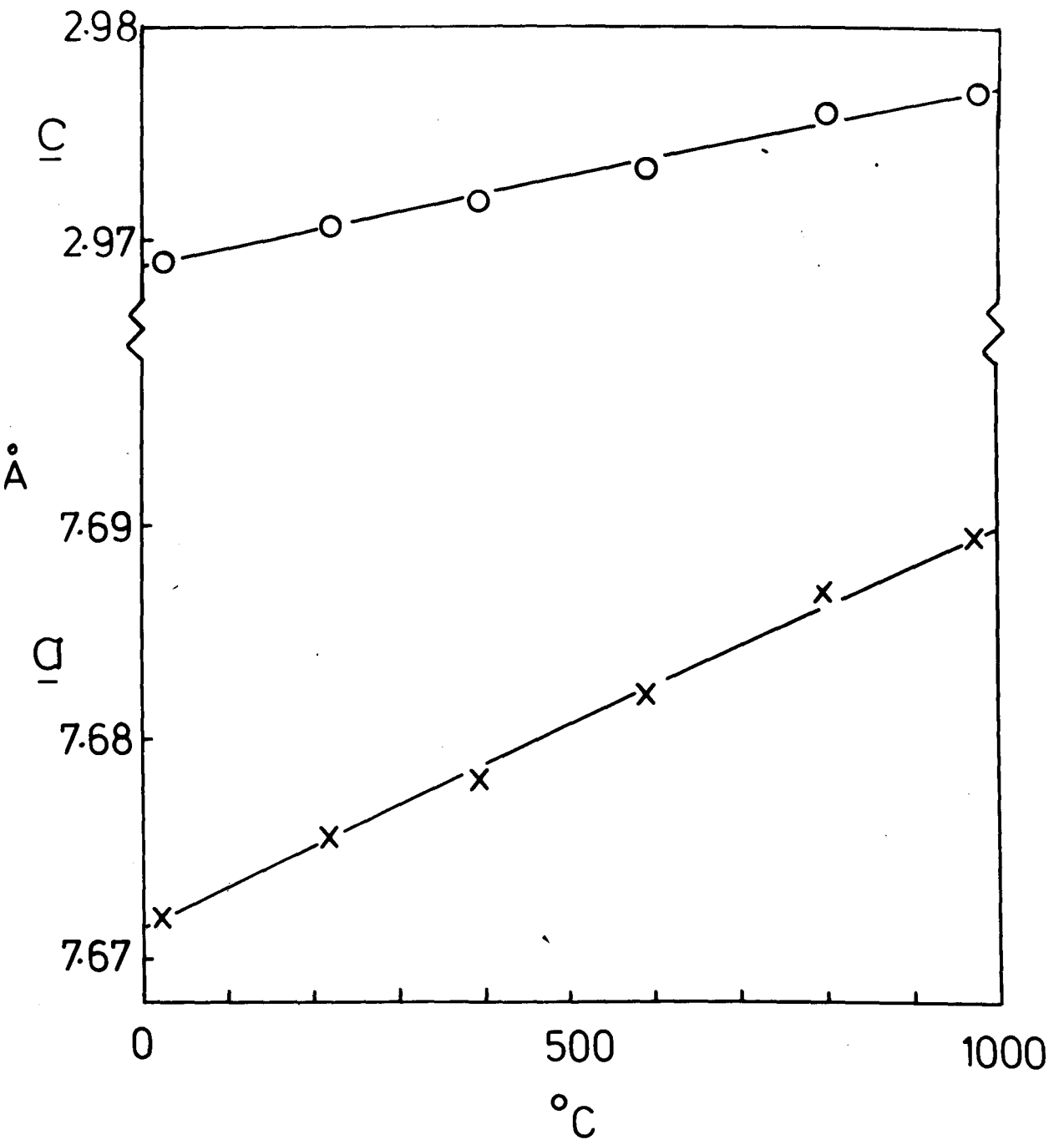

Figure VII.5 Variation of unit-cell dimensions with temperature for β'-magnesium sialons ($z = 2.8$)

acid at 20°C for 30 minutes; it was affected only by hydrofluoric acid. When β'-sialon (z=3) was subjected to similar treatment (Wilson, 1974), it was attacked by sodium hydroxide and hydrofluoric acid.

VII.4(v) Oxidation resistance and thermal decomposition

Hot-pressed block of β'-magnesium sialon (z=2.35) when heated in air at 1200°C for 24h and 240h showed small weight gains of 0.05% and 0.15% respectively. No surface oxidation product was observed or detected by X-ray methods. Similar treatment with hot-pressed Si_3N_4 gave cristobalite as the oxidation product.

The above β'-magnesium sialon was powdered and the fraction between -200 mesh and +300 mesh (53-75 μm) was heated at 1500°C for 16h and 24h in air and weight gains observed were 4.3% and 6.5% respectively. The X-ray analysis of the product for the 24hour-specimen showed 60% β'-magnesium sialon, 30% Si_2N_2O and 10% N-phase. Under comparable conditions β-Si_3N_4 was completely oxidised to cristobalite in six hours and β'-sialon (z=3) oxidised to mullite and cristobalite in 24 hours (Wilson, 1974). These results, although not really quantitative suggest that magnesium sialon has better oxidation resistance than silicon nitride or β'-sialon.

When β'-magnesium sialon (z=2.35) of particle size 53-75 μm was heated in purified nitrogen at 1450°C for

18h there was a weight loss of 7%. X-ray examination showed about 5% spinel as a new phase in addition to the β'-magnesium sialon and 2% 15R-magnesium sialon present originally. Under similar conditions silicon nitride and β'-sialon (z=3) showed weight losses of 7% and 3% respectively (Wilson, 1974). It is calculated that the oxygen potential in the purified nitrogen is $\sim 10^{-16}$ atmospheres and at these low values β'-magnesium sialon undergoes dynamic oxidation:

$$Si_{4.2}\,Al_{1.2}\,Mg_{0.6}\,O_{2.4}\,N_{5.6} + 2.1O_2 = 0.6\,MgAl_2O_4 + 4.2\,SiO\uparrow + 2.8\,N_2\uparrow$$

These crude comparative tests show that β'-magnesium sialon suffers about the same amount of thermal decomposition in nitrogen as β-silicon nitride.

VII.4(vi) Hardness measurements

Vickers hardness measurements using a diamond indentor and a load of 10 Kg gave average value for 10 readings of 1522 VN. This is similar to the corresponding result for β'-sialon (z=3), 1630 VN (Wilson, 1974).

VII.5 Conclusion

The present work shows that β'-magnesium sialons can be produced by different routes and extend

the range of homogeneity of β'-sialon. The physical properties are comparable to β'-sialon but the chemical properties are slightly better.

VIII. Phase Relationships in the Mg-Si-Al-O-N System

VIII.1 The $6MgO-2Al_2O_3-Si_3N_4$ section

This section represented for convenience by the equilateral triangle of Figure VIII.1 cuts across planes of constant M:X ratio. The behaviour diagram was constructed from the results of hot-pressing mixtures of MgO, Al_2O_3 and Si_3N_4 or of $MgAl_2O_4$, Al_2O_3 and Si_3N_4 at 1800°C (see Figure VIII.2). Below the 3M:4X line the weight losses were less than 5^w/o but above it, they increased with increasing MgO (40-90^m/o) to about 40^w/o. Compositions prepared by spinel additions to Si_3N_4 and Al_2O_3 generally show lower weight losses than those from MgO, Si_3N_4 and Al_2O_3. The volatile product was Mg_3N_2 (see Chapter VI) formed according to the equation:

$$Si_3N_4 + 12MgO = 2Mg_3N_2 + 3Mg_2SiO_4$$

Along the Si_3N_4-$MgAl_2O_4$ join β'-magnesium sialon is formed up to 30^m/o $MgAl_2O_4$. Below the 3M:4X line β'-magnesium sialon and X-phase are formed, while above it α-Si_3N_4 is stabilised. This α-structure has a slight distortion relative to pure α-Si_3N_4 and hence is labelled α'. At high spinel concentrations along the Si_3N_4-spinel join, 15R-magnesium sialon appears and with further increase, magnesia spinel remains. The

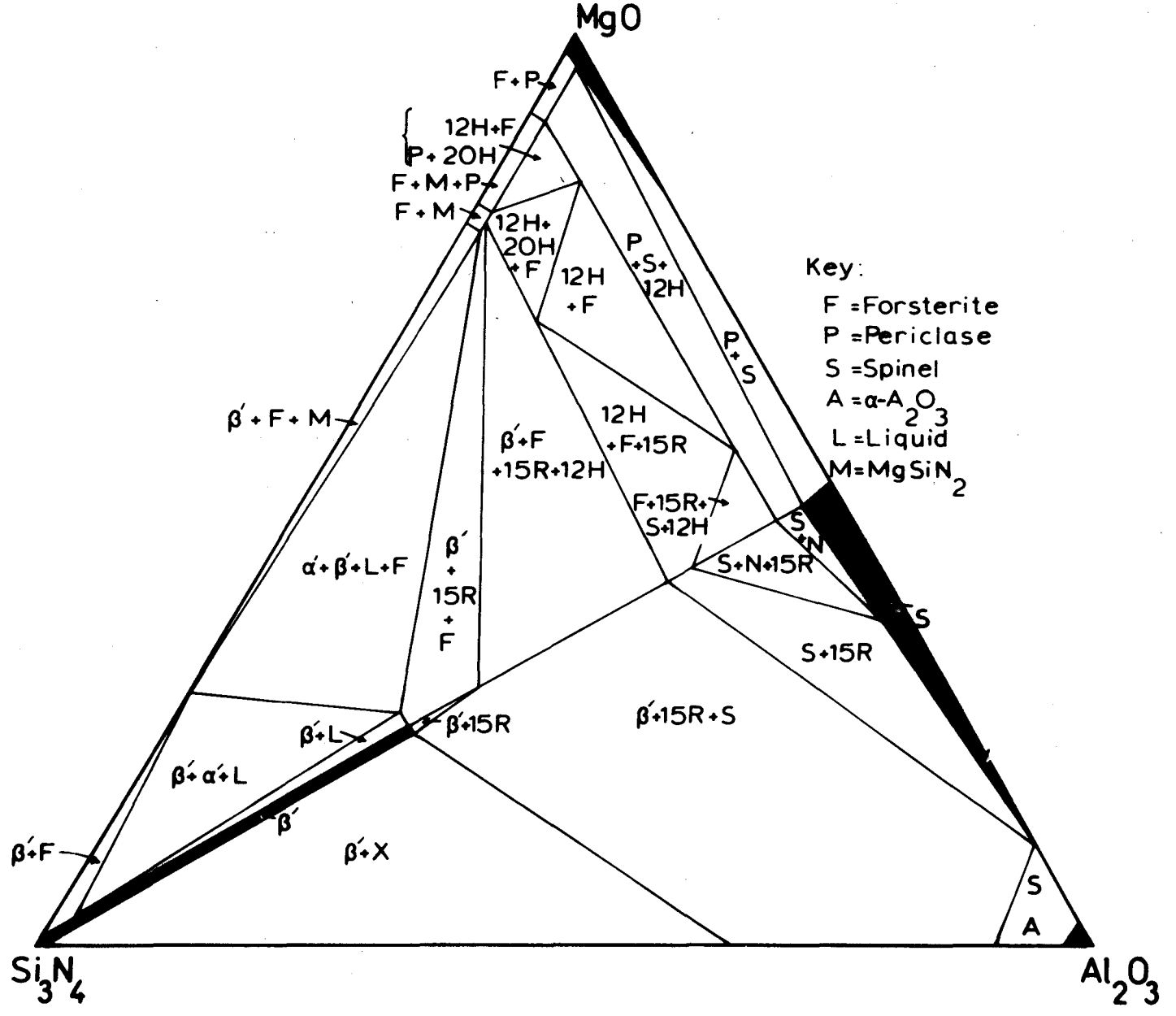

Figure VIII.1 The behaviour diagram of the $MgO-Al_2O_3-Si_3N_4$ sub-system at 1800°C

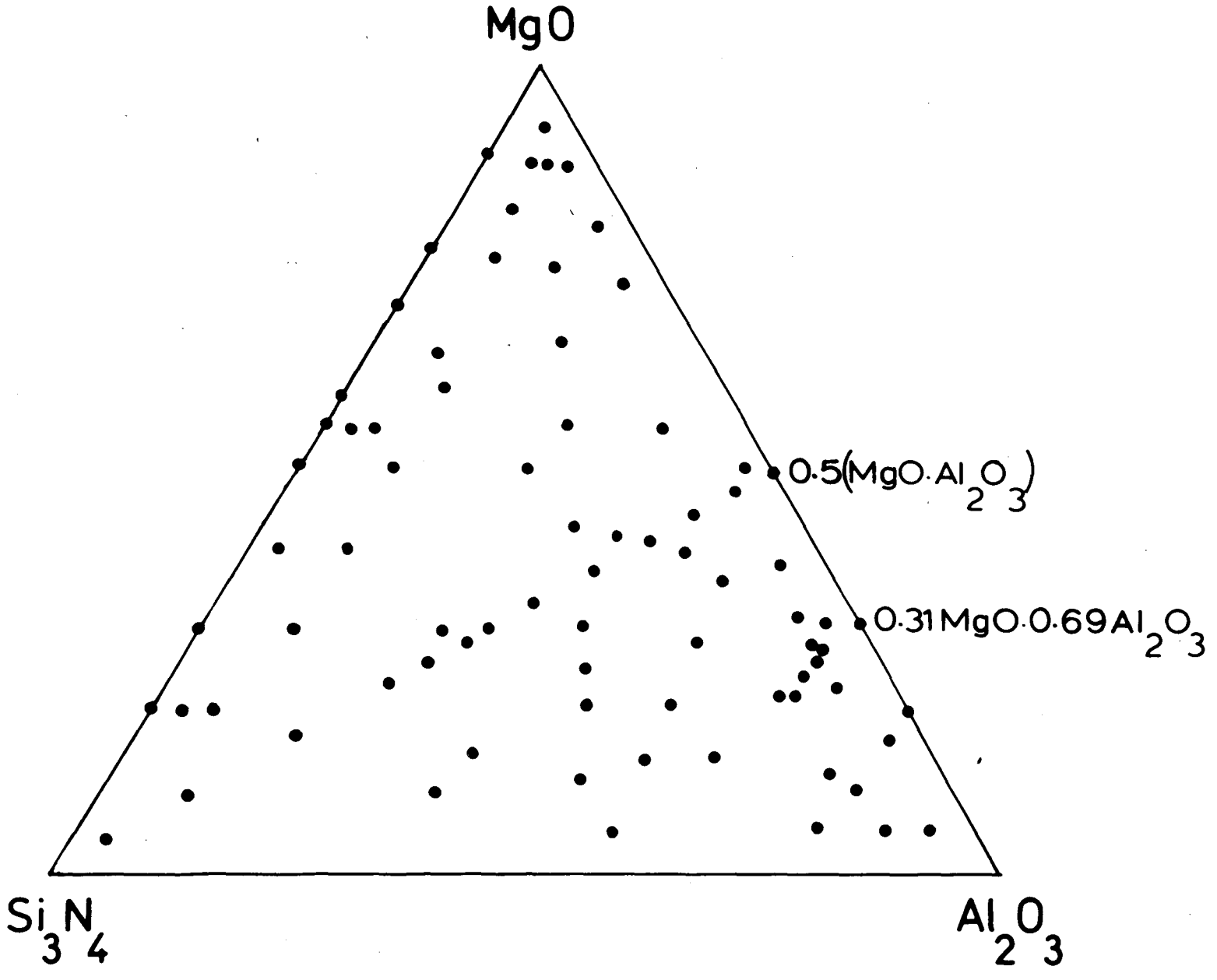

Figure VIII.2 Hot-pressed compositions in the $MgO-Al_2O_3-Si_3N_4$ sub-system

spinel structure can dissolve up to $4^m/o$ Si_3N_4 for Al_2O_3 contents of $50\text{-}70^m/o$.

Below the 3M:4X line and towards the Al_2O_3 rich corner another phase designated "N" appears; it is probably formed below the 3M:4X plane and the maximum amount observed was 20%. N-phase was also observed in the MgO-AlN-Si_3N_4 sub-system, in equilibrium with a vitreous phase and can best be described as a nitrogen-petalite, because the X-ray diffraction pattern is similar to petalite and is listed in Table VIII.1.

With increasing MgO ($30\text{-}40^m/o$) added to equal weights of Si_3N_4 and Al_2O_3 above the 3M:4X line 15R-magnesium sialon is formed together with forsterite and with further increase of MgO ($40\text{-}60^m/o$) a 12H-magnesium sialon phase appears. This is in agreement with the observation, when increasing amounts of MgO were hot-pressed with 15R-sialon to give the following sequence of products:

$$\text{15R-sialon} \xrightarrow{\text{MgO}} \text{15R-magnesium sialon + forsterite} \xrightarrow{\text{MgO}} \text{12H-magnesium sialon + forsterite}$$

The forsterite can be formed by the reaction of Si_3N_4 with MgO :

$$Si_3N_4 + 4MgO = 2MgSiN_2 + Mg_2SiO_4$$

The $MgSiN_2$ that is formed along the join Si_3N_4-MgO disappears with increasing Al_2O_3 because $MgSiN_2$ reacts

Table VIII.1 X-ray diffraction data for N-phase

Orthorhombic unit cell: $\underline{a}$ = 5.628, $\underline{b}$ = 14.328, $\underline{c}$ = 4.969 Å

$CuK\alpha_1$, 1.5.4051 Å

hkl	d_{calc}	d_{obs}	I_{obs}
020	7.164	7.192	vvw
110	5.239	5.232	vw
130	3.642	3.648	ms
111	3.605	3.606	s
040	3.582	3.586	ms
131	2.937	2.941	m
200	2.814	2.817	w
002	2.484	2.486	m
201	2.4496	2.451	m
022	2.347	2.351	vw
221	2.317	2.316	mw
151	2.271	2.270	vw
132	2.052	2.054	m
241	2.022	2.023	w
170	1.924	1.925	m
202	1.863	1.863	w
310	1.860		
171	1.794	1.793	mw
080	1.791		
330	1.746	1.746	m
172	1.521	1.522	mw
133	1.508	1.508	w
312	1.489	1.488	vw
082	1.453	1.453	vvw
281	1.446	1.445	vw
203	1.427	1.428	m
223	1.400	1.401	vvw
370	1.383	1.382	w
420	1.381		
401	1.354	1.354	vvw
243	1.326	1.326	w
440	1.310	1.309	w
173	1.255	1.255	mw
0.10.2	1.241	1.241	vvw
024	1.224	1.224	vw

with alumina to form 12H-magnesium sialon and forsterite (see section VIII.7), for example:

$$32MgSiN_2 + 20Al_2O_3 = 24\,(Mg_{1.25}Si_{1.125}Al_{1.67}O_{2.17}N_{2.56}) + Mg_2SiO_4 + 4SiO\uparrow + 1.28N_2\uparrow$$

At higher MgO concentrations ($\sim 80^m/o$) and higher temperatures ($\sim 1810^oC$) a small amount of 20H-magnesium sialon was observed; when the same compositions were hot pressed between 1600-1700°C, R-phase was formed.

VIII.2 The 3M:4X compositional plane

The behaviour diagram for this plane is given in Figure VIII.3 which was constructed from the results of hot-pressings carried out between MgO, Al_2O_3, SiO_2, Si_3N_4 and AlN at 1800°C for one hour. The hot-pressed compositions are shown in Figure VII.2; weight losses were less than 5% .

The β'-magnesium sialon phase region was discussed in detail in Chapter VII. Pure 15R-magnesium sialon phase is expected to exist in the 5M:6X plane while N-phase probably forms below the 3M:4X plane and so on the 3M:4X plane, mixtures of both phases would be expected. The data for the spinel-forsterite join are based on the results of Schlaudt & Roy (1965); the solubility of $MgAl_2O_4$ in forsterite is $0.5^m/o$ and the solubility of forsterite in $MgAl_2O_4$ is $5.0^m/o$ at 1720°C.

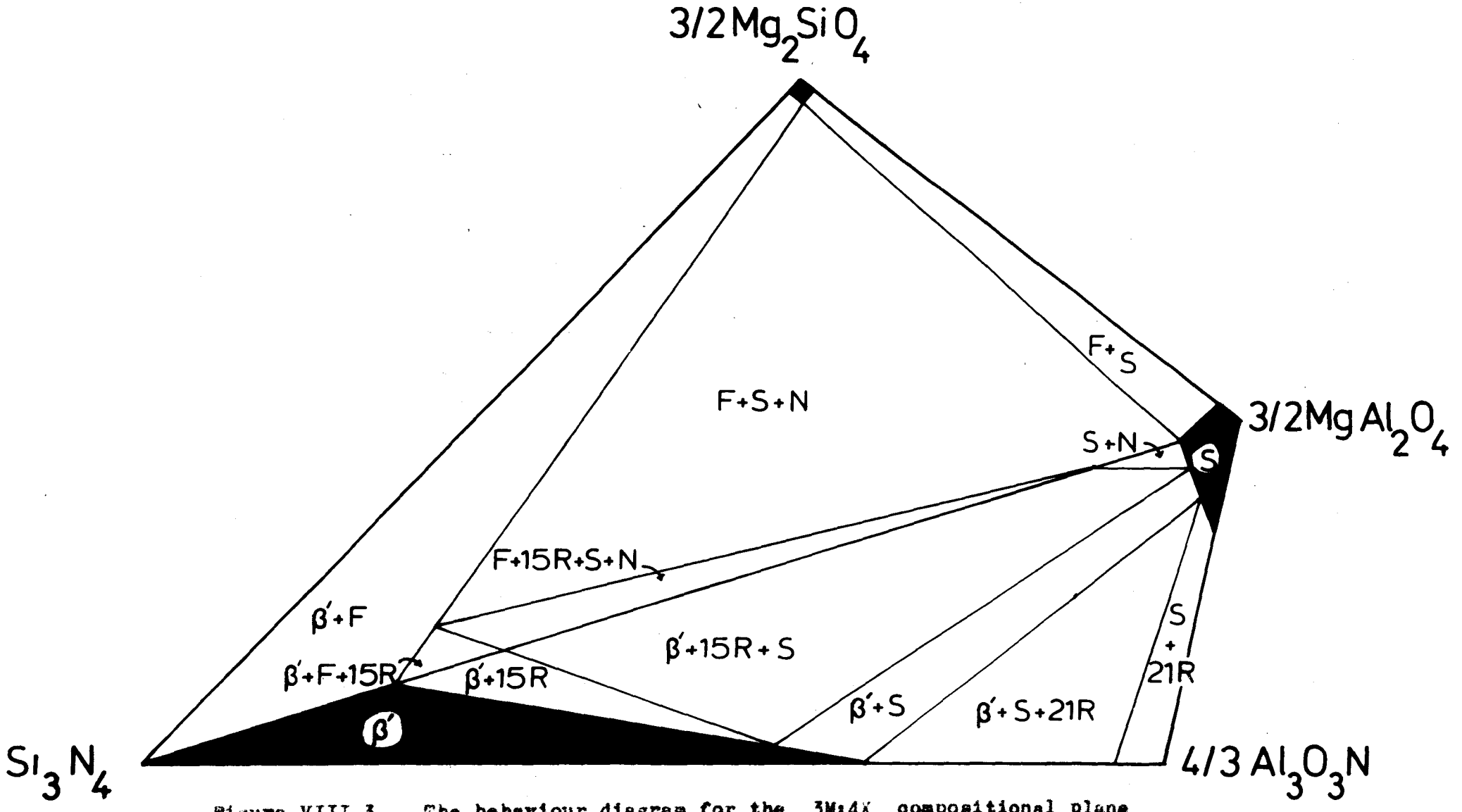

Figure VIII.3 The behaviour diagram for the 3M:4X compositional plane

Between forsterite and spinel, the two-phase region containing both was observed.

Near the Al_3O_3N corner of the 3M:4X plane spinel and 21R magnesium-sialon phases are formed. In the Si-Al-O-N system at compositions richer in Al_2O_3.AlN than the limit of β'-sialon solid solution, the 8H-sialon phase was observed; in this work it was not found.

VIII.3 The $6MgO-4AlN-Si_3N_4$ section

Compositions in this section were prepared by hot-pressing mixtures of Si_3N_4, AlN and MgO at 1700-1800°C for one hour. All the hot-pressed compositions are shown in Figure VIII.4 and the behaviour diagram is shown in Figure VIII.5. This system intersects all the planes of constant M:X from 3M:4X to 1M:1X .

The 20H-magnesium sialon phase was observed nearly pure with only a minor amount of AlN , but it has been drawn as a single-phase region. The traces of aluminium nitride are ignored because they are probably due to incomplete reaction of the larger AlN particles.

The phase designated as "L" ($MgAlSiN_3$) is formed nearly pure in the 1M:1X plane and the R-phase is identical to that observed previously along the MgO-AlN join. There are no anomalies in the observations which are not reconcilable with other sections of the Mg-Si-Al-O-N system.

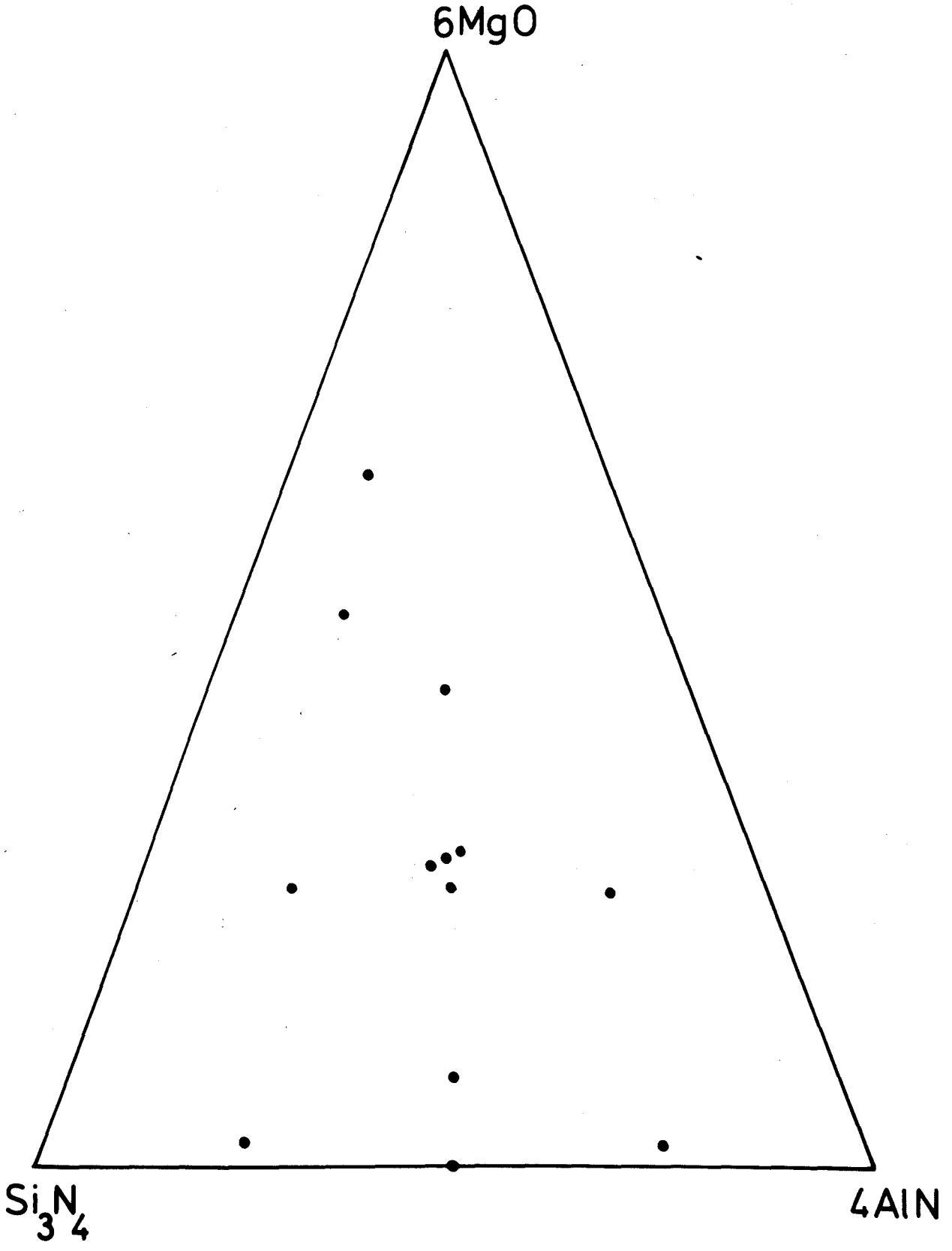

Figure VIII.4 Hot-pressed compositions in the $MgO-AlN-Si_3N_4$ sub-system

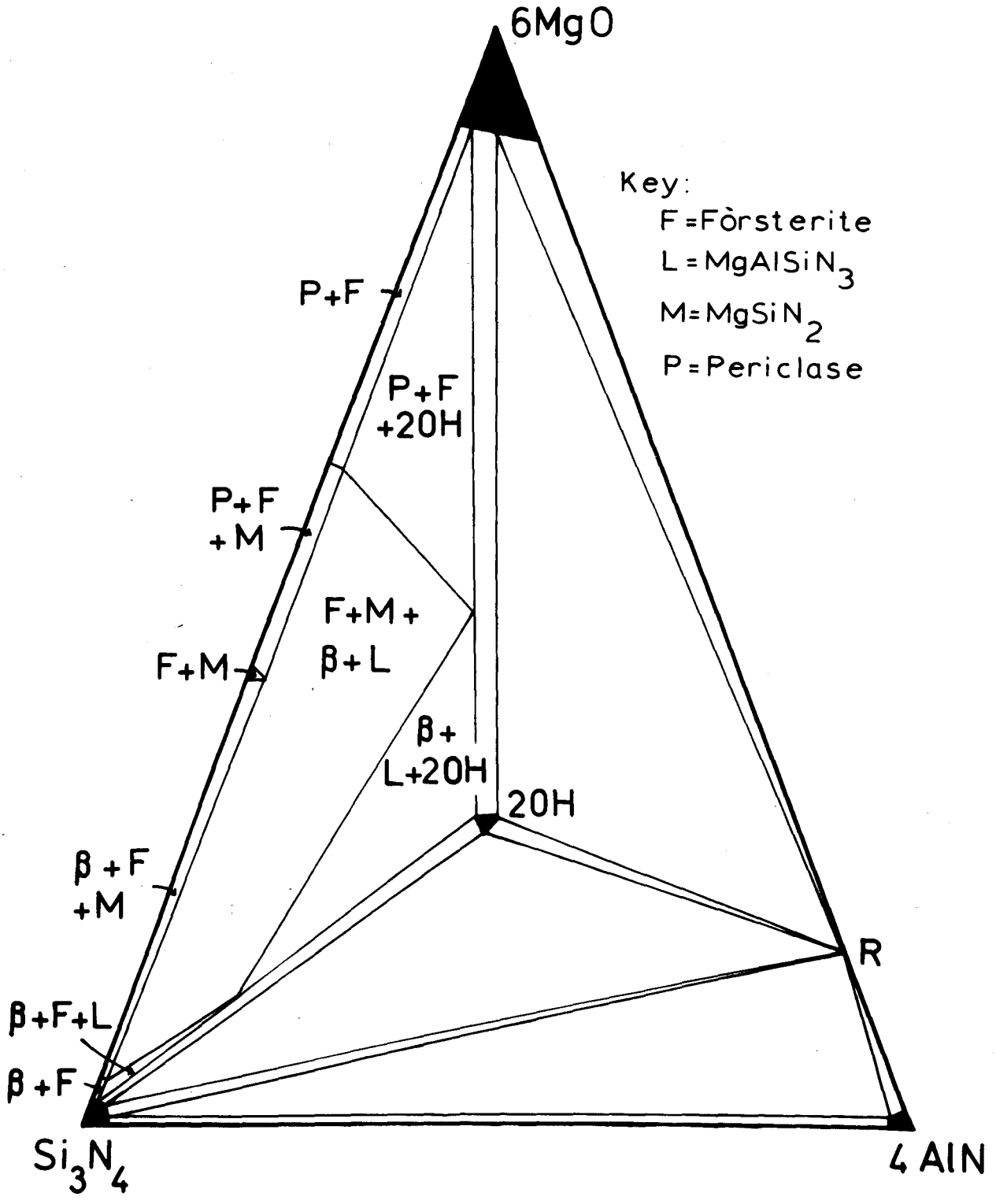

Figure VIII.5 The behaviour diagram for the $MgO-AlN-Si_3N_4$ sub-system at 1800°C

VIII.4 The 1M:1X compositional plane

The behaviour diagram for the 1M:1X plane is given in Figure VIII.6 and was constructed from the results of hot-pressing mixtures of Mg_3N_2, Si_3N_4, AlN and MgO at 1800°C for 30 minutes when weight losses were in the range 3-6%. Pre-prepared $MgSiN_2$ was not used but was formed in situ according to the equation:

$$Mg_3N_2 + Si_3N_4 = 3MgSiN_2$$

The structure of L-phase, observed nearly pure along the join $2MgSiN_2$-4AlN at the composition $Mg_{1.33}Al_{1.33}Si_{1.33}N_{4.00}$, is described in Chapter X.

VIII.5 The 5M:4X compositional plane

A few compositions in this plane were prepared by dry mixing Mg_3N_2, AlN, Si_3N_4 and MgO and hot pressing at 1500°C for 30 minutes. The batch weights were selected so that after volatilisation and oxidation of Mg_3N_2 (see Chapter V) the final composition would lie on the 5M:4X plane. The hot-pressed compositions and the observed phases are shown in Figure VIII.7. The X-ray reflexions of aluminium nitride after reaction were shifted from their normal positions corresponding to unit-cell dimensions of:

AlN^1 $\quad \underline{a} = 3.149$, $\quad \underline{c} = 4.959$ Å

AlN $\quad \underline{a} = 3.114$, $\quad \underline{c} = 4.986$ Å

where AlN^1 is the designation of the distorted structure.

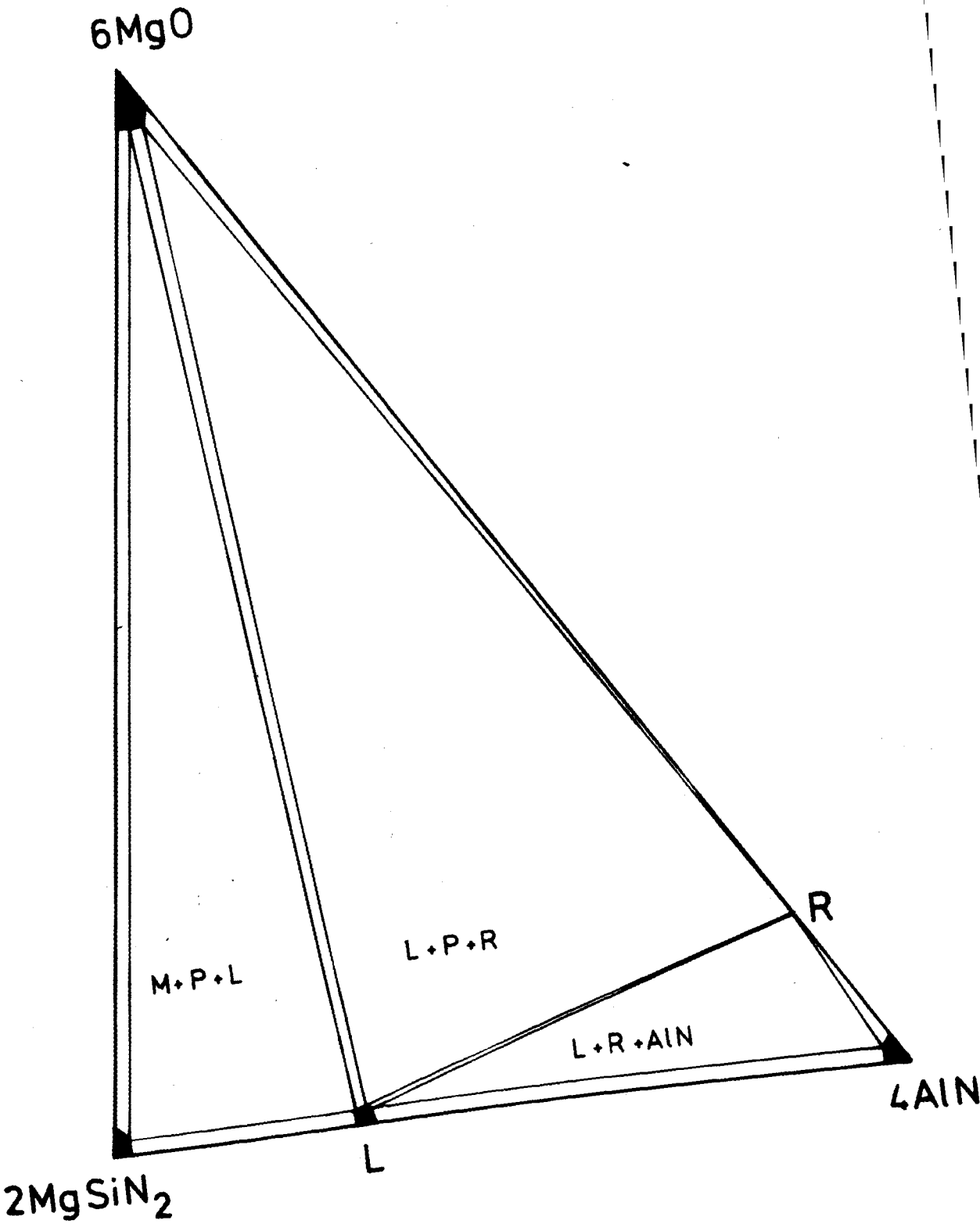

Figure VIII.6 The behaviour diagram for the 1m:1A compositional plane at 1800°C

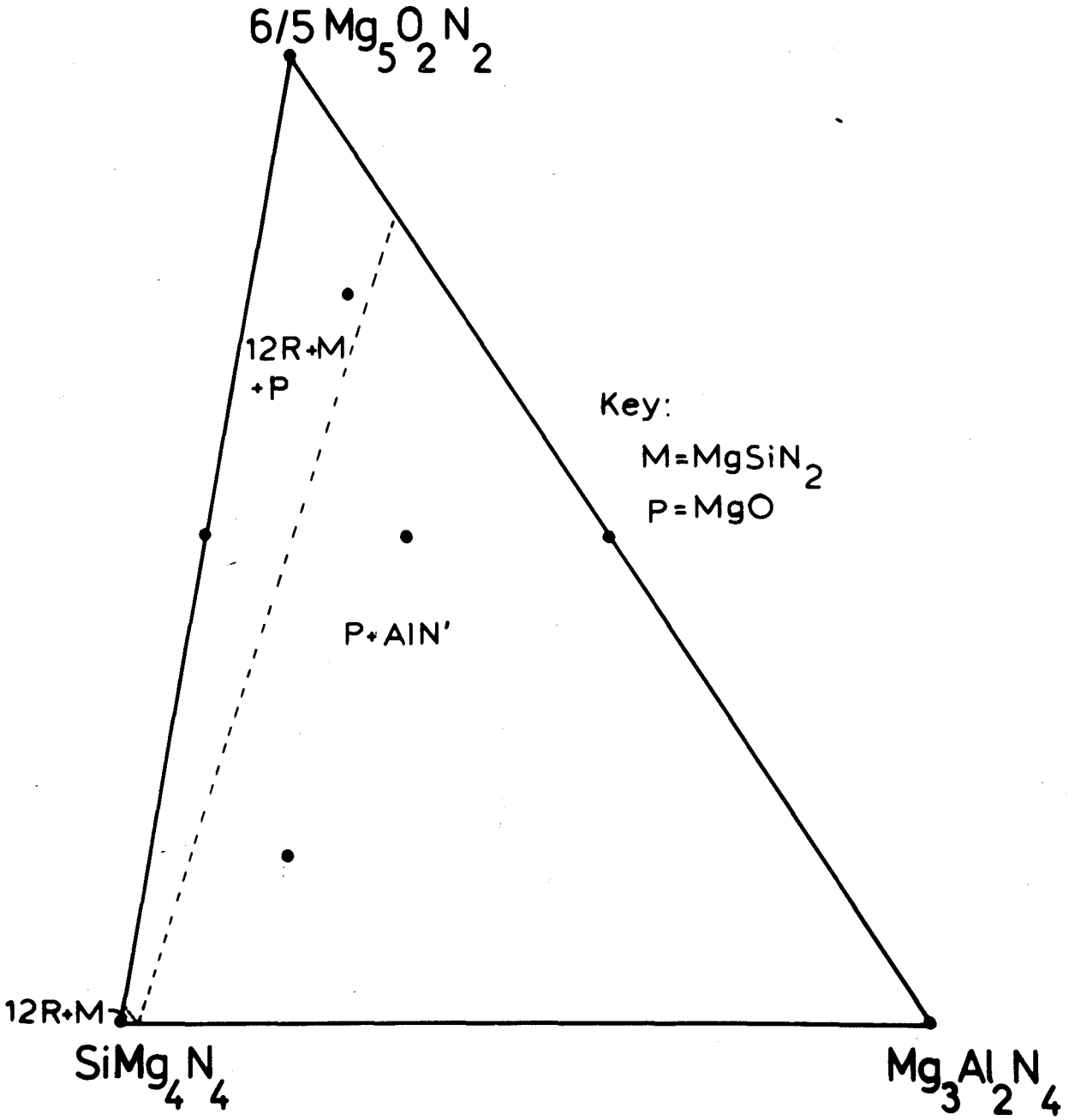

Figure VIII.7 Hot-pressed compositions and phase observations in the 5M:4X compositional plane

VIII.6 Triangular end-sections of the prism (Mg-Si-Al-O-N)

$MgO-Al_2O_3-SiO_2$ phase diagram has been investigated by Osborn & Muan (1960) and is given in modified form in Figure VIII.8 for convenience. The other triangular section Mg_3N_2-AlN-Si_3N_4 has been partially investigated in the present work and a tentative phase diagram is given in Figure VIII.9 from the observations made in the other sub-systems.

VIII.7 The $MgSiN_2$-Al_2O_3 join

The join between $MgSiN_2$ and Al_2O_3 was investigated by hot-pressing Mg_3N_2, Si_3N_4 and Al_2O_3 at 1750°C for 30 minutes. This join cuts across planes of constant M:X atom ratio as the composition varies from 1M:1X to 2M:3X and a schematic diagram to show the phases observed is given in Figure VIII.10. The polytypes are observed at lower M:X ratios than suggested by the starting compositions due to volatilisation of Mg_3N_2 but their order of appearance in going from $MgSiN_2$ to Al_2O_3 with decreasing M:X ratio is as expected; the weight losses of 10-20% were high.

VIII.8 Conclusion

The AlN-polytypes observed in the Si-Al-O-N system are also formed in Mg-Si-Al-O-N system along with new polytype phases. The appropriate polytype is

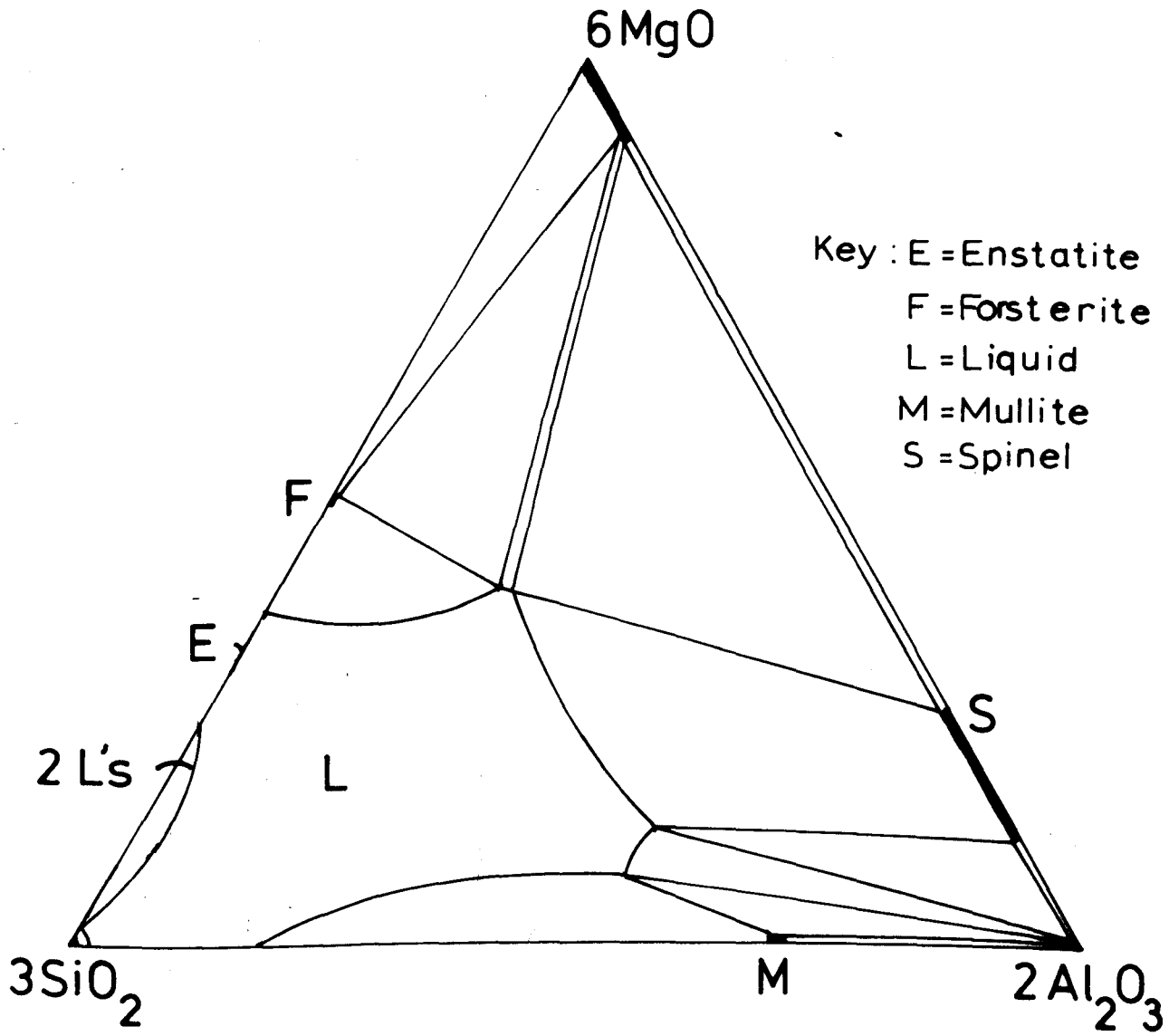

$MgO - Al_2O_3 - SiO_2$ Phase Diagram at 1700 °C

(After Osborn & Muan, 1960)

Figure VIII.8 The $MgO-Al_2O_3-SiO_2$ phase diagram at 1700°C .

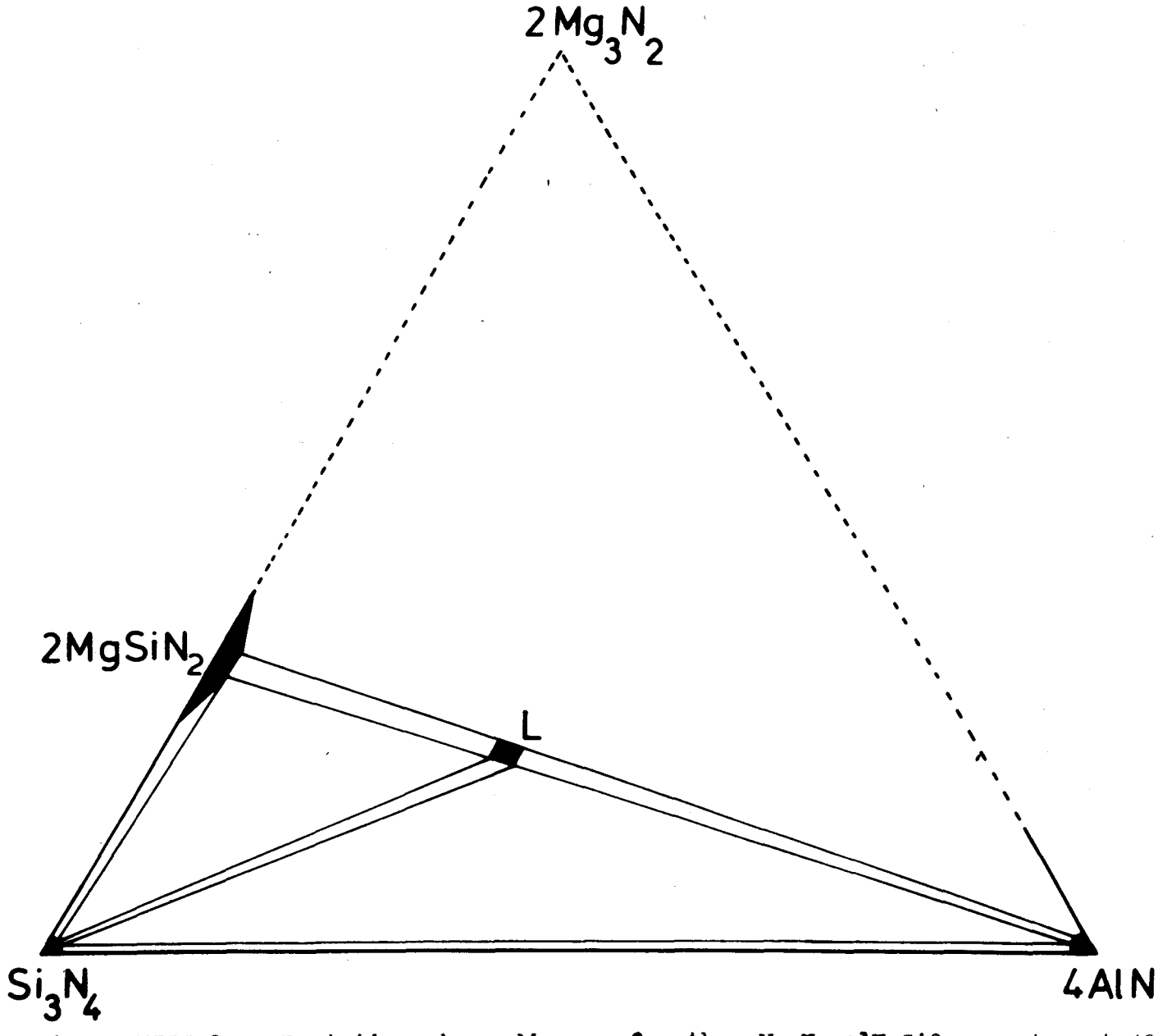

Figure VIII.9 Tentative phase diagram for the Mg_3N_2-AlN-SiO_2 system at 1800°C

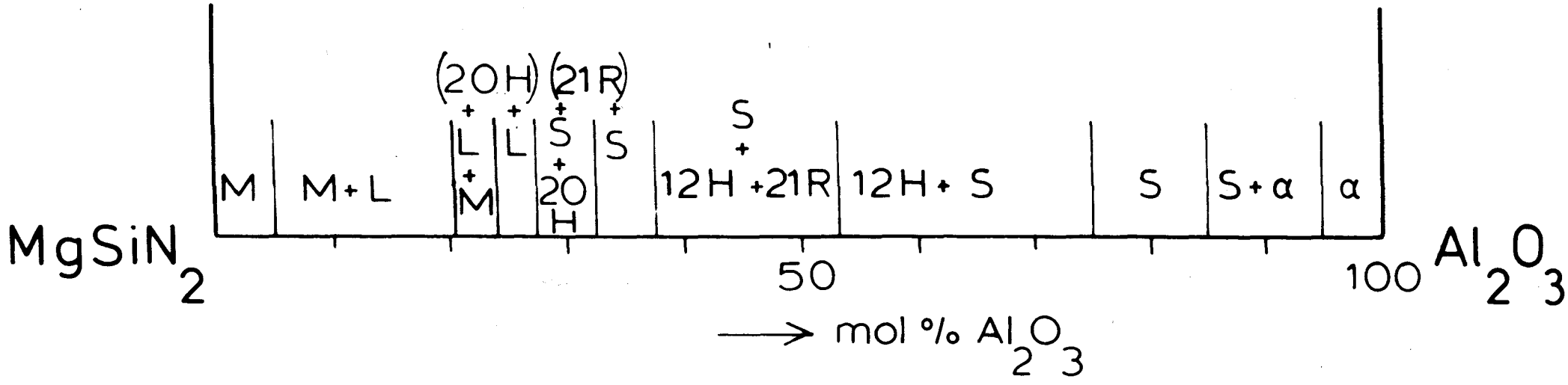

Key:

M = $MgSiN_2$

L = $MgAlSiN_3$

S = Spinel

α = Corundum

Figure VIII.10 A schematic representation of the behaviour of $MgSiN_2$-Al_2O_3 system at 1750°C

formed on the corresponding M:X plane or at a slightly lower M:X ratio due to volatilisation of Mg_3N_2. Further investigation of the constant 2M:3X, 5M:6X, 6M:7X, 7M:8X, 9M:10X and 6M:5X planes should give more information about phase relationships and enable more of the phases to be prepared pure.

IX. Aluminium Nitride Polytypes

IX.1 The structure of aluminium nitride

Aluminium nitride has wurtzite type structure, where the nitrogen atoms are in a hexagonal close-packed arrangement with aluminium atoms, also hexagonal close-packed, occupying one-half of the tetrahedral interstices of the nitrogen-atom packing. The two kinds of atoms are in equivalent positions (see Figure IX.1) with aluminium tetrahedrally co-ordinated by four nitrogens and similarly each nitrogen is tetrahedrally co-ordinated by four aluminium atoms. The stacking sequence of each kind of atom, Al or N, is ABABABAB.....

IX.2 Polytypism

Polytypism is a special kind of one-dimensional polymorphism, exhibited by certain close-packed and layer structures, e.g. SiC, CdI_2, ZnS. These are built up by stacking identical unit layers of structure and differ only in the stacking sequence of these layers. As a consequence, the unit-cell dimensions of the different polytypes are constant in two directions of the plane parallel to the layers and differ only in the stacking direction. Thus, the variable dimension of

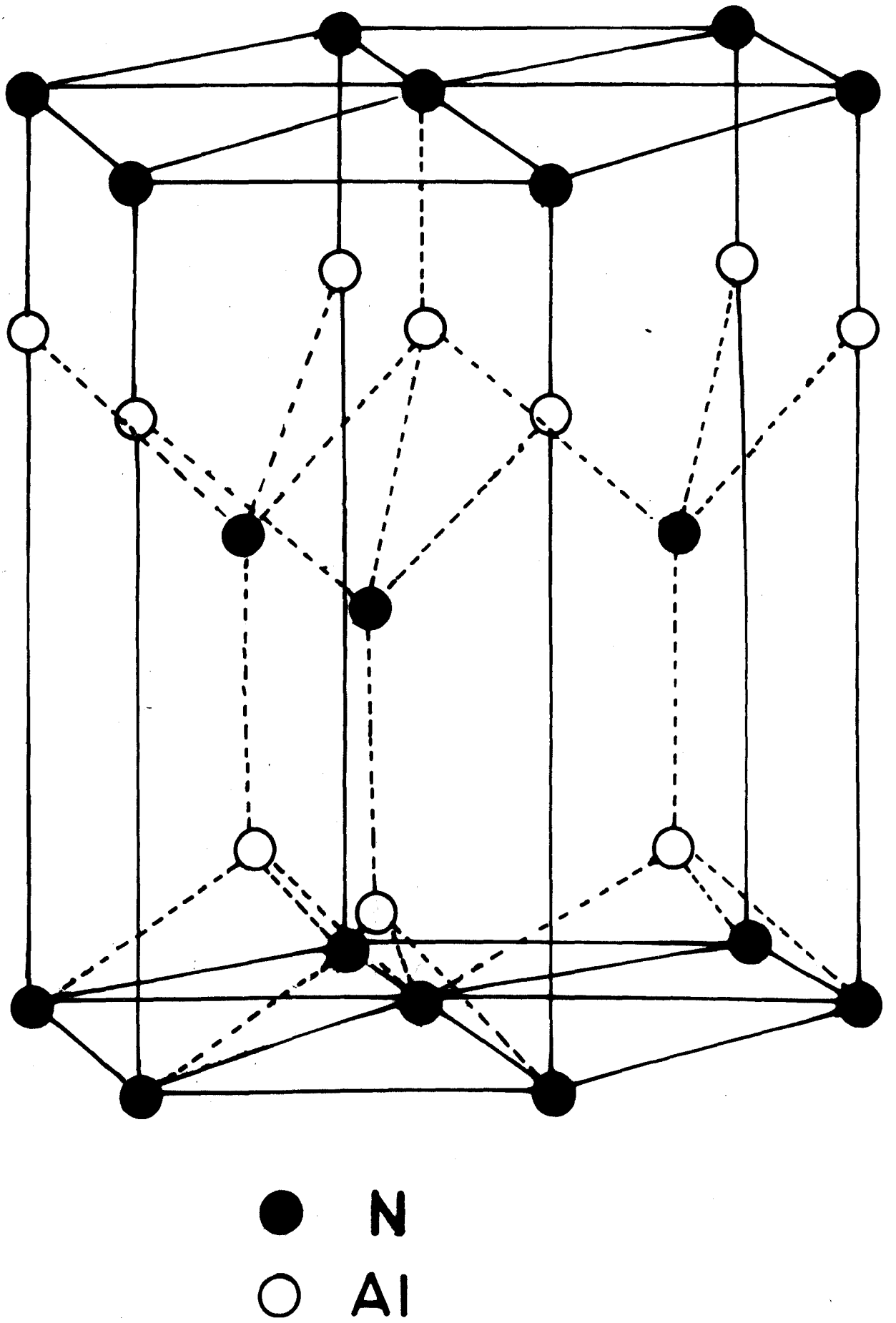

Figure IX.1 Structure of aluminium nitride

the unit-cell must be an integral multiple of a common unit whose value is determined by the distance between successive layers of structure. Polytypism is limited to structures in which the first co-ordination of some atom can be satisfied in more than one way, usually equivalent to cubic versus hexagonal close packing. The various modifications thus have the same first nearest-neighbour relationships and differ only in the second or higher co-ordinations. Therefore they have nearly the same potential energy and hardly differ even in their physical properties. However, the different stacking sequences may result in structures having not only different morphologies but even different lattice types and space groups.

There are special notations used to distinguish the larger number of structurally similar polytypic modifications but in the present work the notation used is due to Ramsdell (1947) and was first applied to SiC. He designated a SiC polytype by the number of layers in the unit cell and added to it the letter H or R to specify the lattice type. Thus a symbol nH represents a structure with a hexagonal cell having n layers along the repeat distance c ; nR represents a rhombohedral unit cell with n layers along c .

AlN-polytypes based on the Al-C-N system have been reported by Jeffrey & Wu (1963, 1966). The series of aluminium carbonitrides are expressed by $(AlN)_n.Al_4C_3$

with n=1 to 4 where the end members are n=0 and ∞, i.e. respectively Al_4C_3 and AlN. The members for which n is odd have space group symmetry $P6_3mc$ with two formula units per cell. Al_4C_3 and members for which n is even have space group symmetry $R\bar{3}m$ and one formula unit per rhombohedral cell.

IX.3 AlN-polytypes in the Si-Al-O-N system

In the Si-Al-O-N system (see Chapter II) six polytypes are observed: 8H, 15R, 12H, 21R, 27R and $2H^{\delta}$. Table IX.1 lists typical unit-cell dimensions for all the polytypes; each structure has a specific M:X composition ratio. The nR polytypes consist of three rhombohedrally-related blocks each of n/3 layers, while the hexagonal nH polytypes consist of two blocks related by a c-glide plane and each containing n/2 layers. Thus, the number of layers per symmetry related block in the five polytypes

	8H	15R	12H	21R	and	27R
is respectively	4	5	6	7	and	9

corresponding to the following M:X ratios

4:5	5:6	6:7	7:8	9:10

The 2H AlN structure with 1M:1X is the end member of this series but a similar 2H structure, designated $2H^{\delta}$, with an expanded c-dimension is obtained at M:X > 9:10

Table IX.1 Tetrahedral AlN-polytypes in the Si-Al-O-N system (after Jack, 1976)

M:X	type	a_h	c_h	c/n	a_r	α_r
4:5	8H	2.988	23.02	2.88		
5:6	15R	3.010	41.81	2.79	14.045	12.30
6:7	12H	3.029	32.91	2.74		
7:8	21R	3.048	57.19	2.72	19.144	9.12
9:10	27R	3.059	71.98	2.67	24.058	7.28
9:10	$2H^{\delta}$	3.079	5.30	2.65		
1:1	2H	3.114	4.986	2.49		

a_r and α_r are the dimensions of the equivalent rhombohedral cell

and $< 1:1$. Polytypes with n even are hexagonal and those with n odd are rhombohedral.

IX.4 15R-magnesium sialon

15R-magnesium sialon is observed when MgO, Si_3N_4, Al_2O_3 mixtures are hot-pressed near the composition $0.4MgO : 0.3Si_3N_4 : 0.3Al_2O_3$ (see Chapter VIII) and occurs most frequently as a minor phase in preparations involving β'-magnesium sialon. 15R-magnesium sialon was obtained 70-90% pure by the following preparative methods:

(1) $20^w/o$ MgO, $40^w/o$ α-Si_3N_4, $40^w/o$ Al_2O_3, hot-pressed at 1800^oC for 30 min.; forsterite and β'-sialon were present as minor phases;

(2) $20^w/o$ MgO, $45^w/o$ Al_2O_3, $35^w/o$ Si_3N_4 hot-pressed at 1700^oC for 30 min.; spinel and β' were minor phases;

(3) powdered β'-magnesium sialon (z=3.2) sintered in N_2 at 1670^oC for 3 hours gave 90% 15R and 10% of unchanged β'-magnesium sialon.

The X-ray diffraction pattern of the 15R-magnesium sialon obtained by method (3) was indexed (see Table IX.2) on the basis of a hexagonal unit cell of dimensions:

$$\underline{a} = 3.024 \text{ , } \underline{c} = 41.59 \text{ Å}$$

It is similar to the non-magnesium containing 15R which has unit-cell dimensions $\underline{a} = 3.010$, $\underline{c} = 41.81$ Å .

Table IX.2 X-ray diffraction data for 15R-magnesium sialon

hexagonal unit cell: $\underline{a}$ = 3.024, $\underline{c}$ = 41.59 Å Cu$K\alpha_1$, 1.54051 Å

rhombohedral unit cell: $\underline{a}$ = 13.971 Å, α = 12.42°

hkl	d_{calc}	d_{obs}	I_{obs}
003	13.86	13.83	w
0015	2.772	2.772	s
101	2.614	2.614	s
102	2.598	2.599	ms
104	2.539	2.537	ms
105	2.498	2.499	ms
107	2.396	2.396	s
108	2.339	2.339	mw
0018	2.312	2.312	mw
1010	2.216	2.217	mw
1011	2.153	2.153	m
0021	1.980	1.980	w
1014	1.964	1.964	mw
1016	1.845	1.844	ms
1017	1.788	1.787	ms
1019	1.679	1.680	mw
1020	1.628	1.614	vw
1022	1.533	1.533	m
110	1.512	1.511	vs
1023	1.488	1.490	m
1025	1.404	1.406	ms
1026	1.365	1.365	ms
1115	1.327	1.328	s
201	1.307	1.307	m
1028	1.292	1.292	m
207	1.279	1.279	m
208	1.270	1.270	m
1031	1.194	1.194	w

The structure suggests that 15R-magnesium sialon must occur pure on the 5M:6X plane.

IX.5 12H-magnesium sialon

12H magnesium sialon was first observed by Bell & Wilson (1973) when 40-60^{m}/o MgO was added to equal weights of Si_3N_4 and Al_2O_3 and hot-pressed at 1600-1800^{o}C. In the present work it is observed over a wide region in the $MgO-Al_2O_3-Si_3N_4$ sub-system (Chapter VIII), and has a range of homogeneity as suggested by different unit-cell dimensions. The indexed diffraction data for the 12H-magnesium sialon is listed in Table IX.3. It was prepared by hot-pressing 35^{w}/o MgO, 32.5^{w}/o Si_3N_4 and 32.5^{w}/o Al_2O_3 at 1800^{o}C for 30 min. The product contained forsterite and 20H-magnesium sialon as impurities. The forsterite was removed by powdering the product to -300 mesh, digesting with hot aqua regia for 30 minutes, filtering and then washing continuously with water until free of acid.

The 12H-magnesium sialon phase was prepared 95% pure in the 6M:7X plane by Buang (1976) at Newcastle. The unit-cell dimensions of the various 12H phases so far examined are:

$MgO-Al_2O_3-Si_3N_4$ system (present work): $\underline{a}$ = 3.073 , $\underline{c}$ = 32.65 Å

6M:7X plane, $Mg_{1.25}Al_{1.67}Si_{1.125}O_{2.17}N_{2.56}$ (after Buang):

$\underline{a}$ = 3.072 , $\underline{c}$ = 32.64 Å

Table IX.3 X-ray diffraction data for 12H-magnesium sialon

hexagonal unit cell: $\underline{a}$ = 3.073, $\underline{c}$ = 32.65 Å Cu$k\alpha_1$, 1.54051 Å

hkl	d_{calc}	d_{obs}	I_{obs}
0012	2.721	2.721	m
100	2.661	2.661	s
101	2.652	2.653	s
102	2.623	2.623	vvw
103	2.585	2.581	mw
104	2.530	2.532	vvw
105	2.464	2.466	mw
106	2.390	2.390	mw
0014	2.332	2.332	vvw
107	2.317	2.317	vvw
108	2.229	2.224	m
1011	1.981	1.979	vvw
1012	1.902	1.902	vw
1013	1.826	1.826	mw
110	1.536	1.539	s
1018	1.499	1.500	m
0022	1.484	1.484	w
1022	1.391	1.392	w
1112	1.338	1.338	m
1022	1.296	1.296	mw
1114	1.283	1.284	mw

$40^{w}/o MgO, 30^{w}/o Si_3N_4, 30^{w}/o Al_2O_3, 1700^{o}C, 1h$ (after Bell & Wilson, 1973):

$\underline{a} = 3.067$, $\underline{c} = 32.68$ Å

12H sialon (after Jack, 1976): $\underline{a} = 3.029$, $\underline{c} = 32.91$ Å

IX.6 21R-polytype phase

A 21R polytype was obtained about 80% pure in the $MgO-Al_2O_3-AlN-Mg_3N_2$ system (Chapter VI) when $50^{m}/o$ MgO and $50^{m}/o$ AlN were hot-pressed at $1850^{o}C$ for one hour. The indexed diffraction data are listed in Table IX.4. Non-magnesium containing 21R polytype was prepared by hot-pressing $50^{m}/o$ Al_2O_3 with $50^{m}/o$ AlN at $1800^{o}C$ for one hour and had spinel and AlN as minor impurity phases. The unit cell of these two 21R polytypes are:

21R (Mg, Al) (O, N) : $\underline{a} = 3.054$, $\underline{c} = 57.17$ Å

21R Al (O, N) : $\underline{a} = 3.048$, $\underline{c} = 57.19$ Å

IX.7 "R"-phase

The phase designated as "R" first observed in the $MgO-Al_2O_3-Si_3N_4$ system by Bell & Wilson (1973) was prepared 70% pure in the present work by hot-pressing $74^{m}/o$ MgO, $11^{m}/o$ Si_3N_4, $15^{m}/o$ Al_2O_3 at $1650^{o}C$ for one hour. It is indexed on a hexagonal unit cell (see Table IX.5) and is similar to the $2H^{\delta}$ structure with an expanded $\underline{c}$-dimension relative to AlN. It therefore probably has additional non-metal atoms M:X > 9:10

Table IX.4 X-ray diffraction data for 21R-(Mg,Al)(O,N) polytype

hexagonal unit cell: $\underline{a}$ = 3.054, $\underline{c}$ = 57.17 Å

rhombohedral unit cell: $\underline{a}$ = 19.141 Å, = 9.15°

hkl	d_{calc}	d_{obs}	I_{obs}
0021	2.723	2.728	m
101	2.642	2.642	s
102	2.633	2.632	m
104	2.600	2.600	vw
105	2.576	2.577	mw
107	2.516	2.516	vw
108	2.480	2.480	mw
1010	2.400	2.400	s
0024	2.382	2.385	w
1011	2.357	2.357	mw
1013	2.266	2.266	mw
1014	2.220	2.220	w
0027	2.118	2.118	vw
1017	2.079	2.079	vvw
1019	1.986	1.990	m
1020	1.941	1.941	w
1022	1.854	1.854	m
1023	1.811	1.811	vw
1025	1.730	1.730	vw
1026	1.691	1.691	vvw
1028	1.617	1.618	vvw
110	1.527	1.526	s
1031	1.513	1.513	w
1032	1.480	1.480	mw
1034	1.419	1.419	vw
1035	1.390	1.389	m
1118	1.376	1.375	vvw
0042	1.361	1.361	vvw
1037	1.334	1.334	w
1121	1.332	1.331	m
201	1.322	1.321	mw
202	1.321		
204	1.317	1.314	vvw
205	1.313		
207	1.305	1.300	vvw
208	1.300		
2010	1.288	1.288	w
1124	1.285	1.285	m
2011	1.281	1.281	vw
2014	1.258	1.259	mw
1040	1.257		
2016	1.240	1.239	w
1127	1.238		
2020	1.200	1.200	vw

Table IX.5 X-ray diffraction data for R-phase

hexagonal unit cell: $\underline{a}$ = 3.090, $\underline{c}$ = 5.253 Å $CuK\alpha_1$, 1.54051 Å

hkl	d_{calc}	d_{obs}	I_{obs}
100	2.675	2.669	vs
002	2.626	2.625	ms
101	2.384	2.383	s
102	1.875	1.875	s
110	1.545	1.543	s
111	1.482	1.489	ms
103	1.465	1.464	ms
200	1.338	1.337	mw
112	1.332	1.332	s
201	1.297	1.296	ms
202	1.192	1.192	ms
104	1.179	1.177	vvw

with disordered stacking faults.

R phase is also observed in the quasi-ternary system Mg-Al-O-N at the composition 0.2MgO:0.8AlN when mixtures of MgO and AlN are hot pressed at 1800°C for 30 min. The X-ray reflexions are diffuse, suggesting a range of homogeneity, and it was not possible to obtain accurate unit-cell dimensions.

IX.8 20H-magnesium sialon

20H-magnesium sialon was obtained nearly pure in the MgO-AlN-Si_3N_4 sub-system (Chapter VIII) by the following preparative route:

(a) the two following compositions (i) 30^w/o Si_3N_4, 36^w/o MgO, 34^w/o AlN, (ii) 30^w/o Si_3N_4, 38^w/o MgO, 32^w/o AlN were hot-pressed separately at 1700°C for one hour to give respective reaction products (i) 70% 20H-phase, 20% AlN, 10% L-phase, trace MgO and (ii) 70% 20H-phase, 20% AlN, 5% L-phase, 5% MgO.

(b) The two products (i) and (ii) were powdered, sieved to -300 mesh, mixed in equal weight proportions and then hot-pressed again at 1800°C for one hour: the product had 90% 20H-phase, 5% AlN and 5% L-phase.

The indexed X-ray diffraction data are listed in Table IX.6. There is no corresponding phase in the Si-Al-O-N system.

The starting composition of the 20H-magnesium sialon was $Si_{2.7}Al_{3.3}Mg_{4.0}O_{4.0}N_{7.0}$, which has the expected 10M:11X ratio. The theoretical density of

Table IX.6 X-ray diffraction data for 20H-magnesium sialon

hexagonal unit-cell: $\underline{a}$ = 3.096, $\underline{c}$ = 52.53 Å cukα_1, 1.54051 Å

hkl	d_{calc}	d_{obs}	I_{obs}
100	2.681	2.681	vs
101	2.678	2.678	vs
102	2.667	2.665	vw
103	2.650	2.650	vw
104	2.627	2.626	s
0020	2.626		
105	2.598	2.612	m
106	2.564	2.564	vvw
107	2.525	2.526	vvw
108	2.482	2.487	m
109	2.436	2.457	ms
1010	2.388	2.386	s
1011	2.338	2.339	vvw
1012	2.286	2.284	w
1014	2.181	2.182	vvw
1015	2.129	2.130	vvw
1016	2.077	2.077	vvw
1018	1.974	1.974	vvw
1020	1.876	1.874	s
1021	1.829	1.828	m
110	1.548	1.548	s
112	1.545	1.545	s
1030	1.466	1.465	ms
1112	1.459	1.461	mw
1116	1.400	1.402	m
200	1.341	1.341	mw

3.22g cm^{-3} is in reasonable agreement with the measured value of 3.16g cm^{-3}.

IX.9 6H and 12R polytype phases

Towards the Mg_3N_2-rich corner of the Mg_3N_2-Si_3N_4-SiO_2-MgO system (Chapter VI) 6H and 12R polytypes are observed, the indexed powder data for which are listed in Tables IX.7 and 8 respectively. The 6H-polytype was prepared 80-85% pure by hot-pressing at 1450°C for 30 min. any one of the following compositions:

(i) Mg_3N_2 (MgO formed in situ by oxidation)

(ii) 98^w/o Mg_3N_2 , 2^w/o MgO

(iii) 96^w/o Mg_3N_2 , 2^w/o MgO , 2^w/o Al_2O_3

The minor phases associated with the above hot pressings were MgO, and 12R polytype and weight losses varied in the range 8-15%. 6H is essentially a Mg-O-N polytype which can dissolve Al_2O_3 or $MgSiN_2$ to a limited extent.

The 12R polytype was prepared by hot-pressing 84^w/o Mg_3N_2, 11^w/o Al_2O_3, 5^w/oSi_3N_4 at 1550°C for one hour. The X-ray photograph showed about 50% 12R, 25% MgO and 25% distorted AlN. It was found in lower yield when Mg_3N_2-Si_3N_4 compositions were hot-pressed (Chapter VI). The X-ray indexing and hence the structure suggest that the ratio of metal to non-metal atoms should be 4M:3X for 6H and 5M:4X for 12R. The unit-cell dimensions compared with AlN are:

Table IX.7 X-ray diffraction data for 6H-polytype

hexagonal unit cell: $\underline{a}$ = 3.549, $\underline{c}$ = 15.99 Å $CuK\alpha_1$, 1.54051 Å

hkl	d_{calc}	d_{obs}	I_{obs}
002	8.00	7.99	m
004	4.00	4.00	mw
100	3.073	3.075	ms
101	3.018	3.017	vs
006	2.667	2.663	ms
103	2.663	-	
104	2.437	2.437	s
105	2.216	2.215	w
106	2.014	2.014	m
008	2.000	2.000	m
107	1.834	1.833	m
110	1.774	1.744	vs
112	1.732	1.773	vvw
114	1.622	1.622	vw
200	1.537	1.537	w
201	1.530	1.530	mw
203	1.476	1.476	m
204	1.434	1.434	mw
118	1.327	1.327	m
1012	1.223	1.223	mw

Table IX.8 X-ray diffraction data for 12R-magnesium sialon

hexagonal unit cell: $\underline{a}$ = 3.442, $\underline{c}$ = 31.33 Å CuKα_1, 1.54051 Å

rhombohedral unit cell: $\underline{a}$ = 10.629 Å, α = 18.64

hkl	d_{calc}	d_{obs}	I_{obs}
003	10.44	10.37	m
009	3.48	3.48	w
101	2.967	2.968	s
102	2.927	2.927	m
104	2.786	2.787	ms
0012	2.610	2.609	m
107	2.481	2.480	m
108	2.372	2.372	w
1010	2.159	2.159	w
0015	2.088	2.088	mw
1013	1.874	1.874	mw
1014	1.790	1.790	w
110	1.721	1.721	ms
118	1.575	1.574	vw
1017	1.567	1.567	vw
207	1.414	1.414	w
1022	1.285	1.285	m

AlN $\underline{a} = 3.114$, $\underline{c} = 4.986$ Å

6H $\underline{a} = 3.549$, $\underline{c} = 15.99$ Å

12R $\underline{a} = 3.442$, $\underline{c} = 31.33$ Å

The $\underline{c}$-dimensions of AlN, 6H and 12R are in approximate ratios of 1:3:6 . This suggests that 6H has 3 layers to a block and it has 2 blocks per repeat distance, while 12R has 4 layers to a block and a repeat distance consisting of 3 blocks. In Be-Si-O-N system (Huseby et al, 1975; Thompson, 1976) a series of polytypes exactly antitypic to the Si-Al-O-N polytypes was observed. The 6H and 12R polytypes are similar to the Be-Si-O-N polytypes but it would appear that the 6H Mg-O-N polytype is analogous to the 9R Be-Si-O-N polytype, and similarly the 12R polytype to the 8H Be-Si-O-N polytype; whereas the beryllium polytypes have a basically hexagonal close-packed non-metal arrangement, the magnesium polytypes have a basically cubic close-packed non-metal arrangement related to cubic Mg_3N_2 .

IX.10 Conclusion

The polytypes in the Si-Al-O-N and related systems based upon AlN represent a new kind, the structures of which are determined by the metal:non-metal atom-ratio, M:X. The following AlN polytype sialons containing magnesium are observed in the Mg-Si-Al-O-N system:

6H	12R	15R	12H	21R	20H	2H[δ]
4M:3X	5M:4X	5M:6X	6M:7X	7M:8X	10M:11X	> 10M:11X
						< 1M:1X

The relationship between mechanical properties and the microstructure of nitrogen ceramics is not known in detail but it is suggested by Komeya, Inoue & Tsuge (1974) that a fibrous morphology (such as that of AlN-polytypes) is advantageous.

The high-temperature properties of some of the AlN-polytypes need further investigation because aluminium nitride itself is a candidate for high-temperature engineering applications and so the polytypes based upon it might well offer improvements, particularly in chemical properties.

X. The Crystal Structure of Magnesium Aluminium Silicon Nitride

X.1 Introduction

The crystal chemistry of ternary nitrides is well documented and some of these have been discussed in Chapter II. Wild, Grieveson & Jack (1972) observed that there was some solid solubility between $MgSiN_2$ and AlN, and discussed the possibility of forming quaternary metal-aluminium-silicon nitride phases of the type $(M,Si,Al)N_2$. An extensive literature search now shows that the $MgSiAlN_3$ prepared in the present work is the first quaternary nitride reported (see Chapter VIII).

X.2 Preparation of pure $MgAlSiN_3$

The maximum amount of the quaternary nitride (L-phase) was observed at the composition $Mg_{1.33}Al_{1.33}Si_{1.33}N_4$. Table X.1 lists compositions that were hot pressed near this to obtain a purer product. In different runs the X-ray reflexions were slightly shifted showing that there was a limited homogeneity range. The highest purity material was prepared by having $3^w/o$ Mg_3N_2 in excess of that required for $Mg_{1.33}Al_{1.33}Si_{1.33}N_4$. It was therefore prepared by hot-pressing $29^w/o$ Mg_3N_2, $38^w/o$ Si_3N_4, $33^w/o$ AlN at 1800^oC for 30 min.; it showed about 90-95% $MgSiAlN_3$ and 5-10% 20H-magnesium

Table X.1 Compositions hot-pressed to prepare $MgAlSiN_3$

	composition*	conditions	X-ray analysis
1.	$Si_{1.5}Al_{1.0}Mg_{1.5}N_{4.0}$	1700°C, H.P., ½h	50%L, 25%AlN, 25%2OH
2.	$Si_{1.33}Al_{1.33}Mg_{1.33}N_{4.0}$	1700°C, H.P., ½h	80%L, 15%AlN, 5%2OH
3.	$SiAl_2MgN_{4.0}$	1700°C, H.P., ½h	70%L, 30%AlN
4.	$Si_{1.33}Al_{1.33}Mg_{1.33}N_{4.0}$	1800°C, H.P., ½h	90-95%L, 5-10%2OH
5.	$Si_{1.33}Al_{1.33}Mg_{1.33}N_{4.0}$	1800°C, H.P., 1h	85%L, 15%2OH
6.	$Si_{1.29}Al_{1.29}Mg_{1.49}N_{4.0}$ (M:X > 1)	1800°C, H.P., ½h	85%L, 10%2OH, 5% H
7.	$Si_{1.32}Al_{1.36}Mg_{1.32}N_{3.96}O_{0.06}$ (M:X < 1)	1750°C, H.P., 1h	85%L, 15%2OH

* runs 1-6 prepared from Si_3N_4, Mg_3N_2 and AlN

run 7 prepared from Si_3N_4, Mg_3N_2, AlN and Al_2O_3

sialon; the weight loss was 3%.

X.3 Unit-cell determination

The following unit-cell dimensions were obtained from 19cm powder photographs taken with LiF monochromated FeKα radiation by Nelson-Riley extrapolation as described in Chapter IV:

$\underline{a}$ = 5.439 ± 0.002 , $\underline{b}$ = 9.399 ± 0.002 , $\underline{c}$ = 4.923 ± 0.002 Å

and are compared with those of $MgSiN_2$ and AlN in Table X.2. The X-ray diffraction pattern was similar to those of $LiSi_2N_3$ and AlN (Figure X.1) and the impurity phase 20H did not show overlaps with any of the $MgAlSiN_3$ reflexions. The strong reflexions of $MgAlSiN_3$ correspond closely in intensity with those of AlN, whilst the "super lattice reflexions" are extremely weak. $MgAlSiN_3$ clearly has a wurtzite-type structure. The cell volume increases only very slightly (see Figure X.2) but the departure from hexagonality increases as Mg+Si increasingly replace Al in the sequence

$$AlN \longrightarrow Mg_{0.33}Si_{0.33}Al_{0.33}N \longrightarrow Mg_{0.5}Si_{0.5}N$$

The powder density of $MgAlSiN_3$, 3.15g cm^{-3}, is in reasonable agreement with the calculated value of 3.20g cm^{-3}.

X.4 Space group

Systematically absent reflexions are hkl with h+k odd

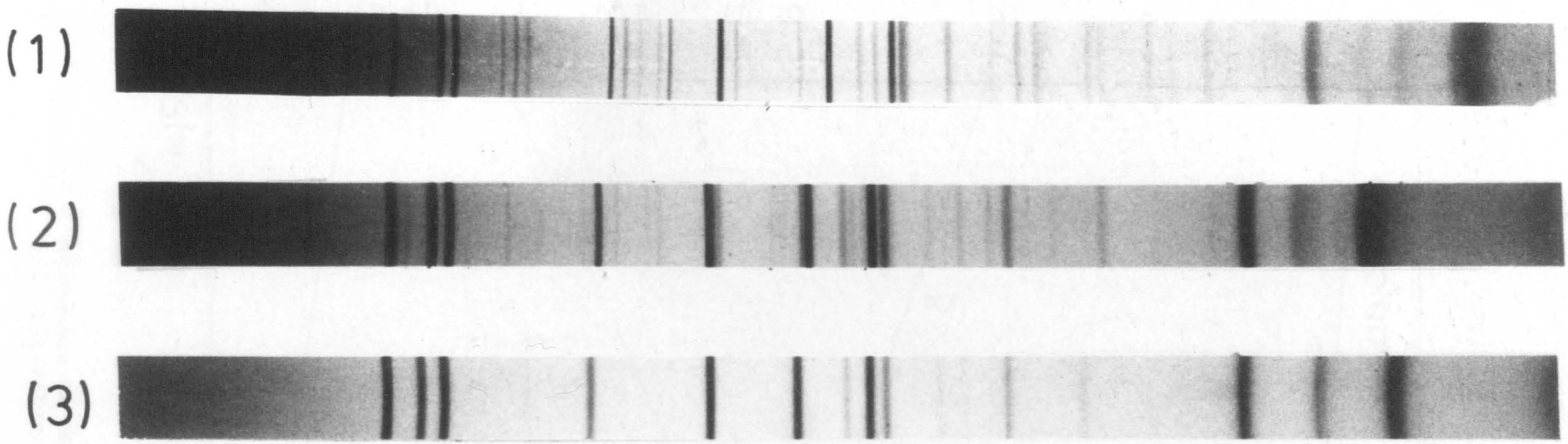

(1) $LiSi_2N_3$ (2) $MgAlSiN_3$ (3) AlN

Figure X.1 19 Cm Powder Photographs on Fe Kα Radiation

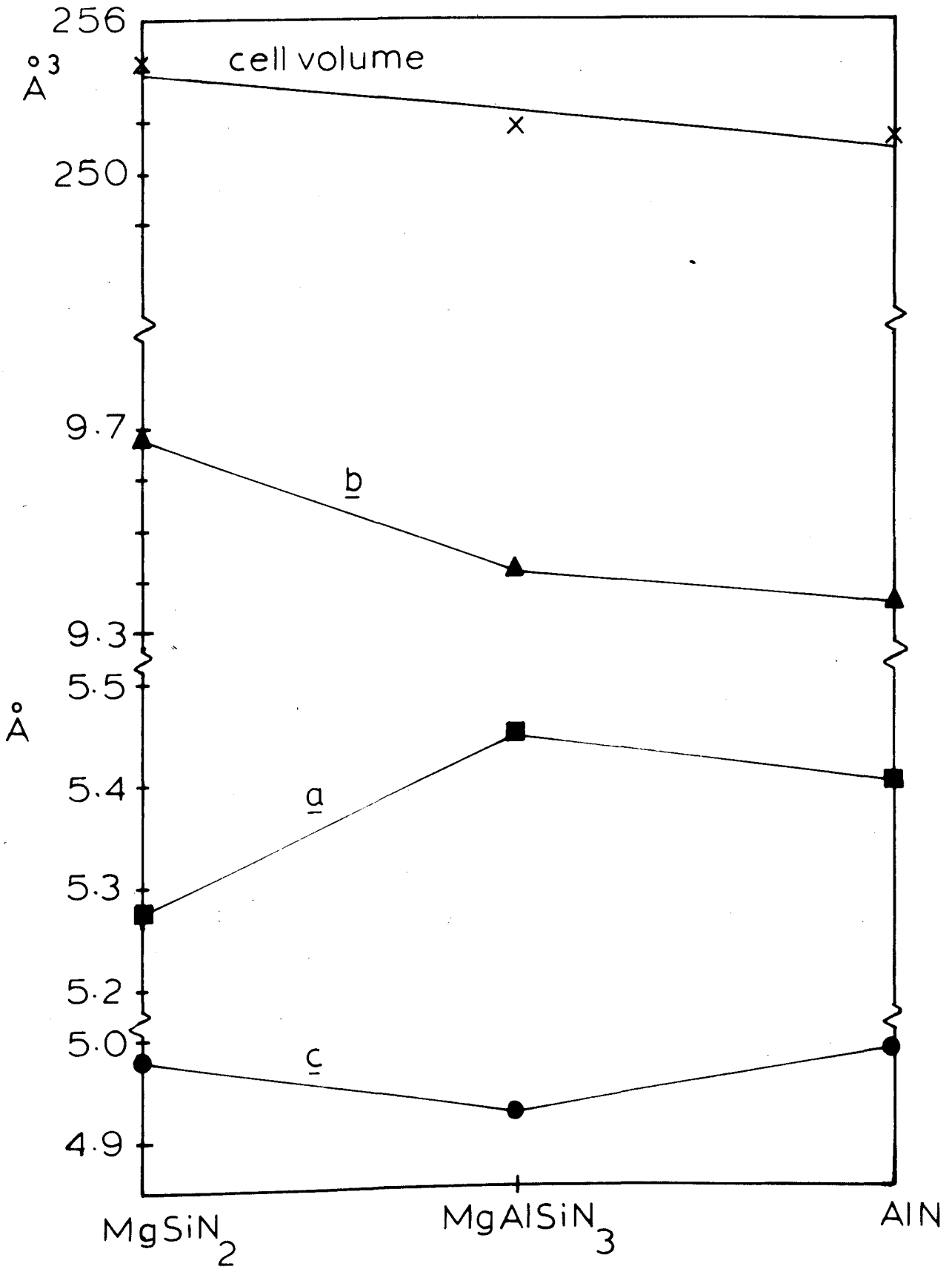

Figure X.2 Variation of unit-cell dimensions and cell-volume for nitrides

Table X.2 Orthorhombic unit-cell dimensions of nitrides

	a(= $\sqrt{3}$a')Å	b(=3a')Å	c=c' Å	b/a	cell volume Å^3
AlN	5.394	9.342	4.986	1.732	251.2
$MgAlSiN_3$	5.439	9.399	4.923	1.728	251.7
$MgSiN_2$	5.275	9.683	4.978	1.836	254.3

where a' and c' are the dimensions of the equivalent pseudo-hexagonal unit

and okl with l odd. Possible space groups are Cc2m (No. 40), Ccmm (No. 63), $Ccm2_1$ (No. 36). Since $LiSi_2N_3$ has $Ccm2_1$, this seemed probable for $MgAlSiN_3$ and because the conventional representation for $Ccm2_1$ is $Cmc2_1$ the a and b dimensions were interchanged for the purposes of structure determination.

X.5 Structure refinement

Thirty intensities were measured corresponding to 73 possible reflexions, 12 of which were too weak to be observed. The final calculated and observed X-ray data are given in Table X.3.

Structure refinement using the SHELL-X program (see Chapter IV) was started using the parameters of $LiSi_2N_3$ (Table X.4 - taken from Taylor & Thompson, 1972) with magnesium in the lithium sites and silicon and aluminium distributed randomly in silicon sites. N1 refers to the nitrogen atom above magnesium while N2 refers to the atom above each silicon or aluminium. In the first data input the parameters underlined in Table X.4 were kept constant and refinement was continued until the R-factor reached 15%. Then the isotropic temperature factor was varied and brought R down to 10%. At this stage anisotropic temperature factors were introduced and refinement reduced R to 7.0%. Then by allowing variation in the atomic positions with the anisotropic factors maintained constant and vice-versa,

Table X.3 X-ray diffraction data for $MgAlSiN_3$

hkl	d_{calc}	d_{obs}	$Sin^2\theta_{calc}$	$Sin^2\theta_{obs}$	I_{calc}	I_{obs}
110	4.7066	4.7041	0.0424	0.0428	0.40	0.99
020	4.6980		0.0425			
111	3.4017	3.3909	0.0811	0.0816	2.31	2.57
200	2.7190	2.7074	0.1269	0.1280	40.37	35.74
130	2.7140		0.1274			
002	2.4610	2.4540	0.1549	0.1558	31.03	28.92
201	2.3800	2.3739	0.1656	0.1665	49.45	39.19
131	2.3767		0.1661			
220	2.3533	—	0.1694	—	0.12	-
040	2.3490		0.1700			
112	2.1809	—	0.1973	—	0.68	-
022	2.1800		0.1974			
221	2.1231	2.1203	0.2082	0.2087	2.00	2.42
202	1.8246	1.8215	0.2818	0.2828	30.43	32.22
132	1.8231		0.2823			
310	1.7799	1.7723	0.2962	0.2987	0.57	1.34
240	1.7775		0.2970			
150	1.7761		0.2974			
222	1.7008	1.6978	0.3243	0.3255	2.51	1.60
042	1.6992		0.3250			
311	1.6738	1.6688	0.3349	0.3369	2.53	3.00
241	1.6719		0.3357			
151	1.6707		0.3362			
330	1.5689	1.5668	0.3812	0.3822	75.81	73.97
060	1.5660		0.3826			
113	1.5492	1.5465	0.3909	0.3923		
331	1.4948		0.4199		0.68	0.70
312	1.4422	1.4398	0.4511	0.4526	2.07	1.77
242	1.4410		0.4519			
152	1.4402		0.4523			
203	1.4047	1.4028	0.4755	0.4768	58.09	49.95
133	1.4041		0.4759			
400	1.3595	1.3582	0.5077	0.5086	18.56	16.12
260	1.3570		0.5095			
223	1.3459		0.5180			
332	1.3229	1.3215	0.5361	0.5373	68.50	59.86
062	1.3212		0.5375			
401	1.3104	1.3077	0.5464	0.5487	34.59	38.53
261	1.3082		0.5482			
420	1.3059		0.5502	—	0.65	-
350	1.3046		0.5513			
170	1.3032		0.5525			
421	1.2623	1.2600	0.5889	0.5910	4.27	2.72
351	1.2611		0.5900			
171	1.2598		0.5912			

Table X.3 contd.

hkl	d_{calc}	d_{obs}	$Sin^2\theta_{calc}$	$Sin^2\theta_{obs}$	I_{calc}	I_{obs}
004	1.2305	1.2299	0.6197	0.6203	4.15	3.87
313	1.2063	1.2048	0.6448	0.6454		
243	1.2056		0.6455			
153	1.2052		0.6460			
114	1.1905	1.1887	0.6620	0.6640	17.16	16.58
024	1.1904		0.6622			
402	1.1900		0.6626			
262	1.1883		0.6644			
440	1.1766		0.6777	—	0.15	-
080	1.1745		0.6802			
422	1.1536	1.1540	0.7051	0.7046	1.91	1.96
352	1.1527		0.7062			
172	1.1517		0.7074			
333	1.1339		0.7298	—	0.38	0.25
204	1.1210	1.1205	0.7466	0.7473	5.14	5.43
134	1.1207		0.7471			
224	1.0904	1.0900	0.7891	0.7897	4.21	4.39
044	1.0900		0.7897			
510	1.0804		0.8038	—	0.12	
370	1.0787		0.8063			
280	1.0782		0.8071			
442	1.0616	1.0605	0.8326	0.8342	1.26	1.70
082	1.0600		0.8351			
511	1.0553		0.8426	—	0.81	
371	1.0537		0.8450			
281	1.0532		0.8458			
403	1.0468	1.0460	0.8562	0.8575	32.50	31.87
263	1.0457		0.8581			
530	1.0274	1.0273	0.8889	0.8891	14.35	12.78
460	1.0266		0.8903			
190	1.0253		0.8926			
423	1.0218		0.8987	—	0.26	
353	1.0211		0.8990			
173	1.0204		0.9011			
314	1.0122	1.0135	0.9159	0.9135	0.36	0.67
244	1.0117		0.9166			
154	1.0115		0.9171			
531	1.0057	1.0057	0.9276	0.9276	42.82	34.14
461	1.0050	1.0050	0.9290	0.9290		
191	1.0037	1.0037	0.9313	0.9313		

Table X.4 Initial atomic parameters

	x	y	z	isotropic temperature factor
Mg	0	0.333	0.500	0.012
Si,Al	0.167	0.167	0	0.012
N1	0	0.333	0.875	0.012
N2	0.167	0.167	0.375	0.012

R was hardly improved to 6.8%. The refinement was terminated at this point and the final atomic parameters are listed in Table X.5.

Throughout the refinement the magnesium parameter z was fixed at 0.5 to define the origin in the z direction. The occupation numbers were kept fixed, because Mg can only be in 4(a) positions of the formula (by analogy with $LiSi_2N_3$).

A fourier map of the electron density of the atoms in xz planes showed that the N atoms were reasonably spherical and were in expected position, which suggested that the structure was correct. The bond lengths and bond angles are given in Table X.6 and 7 respectively. The mean bond lengths are compared with values obtained for nitrides by other workers in Table X.8.

X.6 Discussion

The structure consists of equal numbers of MgN_4 and SiN_4 and AlN_4 tetrahedra sharing corners and linked together in 3-dimensional network. Each (Si,Al) centred tetrahedra is surrounded by 3 (Si,Al) and 3 Mg-centred tetrahedra in its own plane and 4 (Si,Al) and 2 Mg-centred tetrahedra both above and below its plane. Each Mg-centred tetrahedra is surrounded by 6 (Si,Al)-centred tetrehedra in its own plane and 4 (Si,Al) and 2 Mg-centred tetrahedra above and below its plane. The projection on (001) of the atomic arrangement in $MgAlSiN_3$

Table X.5 Final atomic parameters

atom	site	x	y	z
Mg	4(a)	0.000 ±0.000	0.331 ±0.001	0.500 ±0.000
Si,Al	8(b)	0.163 ±0.001	0.165 ±0.001	0.039 ±0.002
N1	4(a)	0.000 ±0.000	0.286 ±0.006	0.966 ±0.010
N2	8(b)	0.185 ±0.003	0.175 ±0.004	0.417 ±0.009

Anisotropic temperature factors

	B_{11}	B_{22}	B_{33}	B_{23}	B_{13}	B_{12}
Mg	0.021 ±0.005	0.016 ±0.006	0.000 ±0.001	-0.013 ±0.006	0.000 ±0.000	0.000 ±0.000
Si,Al	0.014 ±0.003	0.013 ±0.003	0.029 ±0.006	0.004 ±0.001	-0.009 ±0.004	0.002 ±0.003
N1	0.000 ±0.011	0.122 ±0.029	0.178 ±0.053	-0.118 ±0.038	0.000 ±0.000	0.000 ±0.000
N2	0.039 ±0.010	0.036 ±0.011	0.040 ±0.013	-0.025 ±0.009	0.030 ±0.013	-0.017 ±0.009

Table X.6 Bond lengths (Å) in $MgAlSiN_3$

Mg-centred tetrahedron		Si,Al-centred tetrahedron	
$Mg - N1_{(a)}$	= 2.306	$Si,Al - N1_{(a)}$	= 1.704
$Mg - N1_{(b)}$	= 2.088	$Si,Al - N2_{(b)}$	= 1.955
$Mg - N2_{(a)}$	= 1.978	$Si,Al - N2_{(b)}$	= 1.874
$Mg - N2_{(b)}$	= 1.978	$Si,Al - N2_{(c)}$	= 1.780
mean = 2.09 ± 0.13		mean = 1.83 ± 0.10	
$N1_{(b)} - N2_{(a)}$	= 3.418	$N1_{(a)} - N2_{(b)}$	= 3.067
$N1_{(b)} - N2_{(b)}$	= 3.418	$N1_{(a)} - N2_{(a)}$	= 3.059
$N1_{(a)} - N2_{(a)}$	= 3.269	$N1_{(a)} - N2_{(c)}$	= 2.979
$N1_{(a)} - N2_{(b)}$	= 3.269	$N2_{(a)} - N2_{(b)}$	= 3.108
$N1_{(a)} - N1_{(b)}$	= 3.386	$N2_{(a)} - N2_{(c)}$	= 2.982
$N2_{(a)} - N2_{(b)}$	= 3.476	$N2_{(b)} - N2_{(c)}$	= 2.869

Table X.7 Bond angles (°) in $MgAlSiN_3$

Mg-centred tetrahedron:

$N1_{(b)}$ - Mg - $N2_{(a)}$	=	114.4
$N2_{(b)}$ - Mg - $N1_{(b)}$	=	114.4
$N2_{(a)}$ - Mg - $N2_{(b)}$	=	123.0
$N1_{(a)}$ - Mg - $N1_{(b)}$	=	100.7
$N1_{(a)}$ - Mg - $N2_{(b)}$	=	99.2
$N1_{(a)}$ - Mg - $N2_{(a)}$	=	99.2

mean = 109 ± 9

Si,Al-centred tetrahedron:

$N1_{(a)}$ - Si,Al - $N2_{(a)}$	=	113.3
$N1_{(a)}$ - Si,Al - $N2_{(c)}$	=	117.5
$N1_{(a)}$ - Si,Al - $N2_{(b)}$	=	117.9
$N2_{(a)}$ - Si,Al - $N2_{(b)}$	=	108.5
$N2_{(b)}$ - Si,Al - $N2_{(c)}$	=	103.4
$N2_{(a)}$ - Si,Al - $N2_{(c)}$	=	105.9

mean = 111 ± 6

Table X.8 Comparison of mean bond lengths in tetrahedral co-ordination

	Present work	$MgSiN_2$ (Wild et al 1970)	$MgSiN_2$ (David et al 1970)	Mg_3N_2 (David et al 1971)	β-Si_3N_4 (Wild, 1968)	Sialon (Thompson, 1973)
Mg-N	2.09	2.00	1.98	2.13	-	-
Si-N	-	1.84	1.87	-	1.74	-
Al-N = 1.89*						
Si,Al-N	1.83	-	-	-	-	1.77

* In AlN

is given in Figure X.3.

The mean Mg-N bond length agrees with the accepted value (Mg-N=2.12) and the (Si,Al)-N bond length agrees with the averaged bond length for Si-N(1.75) and Al-N(1.89) i.e. 1.82. The mean of the bond angles is nearly equal to the angles in the regular tetrahedron. If Al occupied 4(a) positions and Mg,Si the 8(b) positions, expected mean bond-lengths for the two tetrahedra would be 1.89 and 1.94 respectively and in the case of Si in 4(a) positions and Mg,Al in 8(b) positions the equivalent bond-lengths would be 1.75 and 2.00 respectively. Clearly observed bond-lengths show that Mg occupies the 4(a) positions with Si,Al disordered in 8(b) positions. This is to be expected from the previous work on nitrides, $BeSiN_2$ (Eckerlin, 1967), $MgSiN_2$ (David et al, 1970; Wild et al, 1972), $MnSiN_2$ (Maunaye et al, 1971; Wild et al, 1972), $MgGeN_2$ (David et al, 1970), $LiSi_2N_3$ (David et al, 1973).

The chemical analysis of the hot-pressed $MgAlSiN_3$ sample given in Table X.9 shows the sample to be slightly deficient in magnesium and richer in aluminium than the starting composition.

X.7 Conclusion

The quaternary nitride magnesium aluminium silicon nitride of formula $MgAlSiN_3$ has an orthorhombic

Table X.9 Chemical analysis of $MgAlSiN_3$

(Analysis for metals, carried out at the British Ceramic Research Association)

	w/o
Si_3N_4	37.85
AlN	35.54
Mg_3N_2	25.83
Impurities expressed as oxides	
TiO_2	0.06
Fe_2O_3	0.23
CaO	0.08
K_2O	0.08
Na_2O	0.05
Wo_3	0.28
Co_3O_4	0.06

The composition neglecting the impurities, according to the above chemical analysis is $Mg_{0.94}Al_{1.06}Si_{0.99}N_3 \equiv 2.99M:3.00X$

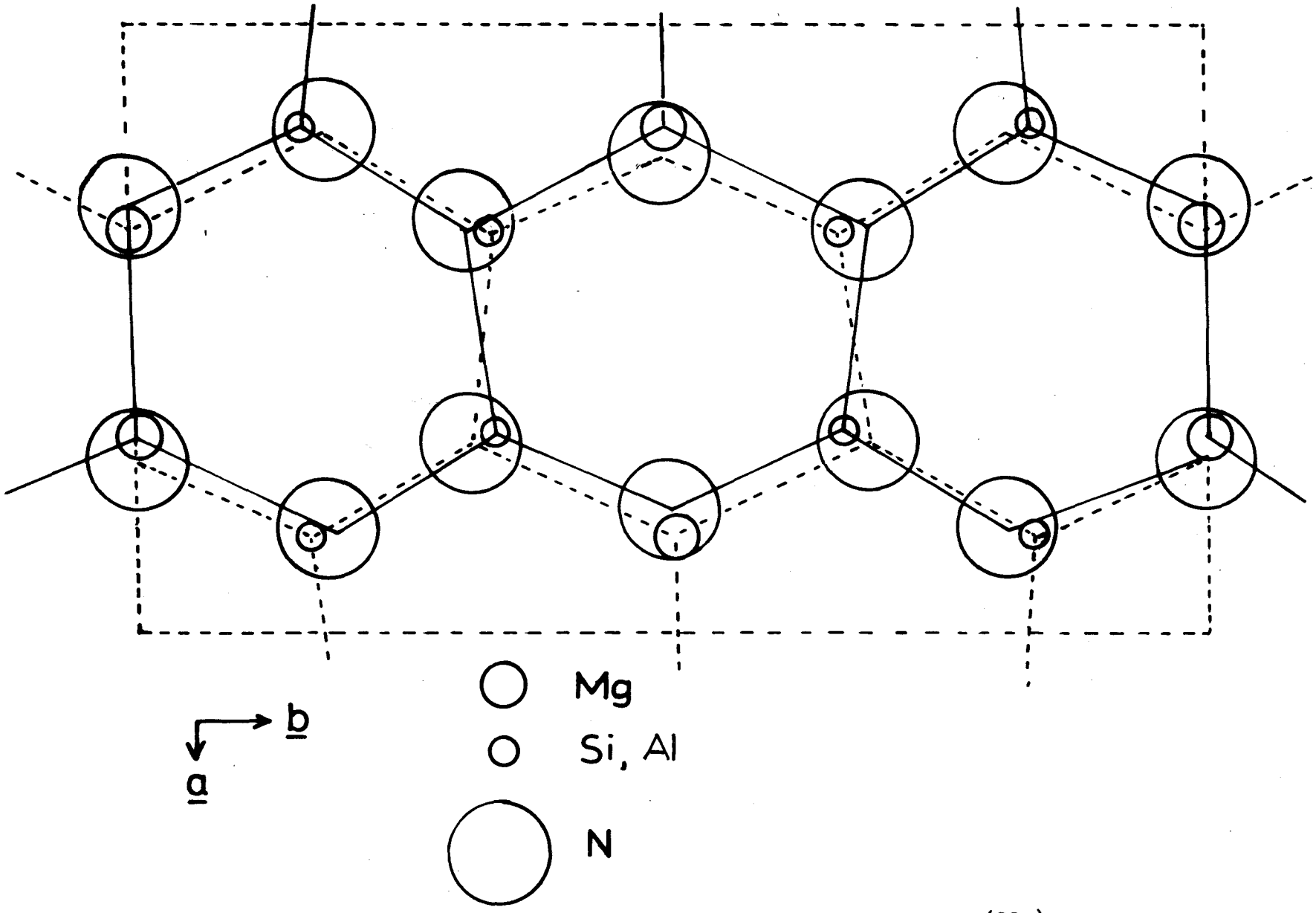

Figure X.3 Atomic arrangement in $MgAlSiN_3$ projected on (001)

structure similar to $LiSi_2N_3$ with space group $Ccm2_1$ and contains four formula weights per unit cell. Magnesium atoms are ordered in 4-fold sites while silicon and aluminium occupy 8-fold sites in a random manner. The structure is based upon that of AlN which, like many other nitrides and oxynitrides, is a wurtzite type.

References

Alper, A.M., McNally, R.N., Ribbe, P.G. & Doman, R.C. 1962 J. Amer. Ceram. Soc., 45, 6, 264.

Arrol, W.J. 1974 "Ceramics for High Performance Applications". Proceedings of the Second Army Materials Technology Conference at Hyannis, November 1973; p. 729

Bayer, G. 1973 Proc. Brit. Ceram. Soc., 22, 39.

Bell, F.R. & Wilson, W.I. 1973 Progress Report (January), Crystallography Laboratory, Department of Metallurgy, University of Newcastle upon Tyne.

Berkbile, C.A. 1970 Corning report No. L1124; Corning Glassworks, Research and Development Laboratory.

Bowen, N.L. & Andersen, O. 1914 Amer. J. Sci., 37, 4, 488.

Bratton, R.J. 1974 J. Amer. Ceram. Soc., 57, 1, 283.

Buang, K.B. 1976 Private communication, University of Newcastle upon Tyne.

Cutter, I.B. & Croft, W.J. 1974 Powder Met. Int., 6, 2.

David, J.P., Lang, J. & Charlot, J.P. 1970 Revue de Chimie Mineral, 7, 121.

David, J.P., Laurent, Y. & Lang, J. 1971 Bull. Soc. Fr. Cristallogr., 94, 340.

David, J., Laurent, Y., Charlot, J.P. & Lang, J. 1973

Bull. Soc. Fr. Mineral Crystallog., 96, 2.

Deeley, G.C., Herbert, J.M. & Moore, N.C. 1961 Powder Met., 8, 145.

Deville, H. & Wöhler, F. 1857 Leibigs. Aim., 104, 256.

Eckerlin, P., Rabenau, A. & Nortman, H. 1967 Z. Anorg. Allg. Chemie., 353, 113,225.

Elmer, T.H. & Nordberg, M.E. 1965 Proceedings of the 7th International Congress on Glass, Brussels, p. 30.

Elmer, T.H. & Nordberg, M.E. 1967 J. Amer. Ceram. Soc., 50, 6, 275.

Evans, A.G. & Davidge, R.W. 1970 J. Mat. Sc., 5, 314.

Forgeng, W.D. & Decker, B.F. 1958 Trans. Met. Soc. A.I.M.E., 343.

Gauckler, L.J., Lukas, H.L. & Petzow, G. 1975 J. Amer. Ceram. Soc., 58, 7-8, 346.

Gazza, G.E. 1973 J. Amer. Ceram. Soc., 56, 662.

Greenwood, N.N. 1968 "Ionic Crystals, Lattice Defects and Stoichiometry". Pub. Butterworths, London.

Grieg, J.W. 1927 Amer. J. Sc. (5), 13, 15, 133.

Hardie, D. & Jack, K.H. 1957 Nature, 180, 332.

Hendry, A., Perera, D.S., Thompson, D.P. & Jack, K.H. 1975 "Special Ceramics 6", Stoke-on-Trent, B. Ceram. R.A.

Huseby, I.C., Lukas, H.L. & Petzow, G. 1975 J. Amer. Ceram.

Soc., 58, 377.

Indrestedt, I. & Brosset, C. 1964 Act. Chem. Scand. 18, 8, 1879.

Jack, K.H. & Wilson, W.I. 1972 Nature Phy. Sc. 238, 28.

Jack, K.H. 1973 Trans. & J. Brit. Ceram. Soc., 72, 376.

Jack, K.H. 1976 J. Mat. Sc., 11, 6, 1135.

Jama, S.A.B., Thompson, D.P. & Jack, K.H. 1975 "Special Ceramics 6", Stoke-on-Trent, B. Ceram. R.A., p. 299.

Jänecke, E. 1907 Z. Anorg. Chem., 53, 319.

Jeffrey, G.A. & Wu, V.Y. 1963 Acta Cryst., 16, 559.

Jeffrey, G.A. & Wu, V.Y. 1966 Acta Cryst., 20, 538.

Keer, H.V., Bodas, M.G., Baudri, A. & Biswas, A. 1974 J. App. Phy., 7, 2058.

Kingery, 1967 "Introduction to Ceramics". Pub. John Wiley & Son, New York.

Kirby, D. 1944 "Pure Oxide Refractories", Metallugia, June.

Komeya, K., Inoue, H. & Tsage, A. 1974 J. Amer. Ceram. Soc., 57, 411.

Lejus, A-M, 1967 Mat. Res. Bull., 2, 837.

Lumby, R.J., North, B. & Taylor, A.J. 1975 "Special Ceramics 6", Stoke-on-Trent, B. Ceram. R.A.

Maunaye, M., L'Haridon, P., Laurent, Y. & Lang, J. 1971

Bull. Soc. Fr. Mineral Cristallogr., 94, 3.

McLean, A.F. 1974 "Ceramics for High-Performance Applications" Proceedings of the Second Army Materials Technology Conference at Hyannis, November 1973.

Messier, D.R. & Gazza, G.E. 1975 J. Amer. Ceram. Soc. 58, 11-12, 538.

Mulfinger, H.O. & Meyer, H. 1963 Glasstech. Ber. 36, 12, 481.

Nuttall, K. & Thompson, D.P. 1974 J. Mat. Sci., 9, 850.

Osborn, E.F. & Muan, A. 1960 "Phase Equilibrium Diagrams of Oxide Systems", Pub. American Ceramic Society and the Edward Orton Jr. Ceramic Foundation.

Oyama, Y. & Kamigaito, O. 1972 Yogo-Kyokai-Sci., 80, 327.

Perelman, V.E. & Roman, O.V. 1974 Proceedings of the First International Conference on the Compaction and Consolidation of Particulate Matter. Powder Technology, Pub. series No. 4, p. 41.

Price, W.M. 1974 Proceedings of the First International Conference on the Compaction and Consolidation of Particulate Matter. Powder Technology, Pub. series No. 4, p. 81.

Priest, H.F., Burns, F.C., Priest, G.L. & Skaar, E. 1973 J. Amer. Ceram. Soc., 56, 395.

Rae, A.W.J.M., Thompson, D.P., Pipkin, N.J. & Jack, K.H. 1975

"Special Ceramics 6", Stoke-on-Trent, B. Ceram. R.A., 347.

Ramsdell, L.S. 1947, Amer. Mineralogist, 32, 64.

Roy, D.M., Roy, R. & Osborn, E.F. 1953 J. Amer. Ceram. Soc., 36, 5, 149.

Ruddelsden, S.N. & Popper, P. 1958 Acta. Cryst. 11, 465.

Schlaudt, C.M. & Roy, D.M. 1965 J. Amer. Ceram. Soc., 48, 5, 248.

Sheldrick, G. 1975 Private communication, University of Cambridge.

Shelly, R.D. & Nicholson, P.S. 1971 J. Amer. Ceram. Soc. 54, 8, 365.

Singer, F. & Singer, S.S. 1963 "Industrial Ceramics" Pub. Chapman & Hall, London.

Smoke, E.J. 1954 "Spinel as Dielectic Insulation", Ceramic Age, May.

Soulen, J.R., Sthapitanoda, P. & Margrave, J.L. 1955 J. Phy. Chem., 59, 132.

Suzuki, H. 1963 Bull. Tokyo Inst. of Technology, 54, 163.

Taylor, A. 1951 J. Sci. Instrum., 28, 200.

Taylor, H. & Thompson, D.P. 1972 Progress Report, Ministry of Defence Contract N/CP.61/9411/67/4B/MP387. University of Newcastle on Tyne.

Taylor, K.M. & Lenie, C. 1960 J. Electrochem. Soc., April, 308.

Terwilliger, G.R. & Lange, F.F. 1975 J. Mat. Sci., 10, 1169.

Thompson, D.P. 1973 Progress Report, July, Ministry of Defence Contract AT/2043/028 AML. University of Newcastle upon Tyne.

Thompson, D.P. 1975 Private communication, University of Newcastle on Tyne.

Thompson, D.P. 1976 J. Mat. Sci., 11, 1377.

Thompson, D.S. & Pratt, P.L. 1967 Science of Ceramics, 3, Edited by G.H. Stewart, Academic Press, New York, p. 33.

Wild, S. 1968 Ph.D. Thesis, University of Newcastle on Tyne.

Wild, S., Grieveson, P. & Jack, K.H. 1968 "The Crystal Chemistry of Ceramic Phases in the Silicon-Nitride-Oxygen and Related Systems", Progress Report No. 1, Ministry of Defence Contract N/CP.61/9411/67/4B/MP387. University of Newcastle on Tyne.

Wild, S., Grieveson, P. & Jack, K.H. 1972 "Special Ceramics 5", Stoke-on-Trent, B. Ceram. R.A., p. 289.

Wild, S., Grieveson, P., Jack, K.H. & Latimer, M.J. 1972 "Special Ceramics 5", Stoke-on-Trent, B. Ceram. R.A., p. 377.

Wilson, W.I. 1974 Ph.D. Thesis, University of Newcastle on Tyne.

Zernike, J. 1955 "Chemical Phase Theory", Deventer, Netherlands, Kluwers Publishing Co. Ltd.